UNIVERSITY OF COPENHAGEN

Master Thesis in Nanoscience

Magnus Fosse Bøe

Majorana surface codes with dislocations

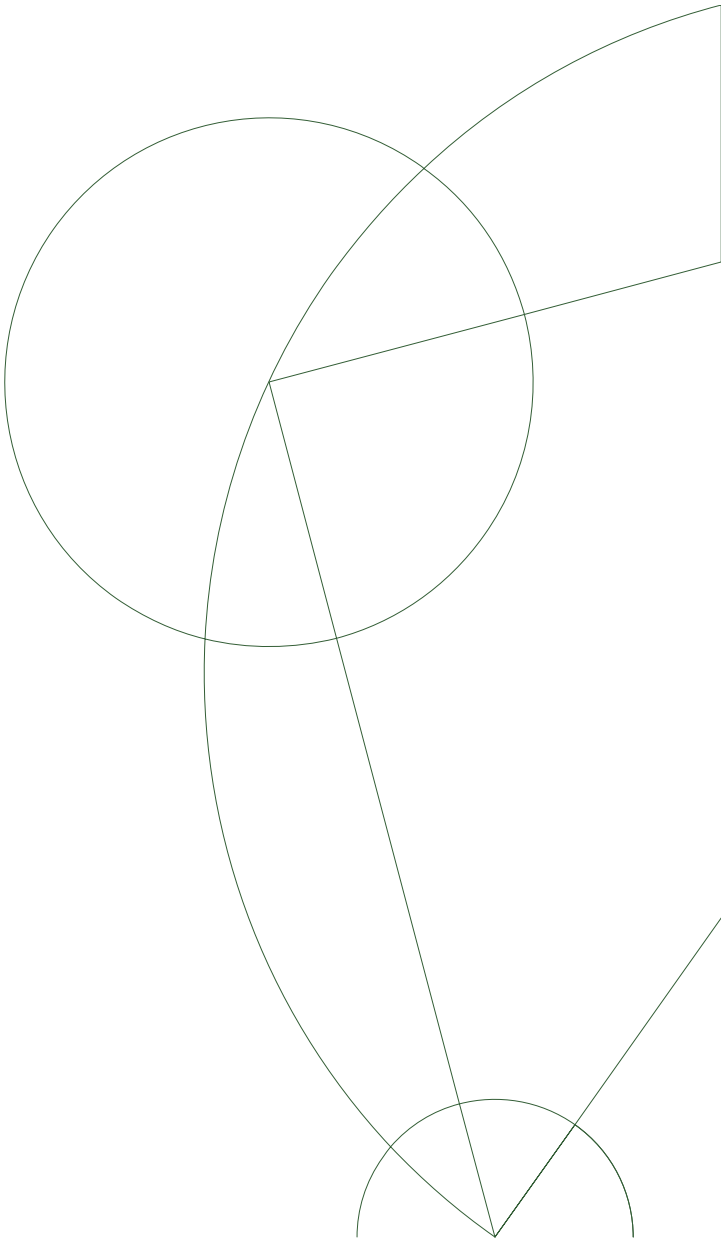

Dr. Michele Burrello and Dr. Karsten Flensberg

August 6, 2018

Abstract

The planar code is at present the most promising proposal for developing fault-tolerant quantum computation. Building on the investigations of twist defects in the toric code model [1, 2], this thesis considers the possibility of constructing computational qubits by introducing dislocations in the planar code.

We review the basic properties of Majorana Fermions (MFs) and the toric code. By use of Schrieffer-Wolff perturbation theory we find that the planar code model with twist defects emerges as the low-energy sector of an array of tunnel coupled Majorana-Cooper boxes (MCBs), with the twist defects being unpaired MFs. We find that the system under investigation can be initialized, and that the MFs can be moved around in the array. By introduction of a modified, split MCB, we are able to perform braiding operations with the MFs. We calculate the Berry phase of the braiding process in two different ways, and confirm that it agrees with the expected result.

Finally, we describe how the state of the system can be measured. This is required in order to observe the non-Abelian statistics of these particles. The operations we can carry out with this system are not enough for universal quantum computation, but in combination with other techniques, such as the T-gate (a $\pi/8$-rotation), implementable through for example magic state destillation [3, 4], universality can be achieved.

Abstrakt

Fladekoden er i øjeblikket det mest lovende forslag til, hvordan man kan udvikle fejltolerant kvanteberegning. Dette speciale bygger videre på forskningen på såkaldte vridninger i Kitaevs toruskode-model [1, 2] og undersøger muligheden for at bygge logiske kvantebits ved at introducere sådanne vridninger i fladekoden.

Vi gennemgår majoranafermionerne og toruskodens grundlæggende egenskaber. Ved brug af Schrieffer-Wolff perturbationsteori finder vi, at lav-energisektoren for et gitter af tunnelkoblede Majorana-Cooper-bokse er ækvivalent med fladekode-modellen med vridninger, hvor vridningerne er uparrede majoranafermioner. Vi finder endvidere, at det undersøgte system kan forberedes i en veldefineret tilstand, og at majoranafermionerne kan flyttes rundt i gitteret. Ved at benytte en todelt Majorana-Cooper-boks er vi i stand til at flette majoranafermioner. Vi udregner den tilhørende Berry-fase på to forskellige måder og bekræfter, at den stemmer overens med de forventede resultater.

Til sidst beskriver vi, hvordan vi kan måle systemets tilstand. Dette er påkrævet for at kunne observere majoranafermionernes ikke-abelske statistik. De operationer, vi kan udføre i det pågældende system, er ikke tilstrækkelige for at kunne udføre universelle kvantebergninger. T-porten er en $\pi/8$-rotation, og kan implementeres gennem for eksempel magic state destillation [3, 4]. I kombination med en T-port kan systemet benyttes for at opnå universel kvanteberegning.

Preface and acknowledgements

This thesis is submitted as the conclusion of the Nanoscience M. Sc. program at the University of Copenhagen.

Firstly, I would like to thank my supervisor, associate professor Michele Burrello, for his invaluable supervision and feedback throughout the project. The work has been a very enriching learning experience. I also want to thank professor Karsten Flensberg for being my co-supervisor.

I would also like to thank the staff and students at the Condensed Matter Theory department of the Niels Bohr Institute for providing a friendly and engaging learning environment.

The Condensed Matter Lunch Club deserves thanks for being a forum where no question or speculation is too far-fetched. I'm grateful for the daily discussions on topics ranging from Chilean avocado cultivation to the Silmarillion.

Finally, I would like to thank my girlfriend, friends and family.

Contents

List of Figures

Introduction

Over the last decades, there has been a lot of interest in the developing field of topological phases of matter. Topological phases are not described by local order parameters and the framework of Landau symmetry-breaking theory, but rather by topological invariants that are concerned with some global property of the system.

Within condensed matter physics, the possibility of realizing Majorana bound states (MBSs) as a topological phase of matter has spurred massive research efforts. The Majorana Fermions (MFs) are of great fundamental interest and the search for them is mainly due to their exotic braiding statistics , which differ drastically from those of Bosons and Fermions [6]. Their technological potential in quantum computation is due to these statistics, and their non-local nature, which allows for robust information processing resilient to local decoherence sources.[7–10]

The idea of MFs in condensed matter systems emerged from an initial proposal by Kitaev [11]. He showed how a spinless p-wave superconducting chain (one-dimensional) could have topologically protected edge modes, in the form of MFs. p-wave superconductors have not been found in nature, and so research has attempted to mimic Kitaev's model in more realistic systems.

Kane and Fu [12] realized that MFs might also arise as surface states of certain topological semiconductors proximitized by a superconductor. Several other proposals have been made, with various systems considered as candidates for hosting MFs [13–16]. In particular, after the work by Kane and Fu, it was suggested to use one-dimensional semiconductor wires proximitized by an s-wave superconductor with strong spin-orbit interaction and a magnetic field oriented along the wire axis [17, 18]. It was predicted that the presence of MFs could be detected by measuring the conductance of such semiconductor wires and finding a quantized conductance peak at the universal conductance value $2e^2/h$ [19–21].

Following a long period of theoretical dominance in the field, an experiment due to Mourik *et al* [22], using tunneling spectroscopy methods, found a characteristic peak in the density of states at zero energy and they concluded that they had likely seen the effect of MFs. Similar observations were shortly after made by several other groups [23–26] in InAs and InSb nanowires. Whether these results are clear indications of the presence of MFs is debated, and more recent experimental efforts have been focussed on ruling out other possible sources for the so-called zero bias conductance peaks. The last years have seen great improvements in material manufacturing, and as a result, peaks

close to the universal conductance value have been found [27]. An overview of the recent progress in the field is provided by the review articles [28, 29]. A key experiment designed to distinguish between the presence of MFs and other likely, non-Majorana sources of similar peaks, has been reported recently [30]. This most recent experiment, in combination with the growing collection of other high-quality investigations give strong reason to believe that semiconductor nanowires under the right conditions host MFs. Chapter 1 of this thesis will review the basic features of MFs.

As mentioned, anyons exhibit exotic statistical evolutions. Systems that host them become topological as a result of the topological nature of these evolutions. Often, topological systems are many-body systems characterized by entangled ground states and localized quasiparticle excitations.

For two-dimensional systems, topological order manifests itself through almost degenerate ground states belonging to a topologically protected subspace of the full Hilbert space. Transformations within this subspace can manipulate information, and the statistical evolution of the quantum states can be tailored to implement quantum algorithms. It is desirable for the nearly degenerate ground states, the states used for computation, to be separated from the continuum of excited states by a gap large enough that perturbations and local noise do not cause transitions from the computational states to more energetic states, and thereby cause computational errors. [7, 31]

Kitaev's toric code model [32] is the pricipal toy model exhibiting topological order. The toric code model will be reviewed in chapter 2. The present work is concerned with the planar code, which is the toric code on a surface without periodic boundary conditions. This model can be realized physically [33–35], as an array of Majorana-Cooper boxes (MCBs) [36–38] where the MBSs are tunnel coupled to those on adjacent islands. Bombín [1] has investigated twist defects in the toric code model, and Zheng, Dua and Jiang [2] have interpreted twist defects in the array of MCBs. A review and extension of this work is provided by chapter 3. In chapter 4, we consider how well-separated twist defects, which are Majorana modes in the MCB array, can be used as non-local qubits resilient to many types of decoherence, and how the planar code setup can be used to braid Majorana modes.

Chapter 1

Introduction to Majorana modes

1.1 The Kitaev chain model

Fermion mode creation and annihilation operators satisfy the relations

$$\{c_i^\dagger, c_j\} = \delta_{i,j}, \quad \{c_i^\dagger, c_j^\dagger\} = 0, \quad \{c_i, c_j\} = 0. \tag{1.1}$$

These operators square to zero, in accordance with the exclusion principle. We can write these complex Fermion operators as linear combinations of real operators, called Majorana operators:

$$c_n = \frac{\gamma_n^a + i\gamma_n^b}{2}, \quad c_n^\dagger = \frac{\gamma_n^a - i\gamma_n^b}{2}. \tag{1.2}$$

Equivalently, we may write the Majorana operators as linear combinations of Fermion operators:

$$\gamma_n^a = c_n^\dagger + c_n, \quad \gamma_n^b = i(c_n^\dagger - c_n). \tag{1.3}$$

We see that the Majorana operators satisfy what is called the Clifford algebra:

$$\{\gamma_m^i, \gamma_n^j\} = 2\delta_{i,j}\delta_{m,n}, \tag{1.4}$$

and that a Majorana operator is its own Hermitian conjugate. It is also evident that any Majorana operator squares to unity. When working with Fermions, we are accustomed to the number operator $c^\dagger c$. Applying this operator to a single Fermion Fock state returns the occupation number of the state. Instead of the number operator, this thesis will mainly use the Fermion parity operator. The Fermion parity operator for a single Fermion mode can be written in terms of the Fermion creation and annihilation

operators, as $1 - 2c^\dagger c$. If the Fermion mode is unoccupied, the parity is even, and $1 - 2c^\dagger c|0\rangle = 1|0\rangle$. Conversely, if it contains a Fermion, the parity is odd, and we have $1 - 2c^\dagger c|1\rangle = -1|1\rangle$. We may also express this as $(-1)^{c^\dagger c}$. For a system containing many Fermions, the parity generalizes to

$$P = (-1)^{\sum_i c_i^\dagger c_i}$$

In terms of Majorana operators, the Fermion parity operator takes the form

$$1 - 2c_n^\dagger c_n = 1 - \frac{1}{2}(\gamma_n^a - i\gamma_n^b)(\gamma_n^a + i\gamma_n^b) = i\,\gamma_b\,\gamma_a$$

In an isolated system, the number of particles cannot change, and the Fermion parity is conserved.

The Majorana modes come in pairs, as linear combinations of a common Fermion mode. It is possible to build a system so that a pair of Majorana modes are well separated and can be treated as individual entities. This means that the Fermion they constitute is a non-local object, which is resilient to local noise. The starting point for the realization of such a system is the Kitaev chain model [11]. Here, we take a similar approach to investigating the Kitaev chains as is done in the online course *Topology in condensed matter* [39].

The Kitaev chain from a spinless p-wave superconductor

Let us consider a one-dimensional, superconducting chain of spinless Fermions, with p-wave coupling. The Hamiltonian governing such a system is

$$H_{SC} = -\mu \sum_{n=1}^{N} \left(c_n^\dagger c_n - \frac{1}{2} \right) - t \sum_{n=1}^{N-1} c_{n+1}^\dagger c_n + \text{H.c} + \Delta \sum_{n=1}^{N-1} c_n c_{n+1} + \text{H.c} \tag{1.5}$$

For convenience, we number the Majorana modes, so that we have

$$c_n = \frac{\gamma_{2n-1} + i\,\gamma_{2n}}{2}$$

We reformulate the chain in terms of Majorana operators. We rewrite the hopping and superconducting pairing terms as follows:

$$\begin{aligned} c_{n+1}^\dagger c_n &= \frac{1}{4}\left(\gamma_{2n+1} - i\,\gamma_{2n+2}\right)\left(\gamma_{2n-1} + i\,\gamma_{2n}\right) \\ &= \frac{1}{4}\left(\gamma_{2n+1}\,\gamma_{2n-1} + \gamma_{2n+2}\,\gamma_{2n}\right) + i\left(\gamma_{2n-1}\,\gamma_{2n+2} + \gamma_{2n+1}\,\gamma_{2n}\right) \end{aligned}$$

$$\begin{aligned} c_n c_{n+1} &= \frac{1}{4}\left(\gamma_{2n-1} + i\,\gamma_{2n}\right)\left(\gamma_{2n+1} + i\,\gamma_{2n+2}\right) \\ &= \frac{1}{4}\left(\gamma_{2n+1}\,\gamma_{2n-1} + \gamma_{2n+2}\,\gamma_{2n}\right) + i\left(\gamma_{2n-1}\,\gamma_{2n+2} - \gamma_{2n+1}\,\gamma_{2n}\right). \end{aligned}$$

When we add to these terms their Hermitian conjugate, the real terms cancel, while the imaginary terms add. The Hamiltonian simplifies to

$$H = -\frac{i\mu}{2}\sum_{n=1}^{N}\gamma_{2n-1}\,\gamma_{2n} - \frac{it}{2}\sum_{n=1}^{N-1}\left(\gamma_{2n-1}\,\gamma_{2n+2} + \gamma_{2n+1}\,\gamma_{2n}\right) + \frac{i\Delta}{2}\sum_{n=1}^{N-1}\left(\gamma_{2n-1}\,\gamma_{2n+2} - \gamma_{2n+1}\,\gamma_{2n}\right)$$

In the case $t = \Delta$, the terms containing $\gamma_{2n-1}\,\gamma_{2n+2}$ cancel, and we are left with

$$H = -\frac{i\mu}{2}\sum_{n=1}^{N}\gamma_{2n-1}\,\gamma_{2n} - \frac{it}{2}\sum_{n=1}^{N-1}\gamma_{2n}\,\gamma_{2n+1} + \frac{i\Delta}{2}\sum_{n=1}^{N-1}\gamma_{2n}\,\gamma_{2n+1}$$

Consider two limits of this model. If we have $\mu \neq 0$, $t = \Delta = 0$, we pair up the Majorana degrees of freedom as indicated in the topmost scenario in figure 1.1. If we however have $\mu = 0$, $t = \Delta \neq 0$, we have the scenario shown in the lower panel of figure 1.1. In this case, the Majorana modes at the end of the chain do not enter the Hamiltonian. Thus, in this phase, the chain has two zero-energy modes at its ends. These two modes in combination constitute a non-local Fermion degree of freedom.

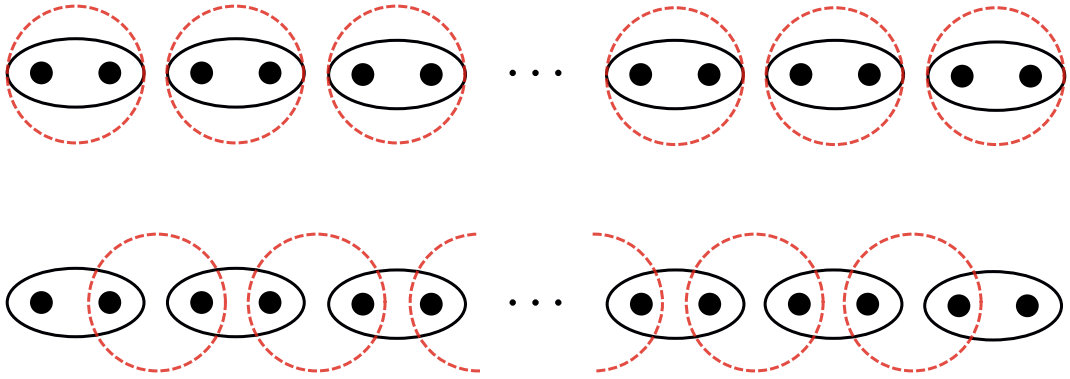

Figure 1.1: The two extreme limits of the p-wave superconducting tight binding chain. The top figure pairs up Majorana modes from the same Fermion site and corresponds to $\mu \neq 0$, $t = \Delta = 0$. The bottom figure pairs up Majorana modes from adjacent sites and corresponds to $\mu = 0$, $t = \Delta \neq 0$.

Equivalence of superconducting chain and Ising chain

Another 1D model which is mathematically equivalent to the superconducting chain is the Ising chain. This model is described by the Hamiltonian

$$H_{Ising} = -J\sum_{n=1}^{N-1}\sigma_n^x\,\sigma_{n+1}^x - h_z\sum_{n=1}^{N}\sigma_n^z$$

We will show how the superconducting chain is equivalent to the Ising chain by use of a Jordan-Wigner transformation, as outlined in [40]. We start by setting $\Delta = \Delta^* = t = t^* = a$, with a being real. This allows us to rewrite

$$-a\sum_{n=1}^{N-1}c_{n+1}^\dagger c_n + \text{H.c} + a\sum_{n=1}^{N-1}c_n c_{n+1} + \text{H.c} = a\sum_{n=1}^{N-1}(c_n - c_n^\dagger)(c_{n+1} + c_{n+1}^\dagger).$$

We introduce the Jordan-Wigner strings which correspond to Fermion creation and annihilation operators:

$$c_n = \left(\prod_{m=1}^{n-1}\sigma_m^z\right)\sigma_n^+, \quad c_n^\dagger = \left(\prod_{m=1}^{n-1}\sigma_m^z\right)\sigma_n^-$$

It can be checked that these operator strings fulfil the appropriate commutation relations. We find

$$(c_n - c_n^\dagger)(c_{n+1} + c_{n+1}^\dagger) = \left(\prod_{m=1}^{n-1}\sigma_m^z\right)(\sigma_n^+ - \sigma_n^-)\left(\prod_{m=1}^{n-1}\sigma_m^z\right)(\sigma_n^z(\sigma_{n+1}^+ + \sigma_{n+1}^-))$$

Operators on different sites commute, and so we can rearrange the string, and use the fact that the σ_z-operators square to one:

$$\begin{aligned}(c_n - c_n^\dagger)(c_{n+1} + c_{n+1}^\dagger) &= \left(\prod_{m=1}^{j-1}\sigma_m^z\right)^2(\sigma_n^+ - \sigma_n^-)(\sigma_n^z(\sigma_{n+1}^+ + \sigma_{n+1}^-)) \\ &= (\sigma_j^+ - \sigma_j^-)(\sigma_j^z(\sigma_{j+1}^+ + \sigma_{j+1}^-)) \\ &= i\sigma_n^y\sigma_n^z\sigma_{n+1}^x \\ &= -\sigma_n^x\sigma_{n+1}^x\end{aligned} \tag{1.6}$$

Where it has been used that the product of two Pauli matrices is

$$\sigma^i\sigma^j = i\varepsilon_{ijk}\sigma^k + \delta_{ij}\sigma^0 \tag{1.7}$$

where σ_0 is the identity matrix of dimension 2 and ε_{ijk} is the antisymmetric Levi-Civita symbol.

Using that $\sigma^{\pm} = (\sigma_x \pm i\,\sigma_y)/2$, we reformulate the summands of the first term of H_{SC} as

$$c_n^\dagger c_n - \frac{1}{2} = \left(\prod_{m=1}^{j-1} \sigma_m^z\right)^2 \sigma_n^- \sigma_n^+ - \frac{1}{2} = \frac{(\sigma_n^x - i\,\sigma_n^y)(\sigma_n^x + i\,\sigma_n^y)}{4} - \frac{1}{2} = \frac{i[\sigma_n^y, \sigma_n^x]}{2} = \sigma_n^z$$

Inserting this result and that of eq. 1.6 into H_{SC}, we get

$$-\mu \sum_{n=1}^{N} \sigma_n^z - a \sum_{n=1}^{N-1} \sigma_n^x\, \sigma_{n+1}^x$$

And see that this is equivalent to H_{Ising} for $\mu = J$ and $a = h_z$.

1.1.1 Investigating the end-modes

In order to find the form of the spinless superconducting chain Hamiltonian in the momentum representation, we proceed by writing it on Bogoliubov-de Gennes form. Introduction of a Nambu spinor, $C^\dagger = (c_1^\dagger, \cdots, c_N^\dagger, c_1, \cdots, c_N)$, containing creation and annihilation operators, enables us to write $H = \frac{1}{2} C^\dagger H_{BdG} C$. This doubles the dimensions of the matrix representation of the Hamiltonian by inclusion of the hole degrees of freedom. As the holes arise from doubling the Hamiltonian, no new information is contained by them. They are therefore related to the electrons by particle-hole symmetry. Introducing Pauli operators τ_i that operate on the particle-hole space, we can write the Hamiltonian kernel, H_{BdG}, compactly as

$$H_{BdG} = -\sum_{n}^{N} \mu\tau_z \otimes |n\rangle\langle n| - \sum_{n}^{N} \Big((t\tau_z + i\Delta\tau_y) \otimes |n\rangle\langle n+1| + \text{H.c.} \Big).$$

In the momentum representation this takes the form

$$H_{BdG} = -\sum_{k} \Big[\big(\mu + 2t\cos(k)\big)\tau_z - 2\Delta \sin(k)\tau_y \Big] \otimes |k\rangle\langle k|, \tag{1.8}$$

and the energies take the form

$$E(k) = \pm\sqrt{(2t\cos(k) + \mu)^2 + 4\Delta^2 \sin^2(k)}.$$

For most values of these parameters, the spectrum is gapped. If $\mu = -2t$, we see that there is a degeneracy for $k = 0$. Similarly, the gap closes at $k = \pi$ for $\mu = 2t$. It is these gap closings and openings which separate the topological and trivial phases. One way to see this, is to consider how the Hamiltonian behaves, close to the gap closing points. We expand H_{BdG} to linear order in the vicinity of $k = 0$ to obtain

$$H_{BdG} \simeq -(2t + \mu)\tau_z + 2\Delta k\tau_y$$

This Hamiltonian is linear in momentum, and is for this reason nicknamed a Dirac Hamiltonian. If we label $-(2t + \mu)$ by m, in analogy with a mass term, we see that the point where m changes sign is the point where the system goes from the topological to the trivial phase. At $m = 0$, the gap is closed, while for m negative or positive in the vicinity of this point, the system is gapped. For the case $m = 0$, the chain is at the transition point from the topological to the trivial phase, and hosts Majorana Fermions with zero energy. To find these modes, we can solve the time-independent Schrödinger equation. If we rewrite the linearized Hamiltonian in the position representation, we have

$$H_{BdG} \simeq m(x)\tau_z - i2\Delta\partial_x\tau_y$$

And $H\Psi(x) = 0\Psi(x)$ becomes

$$0 = m(x)\tau_z - i2\Delta\partial_x\tau_y\Psi(x) \Leftrightarrow \frac{m(x)}{i2\Delta}\tau_z\Psi(x) = \tau_y\partial_x\Psi(x) \Leftrightarrow \frac{m(x)}{2\Delta}\tau_x\Psi(x) = \partial_x\Psi(x).$$

The wave function is an eigenstate of τ_x, and we find it as

$$\Psi(x) \propto \begin{pmatrix} 1 \\ \pm 1 \end{pmatrix} \exp\left(\pm \int_0^x \frac{m(x')}{2\Delta} dx'\right)$$

One of the solutions is normalizable. Which one depends on how $m(x)$ changes sign. We know that $m(x)$ changes sign when the system goes from the trivial to the topological phase and *vice versa*, and so there must always be a zero-energy mode at such a domain wall.

1.1.2 Making the model physical

The Kitaev chain is not a physically realizable model, as it contains spinless fermions. The model can be modified, so that it becomes realistic. The approach to this problem is presented in several sources, for example in the introductory exposition [5]. Here we start from the Hamiltonian kernel

$$H = \left(\frac{k^2}{2m} + \alpha\,\sigma_y\,k - \mu\right)\tau_z + B\,\sigma_z + \Delta\tau_x.$$

We will look at this Hamiltonian term by term, and see how it retains the topological band structure necessary for the appearance of unpaired Majorana modes, even when it is dressed with physical phenomena. The Kitaev chain Hamiltonian of eq. 1.8 can be expanded to second order to yield

$$H_{\mathrm{BdG}} \simeq \sum_k \left[\left(\frac{k^2}{2m} - (\mu + 2t)\right)\tau_z - 2\Delta k\tau_y\right] \otimes |k\rangle\langle k|$$

with m being the effective mass resulting from the expansion. Similarly to how the dimension of the Hilbert space increased when we added the hole degrees of freedom, the inclusion of spin degrees of freedom has the same effect. By addition of a magnetic field B, here in the z-direction, the two spin bands are split, and with a large enough magnetic field, one spin species is topological, while the other one will be trivial.

The spin-orbit coupling term $\alpha\,\sigma_y\,k$ breaks conservation of spin projection in the z-direction, which otherwise would be there due to the fact that the Hamiltonian would commute with σ_z. These two effects, in combination with a physically realistic superconducting s-wave pairing, will effectively make the pairing p-wave, which is the kind of pairing we saw in H_{SC}. Referring to figure 1.2, borrowed from [5], we see how the energy bands change when we introduce the various effects.

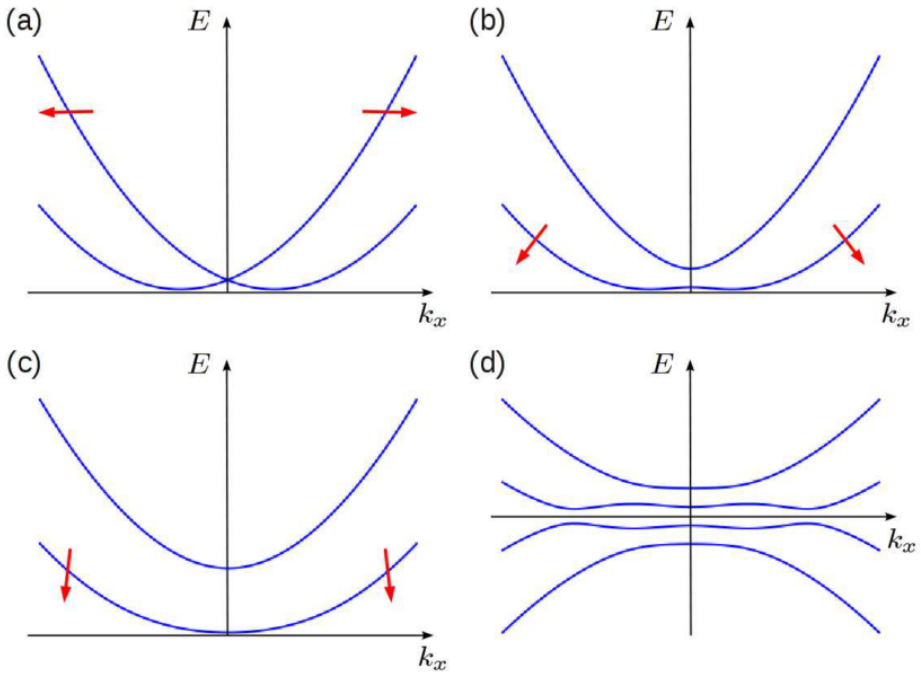

Figure 1.2: Figure borrowed from [5]. (a): A scenario where $B = 0$, $\alpha \neq 0$. The bands are split depending on their spin species with respect to the axis of the spin-orbit coupling. (b): Now, $B \neq 0$, $\alpha \neq 0$. The magnetic field splits the bands, creating a range of momenta without spin degeneracy. (c): The range of momenta without spin degeneracy is seen to grown when the magnetic field is increased. The magnetic field is larger in (c) than in (b). (d): Addition of induced s-wave superconductivity makes one spin species topological, while the other is trivial. Both electron and hole bands are shown in (d).

1.2 Majorana modes and Pauli two-component representations

In this section, we will explain a standard method for constructing a logical qubit from four Majorana modes. Initially, we consider a system of four Majorana modes. We can construct Fermion modes from these Majorana modes, by pairing them up in various ways, as shown in figure 1.3.

We write the six possible Fermion modes in terms of Majorana modes:

$$c_{ab} = \frac{\gamma_a + i\,\gamma_b}{2}, \quad \gamma_a = c_{ab}^\dagger + c_{ab}, \quad \gamma_b = i(c_{ab}^\dagger - c_{ab}) \tag{1.9}$$

As mentioned in the previous subsection, the total number of occupied Fermion modes must remain unchanged in an isolated system. If we consider the four Majoranas as an isolated system, the total Fermion parity must be conserved. This statement is

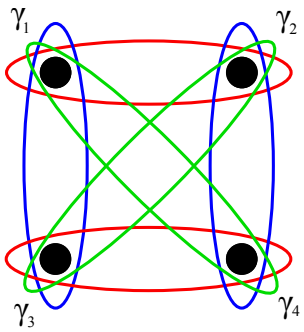

Figure 1.3: Different ways Majorana operators can be paired up to form Fermion operators.

true, independent of how we construct Fermion modes from Majorana modes. This means that a unitary mapping from the basis spanned by occupation number states of modes $\{c_{12}, c_{34}\}$ to the one spanned by $\{c_{14}, c_{23}\}$ must preserve the total Fermion parity. A parity operator can in general be written in terms of Majorana operators as:

$$1 - 2c_{ab}^\dagger c_{ab} = 1 - \frac{1}{2}(\gamma_a - i\,\gamma_b)(\gamma_a + i\,\gamma_b) = -\frac{1}{2}(-i\,\gamma_b\,\gamma_a + i\,\gamma_a\,\gamma_b) = i\,\gamma_b\,\gamma_a$$

Symbolically we have

$$\begin{aligned}(1 - 2c_{12}^\dagger c_{12})(1 - 2c_{34}^\dagger c_{34})|\Psi\rangle &= (1 - 2c_{14}^\dagger c_{14})(1 - 2c_{23}^\dagger c_{23})|\Psi\rangle \\ (i\,\gamma_2\,\gamma_1)(i\,\gamma_4\,\gamma_3)|\Psi\rangle &= (i\,\gamma_4\,\gamma_1)(i\,\gamma_3\,\gamma_2)|\Psi\rangle \\ \gamma_1\,\gamma_2\,\gamma_3\,\gamma_4\,|\Psi\rangle &= \gamma_1\,\gamma_2\,\gamma_3\,\gamma_4\,|\Psi\rangle\end{aligned}$$

where we note that the total Fermion parity for such a four-Majorana system is given by the operator $\gamma_1\,\gamma_2\,\gamma_3\,\gamma_4$.

As the total Fermion parity is conserved, we may split the system into even and odd parity sectors. We let subscripts on the occupation numbers denote which Fermion mode they correspond to: a state $|0_{12}0_{34}\rangle$, in the basis spanned by occupation number states of $\{c_{13}, c_{24}\}$, must be a linear combination of $|0_{13}0_{24}\rangle$ and $|1_{13}1_{24}\rangle$.

When we split the problem into even and odd parity sectors, each sector constitutes a two level system. We define

$$\begin{aligned}|0_{12}0_{34}\rangle \equiv |\mathbf{0}^z_{\text{even}}\rangle, \quad |1_{12}1_{34}\rangle \equiv |\mathbf{1}^z_{\text{even}}\rangle, \\ |0_{12}1_{34}\rangle \equiv |\mathbf{0}^z_{\text{odd}}\rangle, \quad |1_{12}0_{34}\rangle \equiv |\mathbf{1}^z_{\text{odd}}\rangle.\end{aligned}$$

For concreteness, we now consider the even parity sector, and map the two-level system into the familiar algebra of pseudo-spin states. Based on its effect on the pseudo-spin states, we associate $i\,\gamma_2\,\gamma_1$ with the Pauli z-operator, σ_z:

$$i\,\gamma_2\,\gamma_1\,|\Uparrow^z\rangle = -(c_{12}^\dagger - c_{12})(c_{12}^\dagger + c_{12})|0_{12}0_{34}\rangle = c_{12}c_{12}^\dagger|0_{12}0_{34}\rangle = |0_{12}0_{34}\rangle$$
$$i\,\gamma_2\,\gamma_1\,|\Downarrow^z\rangle = -(c_{12}^\dagger - c_{12})(c_{12}^\dagger + c_{12})|1_{12}1_{34}\rangle = -c_{12}^\dagger c_{12}|1_{12}1_{34}\rangle = -|1_{12}1_{34}\rangle$$

The operator $i\,\gamma_4\,\gamma_3$ accomplishes the same, by extracting the parity of the Fermion mode c_{34}. In the even parity sector, these two expressions for the σ_z-operator are equivalent. The total Fermion parity for the even sector is

$$(i\,\gamma_2\,\gamma_1)(i\,\gamma_4\,\gamma_3)|\Psi\rangle = |\Psi\rangle$$
$$(i\,\gamma_2\,\gamma_1)|\Psi\rangle = (i\,\gamma_4\,\gamma_3)|\Psi\rangle$$

while for the odd parity sector, we have

$$(i\,\gamma_2\,\gamma_1)(i\,\gamma_4\,\gamma_3)|\Psi\rangle = -|\Psi\rangle$$
$$(i\,\gamma_2\,\gamma_1)|\Psi\rangle = -(i\,\gamma_4\,\gamma_3)|\Psi\rangle$$
$$(i\,\gamma_2\,\gamma_1)|\Psi\rangle = (i\,\gamma_3\,\gamma_4)|\Psi\rangle.$$

We see that the two equivalent forms of the σ_z-operator in the odd sector are $i\,\gamma_2\,\gamma_1$ and $i\,\gamma_3\,\gamma_4$.

In the even sector, we can represent the σ_x-operator by $i\,\gamma_4\,\gamma_1$, as this operator flips the pseudo-spins:

$$i\,\gamma_4\,\gamma_1\,|\Uparrow^z\rangle = -(c_{34}^\dagger - c_{34})(c_{12}^\dagger + c_{12})|0_{12}0_{34}\rangle = -c_{34}^\dagger c_{12}^\dagger|0_{12}0_{34}\rangle = |1_{12}1_{34}\rangle$$
$$i\,\gamma_4\,\gamma_1\,|\Downarrow^z\rangle = -(c_{34}^\dagger - c_{34})(c_{12}^\dagger + c_{12})|1_{12}1_{34}\rangle = c_{34}c_{12}|1_{12}1_{34}\rangle = |0_{12}0_{34}\rangle.$$

The operator $i\,\gamma_3\,\gamma_2$ has the same effect, and these two expressions for the σ_x-operator are equivalent. In the odd subspace, the two equivalent expressions for this operator are $i\,\gamma_1\,\gamma_4$ and $i\,\gamma_3\,\gamma_2$.

Recalling the product of two Pauli matrices, as given by eq. 1.7, we can find the form of the σ_y-operator as $i\,\sigma_x\,\sigma_z = i(i\,\gamma_4\,\gamma_1)(i\,\gamma_2\,\gamma_1) = i\,\gamma_4\,\gamma_2$, or equivalently, $i\,\gamma_1\,\gamma_3$. The effect of this operator on the pseudo-spin states is as we expect:

$$i\,\gamma_4\,\gamma_2\,|\Uparrow^z\rangle = -i(c_{34}^\dagger - c_{34})(c_{12}^\dagger - c_{12})|0_{12}0_{34}\rangle = -ic_{34}^\dagger c_{12}^\dagger|0_{12}0_{34}\rangle = i|1_{12}1_{34}\rangle$$
$$i\,\gamma_4\,\gamma_2\,|\Downarrow^z\rangle = -i(c_{34}^\dagger - c_{34})(c_{12}^\dagger - c_{12})|1_{12}1_{34}\rangle = -ic_{34}c_{12}|1_{12}1_{34}\rangle = -i|0_{12}0_{34}\rangle$$

In the odd subspace, the two equivalent expressions for this operator are $i\,\gamma_2\,\gamma_4$ and $i\,\gamma_1\,\gamma_3$.

In summary, we have found that for the even subspace, we have

$$\boxed{\sigma_z \equiv i\,\gamma_2\,\gamma_1 \equiv i\,\gamma_4\,\gamma_3, \quad \sigma_x \equiv i\,\gamma_4\,\gamma_1 \equiv i\,\gamma_3\,\gamma_2, \quad \sigma_y \equiv i\,\gamma_4\,\gamma_2 \equiv i\,\gamma_1\,\gamma_3} \tag{1.10}$$

while for the odd subspace, we have

$$\boxed{\sigma_z \equiv i\,\gamma_2\,\gamma_1 \equiv i\,\gamma_3\,\gamma_4, \quad \sigma_x \equiv i\,\gamma_1\,\gamma_4 \equiv i\,\gamma_3\,\gamma_2, \quad \sigma_y \equiv i\,\gamma_2\,\gamma_4 \equiv i\,\gamma_1\,\gamma_3} \tag{1.11}$$

1.2.1 Basis transformations

In order to be able to transform between the different bases, we proceed to find expressions for states in the bases $\{c_{13}, c_{24}\}$, $\{c_{14}, c_{23}\}$ as linear combinations of states in the basis $\{c_{12}, c_{34}\}$. As the total fermion parity is independent of the basis choice, we have that an even parity state in one basis must be a linear combination of even parity states of the other bases.

We identified $\sigma_y \equiv i\,\gamma_1\,\gamma_3$, because $i\,\gamma_1\,\gamma_3\,|0_{12}0_{34}\rangle = i|1_{12}1_{34}\rangle$. Due to parity conservation $|0_{12}0_{34}\rangle = \alpha|0_{13}0_{24}\rangle + \beta|1_{13}1_{24}\rangle$. We see that the operator $c_{13}^\dagger c_{13}$ projects $|0_{12}0_{34}\rangle$ onto $\beta|1_{13}1_{24}\rangle$, as

$$c_{13}^\dagger c_{13}|0_{12}0_{34}\rangle = c_{13}^\dagger c_{13}(\alpha|0_{13}0_{24}\rangle + \beta|1_{13}1_{24}\rangle) = 0 + \beta|1_{13}1_{24}\rangle$$

We rewrite the parity operator in terms of Fermion operators. In accordance with 1.9, we see that

$$2c_{13}^\dagger c_{13} - 1 = \frac{1}{2}(\gamma_1 - i\,\gamma_3)(\gamma_1 + i\,\gamma_3) - 1 = i\,\gamma_1\,\gamma_3$$

Inserting this in the equality $i\,\gamma_1\,\gamma_3\,|0_{12}0_{34}\rangle = i|1_{12}1_{34}\rangle$, we find

$$\begin{aligned}
(2c_{13}^\dagger c_{13} - 1)|0_{12}0_{34}\rangle &= i|1_{12}1_{34}\rangle \\
2c_{13}^\dagger c_{13}|0_{12}0_{34}\rangle &= |0_{12}0_{34}\rangle + i|1_{12}1_{34}\rangle \\
2c_{13}^\dagger c_{13}(\alpha|0_{13}0_{24}\rangle + \beta|1_{13}1_{24}\rangle) &= |0_{12}0_{34}\rangle + i|1_{12}1_{34}\rangle \\
2\beta|1_{13}1_{24}\rangle &= |0_{12}0_{34}\rangle + i|1_{12}1_{34}\rangle
\end{aligned}$$

$$\begin{aligned}
(2c_{13}^\dagger c_{13} - 1)|1_{12}1_{34}\rangle &= -i|0_{12}0_{34}\rangle \\
(-2c_{13}c_{13}^\dagger + 1)|1_{12}1_{34}\rangle &= -i|0_{12}0_{34}\rangle \\
-2c_{13}c_{13}^\dagger(\alpha'|0_{13}0_{24}\rangle + \beta'|1_{13}1_{24}\rangle) &= -i|0_{12}0_{34}\rangle - |1_{12}1_{34}\rangle \\
2\alpha'|0_{13}0_{24}\rangle &= i|0_{12}0_{34}\rangle + |1_{12}1_{34}\rangle
\end{aligned}$$

If we normalize these states, we see that the matrix connecting the states in the number basis of (c_{12}, c_{34}) and (c_{13}, c_{24}) must be

$$\mathbf{U}_{12\to13} = \sqrt{\frac{1}{2}}\begin{pmatrix} i & 1 \\ 1 & i \end{pmatrix}$$

We repeat this for the equality $i\,\gamma_4\,\gamma_1\,|0_{12}0_{34}\rangle = |1_{12}1_{34}\rangle$:

$$\begin{aligned} -(2c_{14}^\dagger c_{14} - 1)|0_{12}0_{34}\rangle &= |1_{12}1_{34}\rangle \\ -2c_{14}^\dagger c_{14}|0_{12}0_{34}\rangle &= -|0_{12}0_{34}\rangle + |1_{12}1_{34}\rangle \\ -2c_{14}^\dagger c_{14}(\delta|0_{14}0_{23}\rangle + \epsilon|1_{14}1_{23}\rangle) &= -|0_{12}0_{34}\rangle + |1_{12}1_{34}\rangle \\ -2\epsilon|1_{14}1_{23}\rangle &= -|0_{12}0_{34}\rangle + |1_{12}1_{34}\rangle \end{aligned}$$

$$\begin{aligned} -(2c_{14}^\dagger c_{14} - 1)|1_{12}1_{34}\rangle &= |0_{12}0_{34}\rangle \\ 2c_{14}c_{14}^\dagger - 1|1_{12}1_{34}\rangle &= |0_{12}0_{34}\rangle \\ 2c_{14}c_{14}^\dagger|1_{12}1_{34}\rangle &= |0_{12}0_{34}\rangle + |1_{12}1_{34}\rangle \\ 2c_{14}c_{14}^\dagger(\delta'|0_{14}0_{23}\rangle + \epsilon'|1_{14}1_{23}\rangle) &= |0_{12}0_{34}\rangle + |1_{12}1_{34}\rangle \\ 2\delta'|0_{14}0_{23}\rangle &= |0_{12}0_{34}\rangle + |1_{12}1_{34}\rangle \end{aligned}$$

Taking the phase factors δ' and ϵ to be positive, we see that the matrix connecting the states in the number basis of (c_{12}, c_{34}) and (c_{14}, c_{23}) must be

$$\mathbf{U}_{12\to14} = \sqrt{\frac{1}{2}}\begin{pmatrix} 1 & 1 \\ 1 & -1 \end{pmatrix}$$

The matrix connecting the states in the number basis of (c_{14}, c_{23}) and (c_{13}, c_{24}) can then be found as

$$\mathbf{U}_{13\to14} = \mathbf{U}_{13\to12}\mathbf{U}_{12\to14} = \mathbf{U}_{12\to13}^\dagger\mathbf{U}_{12\to14} = \frac{1}{2}\begin{pmatrix} 1-i & -1-i \\ 1-i & 1+i \end{pmatrix}$$

$$i\,\gamma_i\,\gamma_j = \mathbf{U}_{kl\to ij}\,i\,\gamma_k\,\gamma_l\,\mathbf{U}_{kl\to ij}^\dagger \tag{1.12}$$

We can visualize these unitary operators as rotations on the Bloch sphere. We label a rotation operator which rotates a state on the Bloch sphere by ϕ radians about a unit axis $\mathbf{n}$ as $\mathbf{R}(\mathbf{n}, \phi, \theta)$.

$$\mathbf{R}(\mathbf{n},\phi,\theta) = \exp(i\theta)\exp\left(\frac{-i\boldsymbol{\sigma}\cdot\mathbf{n}\phi}{2}\right) = e^{i\theta}\left[\boldsymbol{\sigma}_0\cos\left(\frac{\phi}{2}\right) - i\boldsymbol{\sigma}\cdot\mathbf{n}\sin\left(\frac{\phi}{2}\right)\right] \tag{1.13}$$

We define the three axes

$$\mathbf{n}_{12\to13} = (1,0,0), \quad \mathbf{n}_{12\to14} = \sqrt{\frac{1}{2}}(1,0,1), \quad \mathbf{n}_{13\to14} = \sqrt{\frac{1}{3}}(1,1,1),$$

which allows us to write

$$\begin{aligned}
\mathbf{U}_{12\to13} &= \mathbf{R}(\mathbf{n}_{12\to13},\pi/2,\pi/2) = i\,\sigma_0 + \sigma_x \\
\mathbf{U}_{12\to14} &= \mathbf{R}(\mathbf{n}_{12\to14},\pi,-\pi/2) = \sqrt{\frac{1}{2}}(\sigma_x+\sigma_z) \\
\mathbf{U}_{13\to14} &= \mathbf{R}(\mathbf{n}_{13\to14},2\pi/3,0) = \frac{1}{2}(\sigma_0 - i(\sigma_x+\sigma_y+\sigma_z)).
\end{aligned}$$

In the even sector, these unitary transformation operators can be written in terms of Majorana operators by substituting the Pauli operators by parity operators according to 1.10. As an example, we consider the transformation

$$\begin{aligned}
\mathbf{U}_{12\to14} i\,\gamma_3\,\gamma_2\,\mathbf{U}_{12\to14} &= \frac{1}{2}(i\,\gamma_4\,\gamma_1 + i\,\gamma_4\,\gamma_3) i\,\gamma_3\,\gamma_2 (i\,\gamma_4\,\gamma_1 + i\,\gamma_4\,\gamma_3) \\
&= \frac{1}{2}(i\,\gamma_3\,\gamma_2 - 2i\,\gamma_1\,\gamma_2 - i\,\gamma_3\,\gamma_2) = i\,\gamma_2\,\gamma_1
\end{aligned}$$

which clearly rotates the parity operator in the number basis of (c_{14}, c_{23}) into that in the number basis of (c_{12}, c_{34}).

Phase freedom

It is important to note that these basis transformation matrices are only defined up to some phase factors. To see this, consider two vectors containing the states of a two-level system in different bases. Some transformation matrix connects the two bases. Consider as an example the expression of spin states along some direction α expressed in terms of spin states along the some direction β:

$$\begin{pmatrix} |0^\alpha\rangle \\ |1^\alpha\rangle \end{pmatrix} = \mathbf{U}_{\beta\leftarrow\alpha} \begin{pmatrix} |0^\beta\rangle \\ |1^\beta\rangle \end{pmatrix}$$

We can attach a global phase to each state, on both sides of the equation, and for these two-component vectors this corresponds to multiplication by the following unitary matrices.

$$e^{i\alpha_1}\begin{pmatrix}1 & 0\\ 0 & e^{i\alpha_2}\end{pmatrix}\begin{pmatrix}|0^\alpha\rangle\\ |1^\alpha\rangle\end{pmatrix} = \mathbf{U}_{\beta\leftarrow\alpha}e^{i\beta_1}\begin{pmatrix}1 & 0\\ 0 & e^{i\beta_2}\end{pmatrix}\begin{pmatrix}|0^\beta\rangle\\ |1^\beta\rangle\end{pmatrix}$$

If we now shift this phase freedom into the transformation operator, it takes the general form (here we take $\mathbf{U}_{\beta\leftarrow\alpha} = \begin{pmatrix}a & b\\ c & d\end{pmatrix}$):

$$\mathbf{U}'_{\beta\leftarrow\alpha} = e^{-i\alpha_1}\begin{pmatrix}1 & 0\\ 0 & e^{-i\alpha_2}\end{pmatrix}\begin{pmatrix}a & b\\ c & d\end{pmatrix}e^{i\beta_1}\begin{pmatrix}1 & 0\\ 0 & e^{i\beta_2}\end{pmatrix} = e^{i(\beta_1-\alpha_1)}\begin{pmatrix}a & be^{i\beta_2}\\ ce^{-i\alpha_2} & de^{i(\beta_2-\alpha_2)}\end{pmatrix}$$

The set of transformation operators $\{\mathbf{U}_{\gamma\leftarrow\beta}, \mathbf{U}_{\alpha\leftarrow\beta}, \mathbf{U}_{\gamma\leftarrow\alpha}\}$ is defined only up to the set of these phase parameters.

If we interpret the Majorana Fermions as Ising anyons, as presented in for example [31], these basis transformations are related to the fusion matrix for the Ising anyons. Up to an exchange of the basis vectors, the fusion matrix is equivalent to $\mathbf{U}_{12\to14}$. If we interpret the Majorana modes thus, it is customary to take $\alpha_1 = \beta_1 = 0$ and $\alpha_2 = \beta_2$ to get consistency in the fusion equations.

1.3 Braiding

Let us again consider four Majorana modes, defined by

$$c_{12} = \frac{\gamma_1 + i\,\gamma_2}{2}, \qquad c_{34} = \frac{\gamma_3 + i\,\gamma_4}{2}.$$

We wish to exchange two Majorana modes γ_i and γ_j. If we exchange two Majorana particles adiabatically, the state of the system, $|\psi\rangle$, changes accordingly. The change is described by a unitary evolution operator U so that $|\psi\rangle \to U|\psi\rangle$. For the general case, we do not know the details of the Hamiltonian which governs the time evolution of the system, but by other considerations we can elucidate the form of U. [7, 41]

The transformation cannot change the total fermion parity, and for this reason, it must commute with the total fermion parity operator. We also assume that the transformation operator does not depend on the Majorana operators for modes other than those that are exchanged. As it must commute with the total fermion parity, it must contain the product of the operators for the exchanged modes. The parity operator $i\gamma_i\gamma_j$ is Hermitian, and thus an operator $\exp(i(i\gamma_i\gamma_j))$ would be unitary. The most general form U can take, up to a phase, is then $U = \exp(\alpha\gamma_i\gamma_j)$. Keeping in mind that $(\gamma_i\gamma_j)^2 = -1$ we can rewrite this as

$$\begin{aligned} U = \exp(\alpha\gamma_i\gamma_j) &= \sum_n^\infty \frac{1}{n!}\alpha^n(\gamma_i\gamma_j)^n \\ &= \sum_n^\infty \frac{1}{(2n)!}\alpha^{2n}\left[(\gamma_i\gamma_j)^2\right]^n + \sum_n^\infty \frac{1}{(2n+1)!}\alpha^{2n+1}\left[(\gamma_i\gamma_j)^2\right]^n(\gamma_i\gamma_j) \\ &= \sum_n^\infty \frac{1}{(2n)!}\alpha^{2n}(-1)^n + \sum_n^\infty \frac{1}{(2n+1)!}\alpha^{2n+1}(-1)^n(\gamma_i\gamma_j) \\ &= \cos(\alpha) + \gamma_i\gamma_j\sin(\alpha) \end{aligned}$$

In the Heisenberg picture, the time dependent operators are given by

$$\begin{aligned} \gamma_i \to U\gamma_i U^\dagger &= (\cos(\alpha) + \gamma_i\gamma_j\sin(\alpha))\gamma_i(\cos(\alpha)\gamma_i\gamma_j\sin(\alpha)) \\ &= \gamma_i\cos^2(\alpha) - \gamma_i\sin^2(\alpha) - 2\gamma_j\sin(\alpha)\cos(\alpha) \\ &= \gamma_i\cos(2\alpha) - \gamma_j\sin(2\alpha) \\ \gamma_j \to U\gamma_j U^\dagger &= \gamma_j\cos(2\alpha) + \gamma_i\sin(2\alpha) \end{aligned}$$

When a time T has passed, so that γ_i and γ_j have been interchanged, we see that α must take the value $\pm\pi/4$ for the evolution to be correct. If we pick the positive value, we have the exchange

$$\begin{aligned} \gamma_i &\to -\gamma_j \\ \gamma_j &\to \gamma_i\,. \end{aligned}$$

For a complete exchange the time evolution operator then takes the form

$$U_{ij} = \exp(\pm\frac{\pi}{4}\,\gamma_i\,\gamma_j) = 1 \pm \gamma_i\,\gamma_j$$

By the association rules (eq. 1.10) between parity operators and Pauli operators in the even parity subspace, we can write the braiding operators as

$$\begin{aligned} U_{12} &= \exp\left(\mp i\frac{\pi}{4}\,\sigma_z\right) \\ U_{13} &= \exp\left(\mp i\frac{\pi}{4}\,\sigma_y\right) \\ U_{23} &= \exp\left(\mp i\frac{\pi}{4}\,\sigma_x\right). \end{aligned}$$

Where the sign depends on the 'chirality' of the exchange, a concept we return to in more detail later. Expressing the operators in this form facilitates visualization of how the braiding operations rotate the states on the Bloch sphere.

We can also write the evolution operator in the basis $\{|0_{12}0_{34}\rangle, |1_{12}1_{34}\rangle, |0_{12}1_{34}\rangle, |1_{12}0_{34}\rangle\}$. This allows to collect information about the even and odd subspaces in one matrix. In this basis, all the evolution operators will be block diagonal, as they do not mix the even and odd parity sectors. The evolution operator associated with the braiding of γ_1 and γ_2 consists of two blocks. For this pair of Majorana modes, the blocks are identical, as the operator $i\,\gamma_2\,\gamma_1$ is associated with σ_z both for the even and odd subspaces.

$$U_{12} = \begin{pmatrix} e^{-i\pi/4} & 0 & 0 & 0 \\ 0 & e^{i\pi/4} & 0 & 0 \\ 0 & 0 & e^{-i\pi/4} & 0 \\ 0 & 0 & 0 & e^{i\pi/4} \end{pmatrix}.$$

Consider then the evolution operator for the exchange of γ_2 and γ_3. For the even subspace, we associated $\sigma_x \equiv i\,\gamma_3\,\gamma_2$. The block for the even subspace therefore takes the form $\exp(-\pi\,\gamma_3\,\gamma_2\,/4) = \exp(i\pi\,\sigma_x\,/4)$. The association for the odd subspace is the same, and the braiding operator takes the form :

$$U_{23} = \sqrt{\frac{1}{2}} \begin{pmatrix} 1 & 1 & 0 & 0 \\ -1 & 1 & 0 & 0 \\ 0 & 0 & 1 & 1 \\ 0 & 0 & -1 & 1 \end{pmatrix}.$$

The last evolution operator exchanges γ_3 and γ_4. The even subspace block takes the form $\exp(-i\pi\,\sigma_z\,/4)$, while the odd subspace block is $\exp(i\pi\,\sigma_z\,/4)$:

$$U_{34} = \begin{pmatrix} e^{-i\pi/4} & 0 & 0 & 0 \\ 0 & e^{i\pi/4} & 0 & 0 \\ 0 & 0 & e^{i\pi/4} & 0 \\ 0 & 0 & 0 & e^{-i\pi/4} \end{pmatrix}.$$

From these three matrices, all exchange operations can be composed.

Chapter 2

The toric and planar code models

2.1 The toric code model

With his celebrated connection of quantum error correction codes to a physical many-body system, Kitaev [32] opened the field of topological quantum computation. His toric code is defined on a square lattice wrapped on a torus. We will now consider some important aspects of this model.

Consider a square lattice, with qubits (some two-level system, which for concreteness can be thought of as a spin-half particle) on the links of the lattice. Hereafter we refer to these two-level systems simply as spins. The Hamiltonian of the system, in Kitaev's original description, is given by

$$H = -\sum_{v} A(v) - \sum_{p} B(p). \tag{2.1}$$

The four-body vertex interaction term is given by $A(v) = \sigma^x_{v,1}\,\sigma^x_{v,2}\,\sigma^x_{v,3}\,\sigma^x_{v,4}$, where the Pauli operators refer to the four spins surrounding a vertex v. The four-body plaquette interaction term is given by $B(p) = \sigma^z_{p,1}\,\sigma^z_{p,2}\,\sigma^z_{p,3}\,\sigma^z_{p,4}$, where the Pauli operators refer to the four spins surrounding a plaquette p. Such plaquette and vertex terms are shown in 2.1.

As two neighbouring vertex and plaquette operators share an even number (two) of anticommuting operators, they commute. All vertex and plaquette operators therefore commute. Symbolically, we write $[A_i, A_j] = [B_i, B_j] = [A_i, B_j] = 0$. The terms commute with the Hamiltonian. Due to this, they can be replaced by their eigenvalues. The ground state of the model is characterized by the condition that the vertex and plaquette operators all have eigenvalue 1, as this minimizes the energy. We will now find the ground state of the model, before we consider the more symmetric reformulation of the model, due to Wen. [42]

If we work in the z-basis, the requirement on the plaquette operators is satisfied if an even number of spins surrounding a plaquette are aligned in the z-direction. Imagine the case where all spins are aligned with the negative z-direction. $B(p)$ would then be 1 for all plaquettes. Consider then having two or four spins surrounding a plaquette

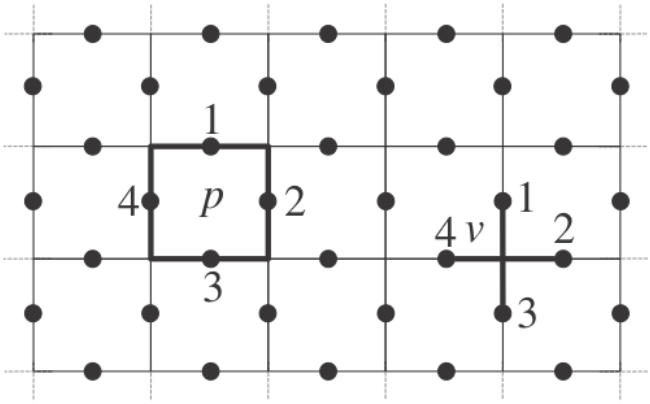

Figure 2.1: Lattice with spin-1/2 degrees of freedom on the links. The vertex and plaquette operators of the Hamiltonian are indicated by thick lines and labels v and p, respectively.

aligned in the positive z-direction. For all plaquette operators to now have the value 1, the neighbouring plaquettes must also have an even number of spins aligned in the positive z-direction. It is evident that the spins aligned in the positive z-direction must form closed loops in the background of spins in the negative z-direction.

A vertex operator, $A(v)$, will flip all the spins surrounding the vertex it is applied to. The new state satisfies the condition $B(p) = 1$, but it is a different state from the one prior to the application of the vertex operator. Applying vertex operators on vertices close to one another can create loops of spins oriented oppositely to the background.

The ground state of the surface code is a linear combination of such loops, oriented oppositely to the background. These closed loops are equally weighted in the superposition. This state will have the eigenvalue 1 for all plaquette operators, and the application of a vertex operator will transform a loop state $|l\rangle$ into a loop state $|l'\rangle$ while conversely, the state $|l'\rangle$ is transformed into $|l\rangle$. As both loops are included in the ground state, the ground state is also an eigenstate of the vertex operators.

To create this superposition of different loop states, we use that a loop may be constructed by using different vertex operators. To see this more clearly, consider two neighbouring vertices. In a background of spins aligned in the negative z-direction, a vertex operator would create a small loop of four spins in the positive z-direction. Applying the neighbouring vertex operator would extend the loop, and by application of a series of vertex operators, arbitrarily shaped loops could be created. We note that these loops would be contractible. The opposite would be non-contractible loops, by which we mean loops that encircle the torus in either the poloidal or toroidal direction, and cannot be constructed, only deformed, by application of vertex operators. With this in mind, we see that the ground state for the toric code model can be written as

$$|\psi\rangle = \prod_p \sqrt{\frac{1}{2}}(\mathbb{I} + B(p))|\alpha\rangle,$$

where the state $|\alpha\rangle$ is the state with all spins aligned with the negative z-direction. Wen's reformulation of the model brings the Hamiltonian to a more symmetric form:

$$H = -\sum_{\mathbf{r}} A_{\mathbf{r}}, \quad A_{\mathbf{r}} \equiv \sigma^x_{\mathbf{r}}\sigma^z_{\mathbf{r}+\mathbf{i}}\sigma^x_{\mathbf{r}+\mathbf{i}+\mathbf{j}}\sigma^z_{\mathbf{r}-\mathbf{j}}$$

with $\mathbf{i} = (1, 0)$ and $\mathbf{j} = (0, 1)$. One such plaquette operator is shown in figure 2.2. To go from Kitaev's original formulation to the form above, we rotate the lattice by $\pi/4$ rad, and perform basis rotations along every other lattice diagonal. Specifically, the unitary mapping $\mathbf{U} = \sqrt{\frac{1}{2}}\begin{pmatrix} 1 & 1 \\ 1 & -1 \end{pmatrix}$ is applied to all vertices along the horizontal links in Kitaev's model. In order to treat the Wen model efficiently, we let $\mathbf{k} = (i, j)$ index the spins on the vertices of the lattice. A plaquette operator $A_{\mathbf{k}}$ squares to one, and has eigenvalues ± 1. These eigenvalues can be written $e^{in\pi}$ where n takes one of the two values $\{0, 1\}$. If the plaquette is not excited, $n = 0$, while if it is excited, $n = 1$. The ground state must be characterized by $A_{\mathbf{k}} = 1$ for all plaquettes, as in Kitaev's formulation. In the Kitaev formulation, we distinguished between two operator types, namely plaquettes and vertices. In the Wen model, the operator for each plaquette takes the same form. To keep the distinction, which will become important when we discuss excitations, we employ the terms even and odd plaquettes. We assign different colours to the two kinds of plaquettes, as shown in figure 2.2. The assignment of colours to the plaquettes is arbitrary, and the colours could be inverted without any change to the model.

For Wen's reformulation, it remains true that two neighbouring plaquette operators share an even number (two) of anticommuting operators. Thus they commute. All plaquette operators therefore commute, and they commute with the Hamiltonian. With this in mind, we map the ground state of the Kitaev formulation into that of the Wen formulation:

$$|\psi\rangle = \prod_{k \in \text{even plaquettes}} \sqrt{\frac{1}{2}}(\mathbb{I} + A_k)|\alpha\rangle$$

where the state $|\alpha\rangle$ is the configuration in which all spins are aligned with the direction of the spin operators of the odd plaquettes.

2.1.1 Excitations of the toric code

We will now discuss excitations of the toric code, and start from the framework of Kitaev's formulation. Quasiparticle excitations of the toric code can be created by the

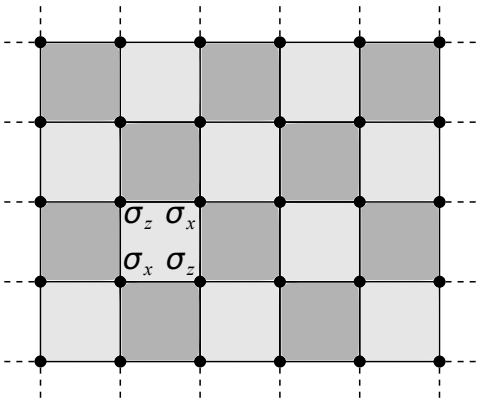

Figure 2.2: Lattice, rotated $\pi/4$ rad relative to Kitaev's original lattice. Spin-1/2 degrees of freedom live on the vertices of the lattice. A plaquette operator in the Wen formulation of the toric code is indicated.

application of a single spin operator on a site. By applying σ^z to a lattice site, the neighbouring vertex operators will have their eigenvalues changed. This is because the vertex operators are products of σ^x-operators, which anticommute with σ^z-operators. Similarly, the application of σ^x flips the eigenvalue of the neighbouring plaquette operators. We distinguish three different quasiparticle excitations: those connected with flipped vertex operators we label e-anyons; those connected with flipped plaquette operators we label m-anyons; those resulting from applying both $\sigma^z$and σ^x, i.e.the combination of an e- and an m-anyon, we label ϵ-anyons. An operator with eigenvalue -1 hosts a quasiparticle excitation.

The quasiparticle excitations are called e- and m-particles in analogy with the anyon models studied by Wilczek, which contained integer electric charges and magnetic flux-carrying vortices. [43, 44] Because of their mutual exchange statistics e- and m-particles are anyons. [7]

In the Wen formulation, an excitation results from a spin operator which flips the state of two diagonally neighbouring plaquettes. If the single spin operator applied is σ^z, it will flip the top right and bottom left plaquettes in the set of four plaquettes surrounding the site, as these have a σ^x operator on the central site. Similarly, if the operator applied is σ^x, the top left and bottom right plaquettes are flipped. In this model, too, a plaquette hosting a quasiparticle excitation will have eigenvalue -1. However, we no longer have vertex- and plaquette-operators, and so we must distinguish between two kinds of plaquettes in this model: those that host e-particles, and those that host m-particles. This distinction correpsponds to the distinction made above between even and odd plaquettes.

An interesting question is: what happens if we apply a string of Pauli operators. We recall that the ground state of the toric code is an equally weighted superposition of closed loops of spins oriented oppositely to the background spins. Closed loops do not represent excitations, then, as they leave no operator with an eigenvalue of -1. A string

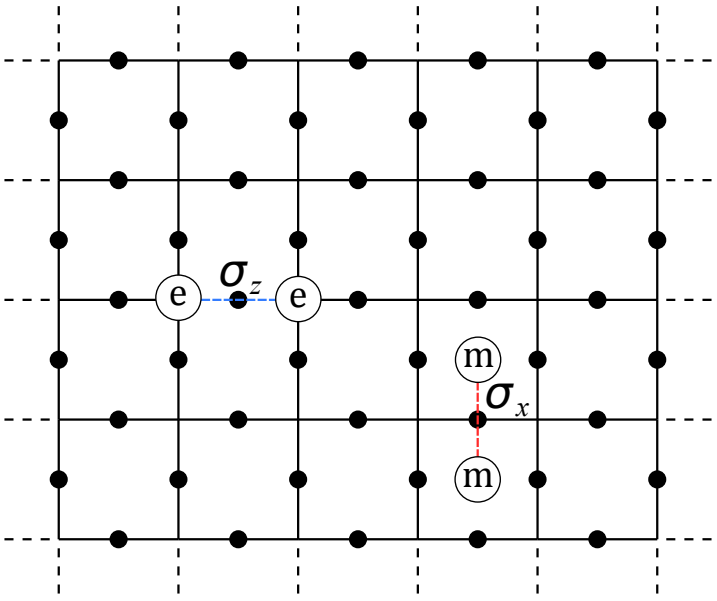

Figure 2.3: Application of σ_z- and σ_x-operators create pairs of e- and m-type particles, respectively, as excitations of the neighbouring vertices and plaquettes.

which is not a closed loop, however, behaves differently. In the Kitaev formulation, a string of σ_x-operators have no effect on the vertex operators. For concreteness, we consider a short string $S = \sigma_x^2 \, \sigma_x^1$ acting on the numbered spins in figure 2.4. The action of σ_x^1 is to flip the eigenvalue of the neighbouring plaquettes. σ_x^2 also flips the eigenvalue of the neighbouring plaquette operators, and that means that the plaquette between spins 1 and 2 has been flipped twice, and its eigenvalue is 1. The plaquette above spin number 2 now has eigenvalue -1, and hosts the excitation. It is evident that application of σ_x (σ_z) on a spin in a plaquette (vertex) with eigenvalue -1 shifts the excitation to the neighbouring plaquette (vertex). The way string operators translate quasiparticle excitations is shown in the transition from 2.4a to 2.4b.

It is important to note that string operators of the m-kind (e-kind) are deformed when multiplied by plaquettes (vertices). If the plaquettes (vertices) do not host excitations, their eigenvalue is one, and multiplying a string by such an operator amounts to applying the identity. This is shown in figure 2.5, where a string of σ_z-operators has excitations of the e-kind at its endpoints. The string can be changed by multiplication by the marked plaquette operator, which takes the value 1. The σ_z-operator shared by the string and the plaquette squares to unity, while the rest of the operators constituting the plaquette become part of a deformed string. As we can deform the string without otherwise changing the system, it is clear that the shape of such strings has no physical meaning in this model, but the locations of its endpoints, which are the plaquettes or vertices hosting excitations, do.

As a final example of some of the properties of string operators in this model, we again consider strings of σ_z-operators, which have excitations of the e-kind at their

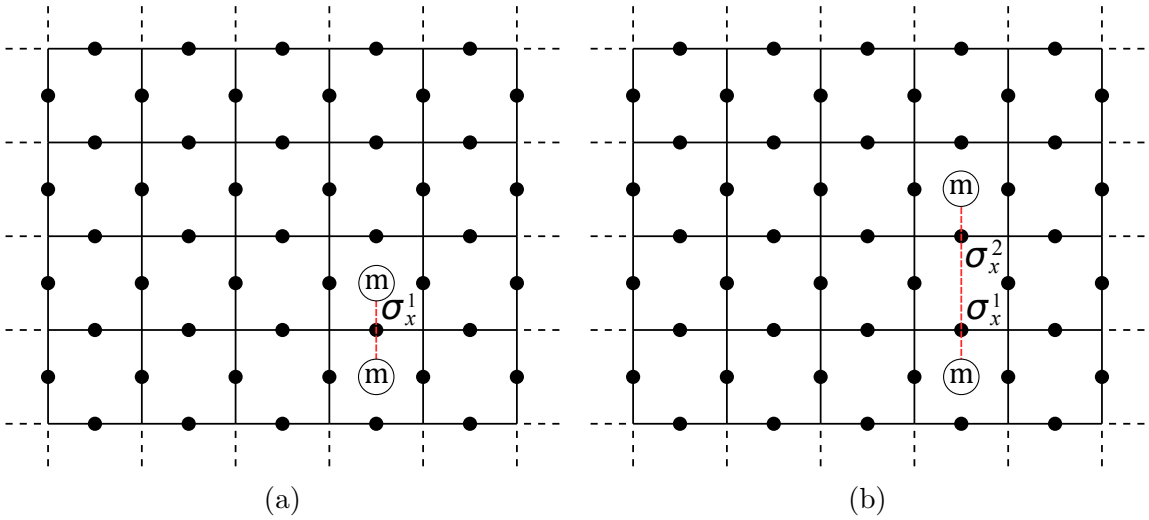

Figure 2.4: In (a), a single σ_x-operator creates two excitations on neighbouring plaquettes. In (b), two σ_x-operators create four m-particles. Two of these are located on the same plaquette, and they annihilate one another, effectively giving an extended σ_x-string with m-anyons at the endpoints.

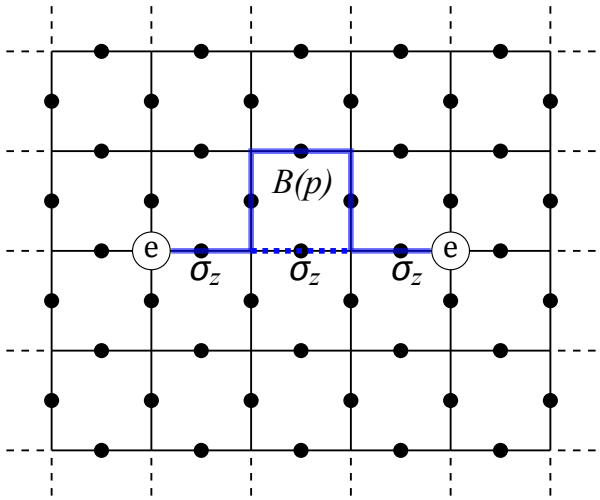

Figure 2.5: A string of three σ_z-operators is deformed through multiplication with one of the plaquettes.

endpoints. These are marked blue in figure 2.6. We label the topmost one $S_{z,t}$, and the bottommost one $S_{z,b}$. We can make a closed loop of σ_x-operators. This σ_x-loop is marked red in figure 2.6. We label it L_x. The eigenvalue of this loop will tell us whether an odd number of the vertices encircled by the loop hosts an e-type excitation. There are two ways to see this. The L_x is the product of the four vertices it encircles. If one of these hosts an excitation, its eigenvalue would be -1, and accordingly, the eigenvalue

of L_x would be -1. Alternatively, we can consider the commutation relations between the excitation strings and L_x. $S_{z,b}$ shares two anticommuting operators with L_x and hence the two operators commute. $S_{z,t}$ shares only one anticommuting operator with L_x, which means that the $S_{z,t}$ and L_x anticommute.

For the ground state, $|\psi\rangle$, we have that $L_x|\psi\rangle = |\psi\rangle$. If we apply L_x to the two excited states $S_{z,b}|\psi\rangle$ and $S_{z,t}|\psi\rangle$, we get $L_x S_{z,b}|\psi\rangle = S_{z,b}L_x|\psi\rangle = S_{z,b}|\psi\rangle$ and $L_x S_{z,t}|\psi\rangle = -S_{z,t}L_x|\psi\rangle = -S_{z,t}|\psi\rangle$. This shows that the loop operator can be used to detect an e-type excitation. One could argue similarly for a loop of σ_z-operators and m-type excitations.

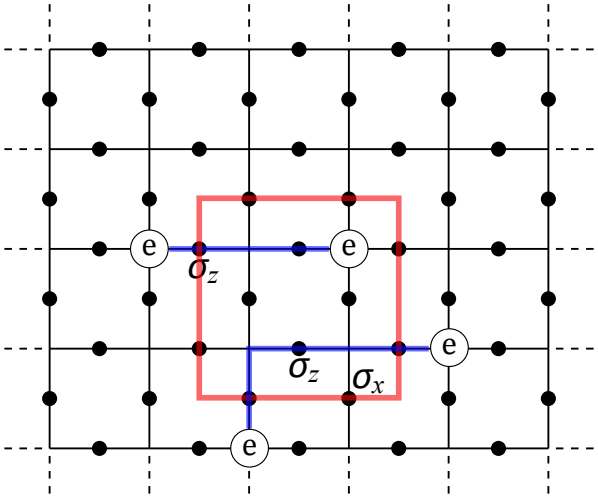

Figure 2.6: A loop of σ_x-operators (in red) intersects strings of σ_z-operators (in blue). The loop operator can detect whether it encloses an even or odd number of e-particles.

2.1.2 Ground state degeneracy

Degeneracy from a counting argument

Let us consider a lattice of dimensions $N \times N$ wrapped on a torus. The ground state contains no quasiparticle excitations, and is defined by

$$A(v)|\psi\rangle = |\psi\rangle, \quad B(p)|\psi\rangle = |\psi\rangle,$$

for all vertices and plaquettes. There are $2N^2$ spins on the lattice, and $2N^2$ of the conditions above. N^2 for the set of plaquettes, and N^2 for the set of vertices. For the ground state it must hold that

$$\prod_v A(v) = 1, \quad \prod_p B(p) = 1.$$

This implies that there is one plaquette eigenvalue which is not independent from the rest of those in the set. The same is true for the set of vertices. The number of constraints on the plaquette operators is therefore $N^2 - 1$. The same is true for the number of constraints on the vertex operators. We can then find the degeneracy as

$$\frac{2^N}{2^{2(N-1)}} = 4.$$

Degeneracy from an argument using string operators

If we again consider a lattice of dimensions $N \times N$ wrapped on a torus, we will look at the degeneracy of the model by use of string operators. We can find four operators, which commute with the Hamiltonian, and which cannot be constructed as products of plaquette and vertex operators. These operators form incontractible loops on the torus. Two such operators encircle the torus in the toroidal direction, while the other two encircle it in the poloidal direction. We label the operators by either T or P for the toroidal and poloidal directions, with a subscript denoting whether the string is of the x- or z-kind. These operators are shown in figure 2.7. The figure illustrates a torus, where the sites along the bottom are the same sites as those along the top, indicated by circles which are not filled in. Similarly, the sites along the right edge are the same as those along the left. The operator P_z shares no sites, and hence no operators, with T_z. They therefore commute. P_z crosses T_x at one site. On this site, P_z has a σ_z-operator, while T_x has a σ_x-operator. P_z and T_x therefore anticommute. Summarizing such observations, we find the following relations for the four operators:

$$\begin{aligned} &[T_x, P_x] = [T_z, P_z] = [T_x, T_z] = [P_x, P_z] = 0 \\ &\{T_x, P_z\} = \{T_z, P_x\} = 0 \end{aligned}$$

The operators all square to unity and have eigenvalues ± 1. We take a state $|T_z = 1, P_z = 1\rangle$. We see how this state behaves when we apply the operators T_x, P_x and $T_x P_x$ to it:

$$\begin{aligned} &P_z|T_z = 1, P_z = 1\rangle = +|T_z = 1, P_z = 1\rangle \\ &P_z(T_x|T_z = 1, P_z = 1\rangle) = -T_x P_z|T_z = 1, P_z = 1\rangle \qquad = -(T_x|T_z = 1, P_z = 1\rangle) \\ &\qquad\qquad = P_z|T_z = 1, P_z = -1\rangle \end{aligned}$$

The effect of T_x is, as we see, to change the state into one with eigenvalue -1 under P_z. This state is still a ground state, as T_x commutes with the Hamiltonian, and thus cannot change the energy. Similarly, for P_x we have:

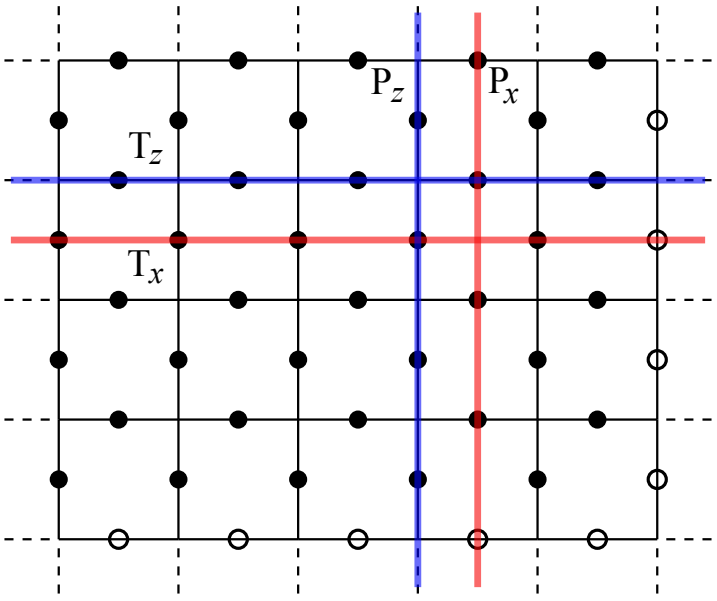

Figure 2.7: Strings of σ_x- and σ_z-operators which are symmetries of the system are shown in red and blue, respectively. The system is a torus, indicated by the hollow lattice sites along the right and bottom edges. From the commutation relations of these symmetries, we may find the degenerate ground states of the system.

$$
\begin{aligned}
&T_z|T_z = 1, P_z = 1\rangle = +|T_z = 1, P_z = 1\rangle \\
&T_z(P_x|T_z = 1, P_z = 1\rangle) = -P_xT_z|T_z = 1, P_z = 1\rangle \qquad = -(P_x|T_z = 1, P_z = 1\rangle) \\
&\qquad\qquad\qquad\qquad\qquad\qquad\qquad\qquad\qquad\qquad\qquad\quad = T_z|T_z = -1, P_z = 1\rangle
\end{aligned}
$$

Finally, we may combine P_x- and T_x-operators:

$$
\begin{aligned}
&P_z|T_z = 1, P_z = 1\rangle = +|T_z = 1, P_z = 1\rangle \\
&P_z(P_xT_x|T_z = 1, P_z = 1\rangle) = -(P_xT_x|T_z = 1, P_z = 1\rangle)
\end{aligned}
$$

$$
\begin{aligned}
&T_z|T_z = 1, P_z = 1\rangle = +|T_z = 1, P_z = 1\rangle \\
&T_z(P_xT_x|T_z = 1, P_z = 1\rangle) = -(P_xT_x|T_z = 1, P_z = 1\rangle)
\end{aligned}
$$

We conclude that

$$
\begin{aligned}
&P_x|T_z = 1, P_z = 1\rangle = |T_z = -1, P_z = 1\rangle, \\
&T_x|T_z = 1, P_z = 1\rangle = |T_z = 1, P_z = -1\rangle, \\
&P_xT_x|T_z = 1, P_z = 1\rangle = |T_z = -1, P_z = -1\rangle.
\end{aligned}
$$

These three states, in addition to the state $|T_z = 1, P_z = 1\rangle$ make up the set of four distinct ground states for the toric code model. As we have seen, they can be described by incontractible string operators.

2.1.3 The planar code

The planar code is the toric code without periodic boundary conditions. The absence of this periodicity affects the properties of the model. We begin by considering how the ground state degeneracy is different for this model. How we define the boundaries and whether we include modifications in the Hamiltonian to account for boundary effects determines the ground state degeneracy.

In the Kitaev formulation, it is useful to distinguish between two types of boundaries which can arise. The two different kinds of boundaries are shown in figure 2.8. The blue line connects two edges where there are incomplete plaquette operators. We call these edges rough edges, due to the way the lines of the lattice poke out along them. The red line connects two edges where there are incomplete vertex operators. These, we call smooth edges, due to the absence of lattice lines protruding from them. The Hamiltonian does also contain the incomplete plaquette and vertex operators. We want to construct a string operator connecting two edges, while being a symmetry of the system. In order to commute with the Hamiltonian, such a string must have σ^z-operators (σ^x-operators) on the lattice sites situated at rough (smooth) edges. For a string starting on a rough edge, this means that it will anticommute with the vertex operator containing the site on the edge, unless it shares two σ^z-operators with the vertex. If one extends this argument, it becomes clear that only a string of σ^z-operators which runs from one rough edge to the other is a symmetry string connecting those two edges. Similarly, we find that a string of σ^x operators connecting the smooth edges is also a symmetry. These two strings, respectively labelled H_z (blue) and V_x (red) are shown in figure 2.8.

H_z and V_x anticommute, and both commute with the Hamiltonian. This leads to a twofold topological degeneracy. The topological aspect of these states is that they are labelled by non-local, non-contractible symmetries. If the system had all smooth or all rough edges, there would be no such degeneracy. It is only present when the kind of edge alternates between rough and smooth.

A recent paper by Brown *et al* [45] introduced two-operator boundary terms for the planar code model. Such an approach provides an alternative view on the degeneracy of the planar code, as the system will have unpaired Majorana modes at its corners accounting for the ground state degeneracy.

2.2 Introduction of twist defects

A twist defect results from a dislocation of the lattice. The kind of dislocations we will consider is one that introduces pentagonal plaquettes in the system. Such a dislocation

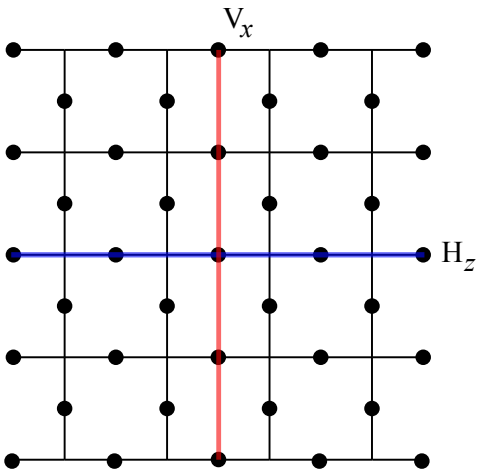

Figure 2.8: Strings of σ_x- and σ_z-operators which are symmetries of the system are shown in red and blue, respectively. From the commutation relations of these symmetries, we may find the degenerate ground states of the system.

is shown in figure 2.9a, where the lattice sites are numbered for later discussion. The lattice dislocations introduce lines that alter the type of anyonic excitations that cross it. This means that upon crossing a dislocation line, an e-type excitation would become an m-type excitation and *vice versa*. We see this effect in figure 2.9b as the result of a mismatch in the colouring of the plaquettes along the dislocation line, drawn in red. The twist defects make it impossible to define the checkerboard pattern consistently, and so, the dislocation lines can be drawn in various ways, depending on the colouring of the plaquettes. An alternative coulouring of the plaquettes, with associated dislocation lines, is shown in figure 2.13.

Twist is a term we use to describe the lattice sites from which dislocation lines originate. It is a topological defect, and a string symmetry operator (which commutes with the Hamiltonian) that encircles the twist once cannot close on itself, as it has gone from residing in dark plaquettes to residing in light ones. If a string operator encircles a twist twice, however, it can close on itself. The introduction of twist defects in the toric code introduces new kinds of plaquettes in the Hamiltonian. In addition to the regular plaquette terms, we have pentagonal plaquette terms and parallelogram plaquette terms. These terms enter in the Hamiltonian. The left and right pentagonal plaquettes, in terms of the numbering of the lattice sites shown in figure 2.9a take the forms

$$A_{\text{left}} = \sigma_1^z \, \sigma_2^x \, \sigma_8^z \, \sigma_9^y \, \sigma_{10}^x, \quad A_{\text{right}} = \sigma_3^z \, \sigma_4^y \, \sigma_5^x \, \sigma_6^z \, \sigma_7^x,$$

respectively. The pentagonal plaquettes are separated by parallelogram plaquettes. The further apart the pentagons are, the more parallelogram plaquettes will there be

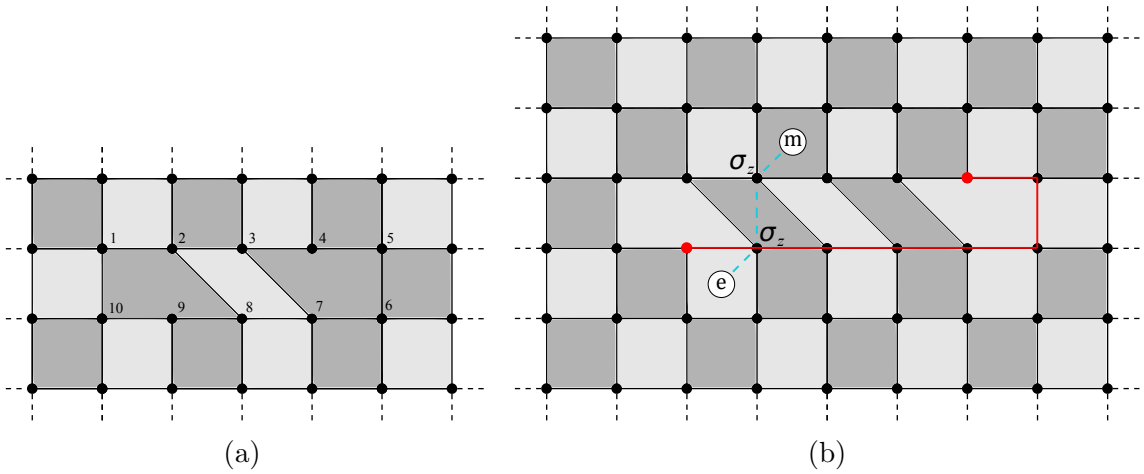

Figure 2.9: (a) shows a system with dislocations resulting in pentagonal plaquettes. When anyonic excitations are moved across the dislocation line drawn in red in (b), they change their type. This is shown for the string of σ_z-operators which move a particle across the line.

in the Hamiltonian. The paralellogram plaquette, in terms of the numbering in 2.9a, takes the form:

$$A_{\text{para}} = \sigma_2^z \, \sigma_3^x \, \sigma_7^z \, \sigma_8^x \, .$$

It might be useful to quickly connect these visual representations of operators with their written form as strings of Pauli operators. If a central vertex is connected to two neighbouring vertices, we can see what kind of operator we should associate with the central vertex via the schematic shown in figure 2.10. The four leftmost kind of vertices will have σ_z-operators associated with them, the two middle ones σ_x-operators and the rightmost pair σ_y-operators.

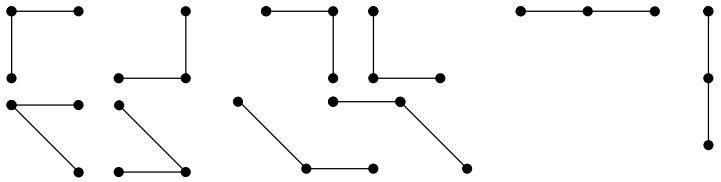

Figure 2.10: The different kinds of vertices that arise in a model with dislocations. The four vertices to the left correspond to σ_z-operators, the four in the middle to σ_x-operators and the two on the right to σ_y-operators.

This association produces the plaquettes of Wen's toric code reformulation, as well as the correct expressions for the pentagonal and parallelogram plaquettes. For the six schematics corresponding to σ_z- and σ_x-operators, we note that the angles between

the lines need not be perpendicular (but for the σ_y schematics they will be). In the simple geometric illustrations we employ, the angle spanned by the lines connected to the central vertex can also take the values $\pi/4$ rad and $3\pi/4$ rad, as shown for the σ_z and σ_x-operators. This is indeed the case for some of the vertices in the pentagonal plaquettes, and all of the vertices in the parallelogram plaquettes.

With the introduction of these new plaquettes in the Hamiltonian, all terms still mutually commute. With the square plaquettes with which they share two sites, the pentagonal plaquettes anticommute twice, resulting in overall commutation. The two pentagonal plaquettes commute with one another, as they have anticommuting operators on their two shared sites. Parallelogram plaquettes also mutually commute, as they have two anticommuting operators on shared sites. For the same reason they commute with pentagonal plaquettes, as well as with square plaquettes.

For the ground state, we require that all plaquettes, including the newly introduced ones, take the value 1.

If one pair of twist defects is introduced, the number of stabilizer terms in the Hamiltonian is reduced by 1, as we go from having three tetragonal plaquette terms to two pentagonal plaquette terms. As per a counting argument, as described in 2.1.2, a reduction in the number of constraints by 1 will double the degeneracy.

The degeneracy introduced in this way is between the two states which would have had opposite eigenvalues for the tetragonal plaquette which disappears when the dislocations are introduced. We term this central plaquette C. It is shown in figure 2.11, both in the presence and absence of twist defects.

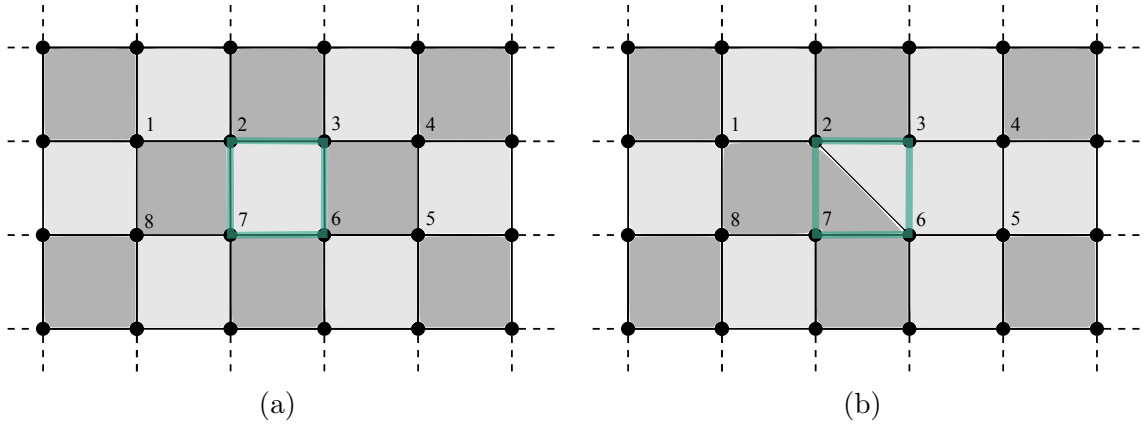

Figure 2.11: The central plaquette in the absence, (a), and presence, (b), of twist defects.

In terms of the numbering introduced in figure 2.11, it takes the form

$$C = \sigma_z^2 \, \sigma_x^3 \, \sigma_z^6 \, \sigma_x^7 \, .$$

This operator commute with both the pentagonal plaquettes, as well as with all square plaquettes. Thus it commutes with the Hamiltonian, and is a symmetry operator.

As it it is one of the regular plaquettes of the model without twist defects, it is a symmetry operator for the system both with (figure 2.11b), and without (figure 2.11a) twist defects.

The operator C has the eigenstates

$$|C = +1\rangle, \quad |C = -1\rangle.$$

For the ground states, we require that all plaquettes take the eigenvalue 1. This means that C multiplied by any other plaquette, for the ground state, results in an equivalent operator. If we take the two products CA_{left} and CA_{right}, we get

$$\begin{aligned} CA_{\text{left}} &= (\sigma_z^2\,\sigma_x^3\,\sigma_z^6\,\sigma_x^7)(\sigma_z^1\,\sigma_x^2\,\sigma_z^6\,\sigma_y^7\,\sigma_x^8) = \sigma_z^1(i\,\sigma_y^2)\,\sigma_x^3\,\sigma_0^6(i\,\sigma_z^7)\,\sigma_x^8 \\ &= -\,\sigma_z^1\,\sigma_y^2\,\sigma_x^3\,\sigma_z^7\,\sigma_x^8 \\ CA_{\text{right}} &= (\sigma_z^2\,\sigma_x^3\,\sigma_z^6\,\sigma_x^7)(\sigma_z^2\,\sigma_y^3\,\sigma_x^4\,\sigma_z^5\,\sigma_x^6) = \sigma_0^2(i\,\sigma_z^3)\,\sigma_x^4\,\sigma_z^5(i\,\sigma_y^6)\,\sigma_x^7 \\ &= -\,\sigma_z^3\,\sigma_x^4\,\sigma_z^5\,\sigma_y^6\,\sigma_x^7 \end{aligned}$$

We will return to these operator throughout this thesis. We assign labels to them as follows:

$$P_L = CA_{\text{left}} = -\,\sigma_z^1\,\sigma_y^2\,\sigma_x^3\,\sigma_z^7\,\sigma_x^8, \quad P_R = CA_{\text{right}} = -\,\sigma_z^3\,\sigma_x^4\,\sigma_z^5\,\sigma_y^6\,\sigma_x^7 \tag{2.2}$$

These operators are sketched in figure 2.12. The illustration does not show whether the operator on a site is of the x-, y- or z-kind, but shows the vertices included in each operator. These operators are string operators ending on the twist defects. We will use these operators to label the degenerate ground states. Their effect on the states is evident:

$$\begin{aligned} P_L|C = +1\rangle = P_R|C = +1\rangle &= +|C = +1\rangle, \\ P_L|C = -1\rangle = P_R|C = -1\rangle &= -|C = -1\rangle \end{aligned} \tag{2.3}$$

Consider an adiabatic transition from the system in figure 2.11a to the one in 2.11b. The system starts out in the lowest energy state, namely $|C = +1\rangle$. Once the system has become that of 2.11b, it is still in the state $|C = +1\rangle$. The crucial difference is that the state $|C = -1\rangle$ now has the same energy. This means that such an adiabatic transition creates a qubit, and initializes the system in a known qubit state. This initialization procedure is instrumental to any quantum computation, as explained by DiVincenzo in his collection of criteria for a functioning quantum computer [46]. An essential part of the physical realization of the planar code will turn out to be this initialization step.

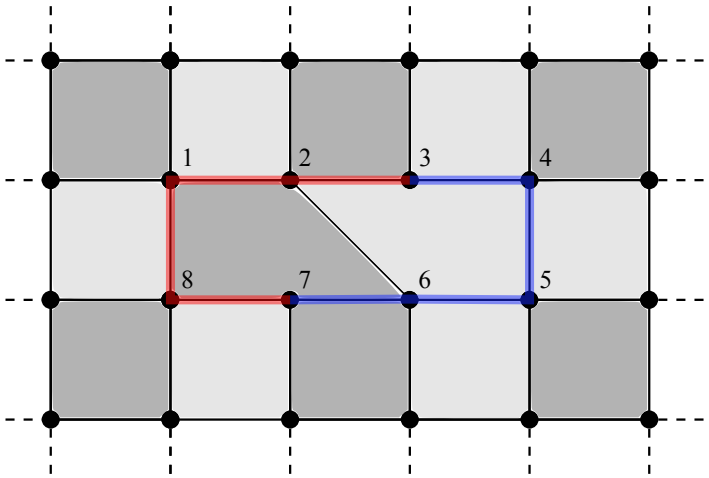

Figure 2.12: The string operators labelling the ground states are sketched. CA_{left} and CA_{right} are drawn in red and blue, respectively.

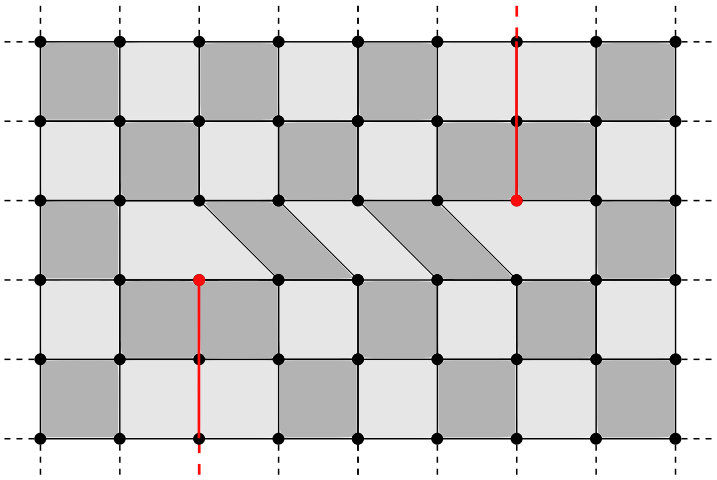

Figure 2.13: The dislocation lines are drawn in red. The operator Y is a string of σ^y-operators along these lines.

2.2.1 An alternative approach to degeneracy

Consider one of the σ_y-string symmetries shown in red in figure 2.13. This operator commutes with the Hamiltonian, and is thus a symmetry. If we interpret it in terms of the e- and m-particles of the toric code, we see that it initially creates a pair of e- and a pair of m-paticles, or alternatively, creates a pair of ϵ-particles. It then moves a ϵ-particle to the edge of the system, while moving the other onto the pentagonal plaquette at its other end. We label this operator Y.

The operator Y anticommutes with the strings P_R and P_L, which we use to la-

bel the degenerate ground states. P_R and P_L, as we have shown, commute with the Hamiltonian. We have the following relations

$$[H, P_R] = 0, \quad [H, Y] = 0, \quad \{Y, P_R\} = 0$$

Consider the previously introduced state $|C = +1\rangle$. It is an energy eigenstate, and also an eigenstate of P_R. Furthermore, $Y|C = +1\rangle$ is also an energy eigenstate:

$$\begin{aligned} H|C = +1\rangle &= E_{C=+1}|C = +1\rangle \\ HY|C = +1\rangle &= YH|C = +1\rangle = E_{C=+1}Y|C = +1\rangle \end{aligned}$$

The states are degenerate. Now we show that $|C = +1\rangle$ and $Y|C = +1\rangle$ are different states. This is done by considering the effect of P_R on these states:

$$\begin{aligned} P_R|C = +1\rangle &= +|C = +1\rangle \\ P_R Y|C = +1\rangle &= -YP_R|C = +1\rangle = -Y|C = +1\rangle \end{aligned}$$

This implies that the state $Y|C = +1\rangle$ is equivalent to the state $|C = -1\rangle$, as it is an eigenstate of P_R with eigenvalue -1. To conclude, we have seen that the states $|C = +1\rangle$ and $|C = -1\rangle$ are degenerate, and that the ground states can be labelled by string operators P_R and P_L

Chapter 3

A physical planar code model

3.1 Getting the planar code from a physical system

The physical system we consider in this thesis is similar to that considered by [33–35]. The primary building block of the system is a so-called Majorana-Cooper box (MCB). This is a system consisting of two semiconducting InAs or InSb nanowires, which under the right conditions may each host Majorana Fermions at both its ends [22, 24, 47]. The nanowires are proximitized by a common s-wave superconductor. The wires are parallel, so that a magnetic field can be applied perpendicular to the wires. Along with the induced superconductivity and the spin-orbit coupling, this is one of the conditions that need to be fulfilled in order for the wires to be in the topological phase [17, 18]. We recall here our introductory discussion of the physical realization of Majorana modes. Assembling many such MCBs in an array with all nanowires parallel, one creates a network of Majorana modes, localized at the end of the wires.

Between Majorana modes on neighbouring islands, we introduce tunnel couplings, which can be varied. Experimental implementation of this could be through the gatemon architecture. [48]

The simple model we employ is a toy model used to approximate the physical reality. We pictorially represent such a system as shown in figure 3.1. The eight framed islands constitute a subsection of this system which we will study in detail.

We can model such a system with the Hamiltonian $H = H_0 + V$, where H_0 is the the sum of charging energies for the individual islands. The charging energy is $E_C(N+q_{\text{ind}})^2$ where N is the number of electrons on the superconducting island and q_{ind} is the induced charge. The most favourable number of electrons can be changed by varying the induced charge. This is usually done by applying some gate voltage, as $q_{\text{ind}} = eV_{\text{gate}}$. By tuning the gate voltage, one can therefore choose whether the energetic minimum occurs for an even or odd number of electrons, N. We recall from section 1.2 that the parity of a set of four Majoranas takes the form $P = \gamma_a \gamma_b \gamma_c \gamma_d$. As a low-energy description of the charging energy for island n, H_0^n, we therefore take $H_0^n = -\Delta \gamma_n^u \gamma_n^r \gamma_n^d \gamma_n^l$ [33]. n labels the island, while the superscript labels the individual Majorana modes on each island, as shown in figure 3.2.

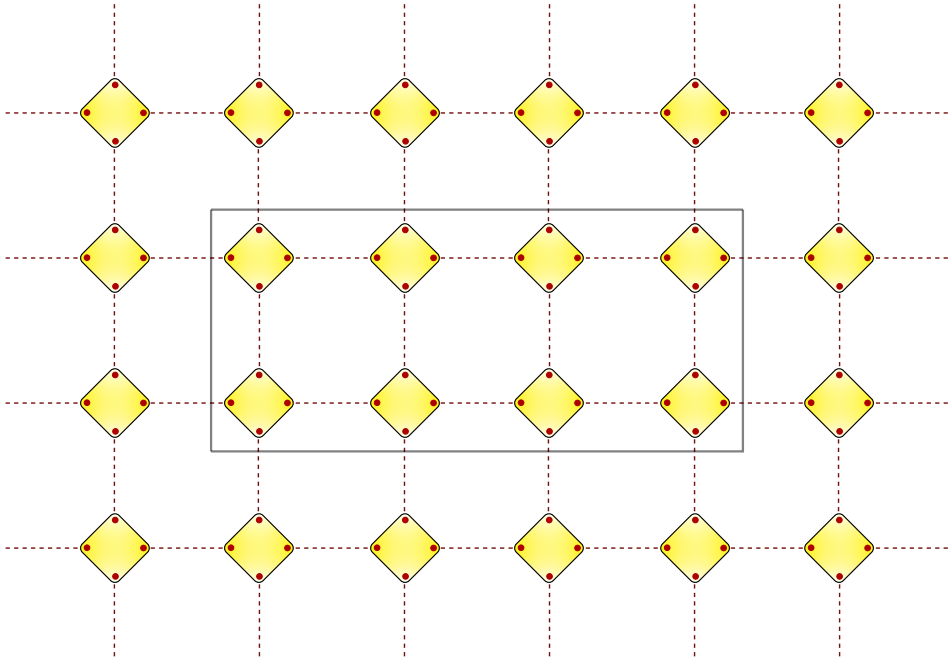

Figure 3.1: Pictorial representation of the physical system. Superconducting islands with parallel nanowires hosting zero-energy Majorana modes are arranged in an array, with tunnel couplings between Majorana modes on adjacent islands indicated by dotted lines. The section of interest of the system is demarcated by the grey rectangle.

The second term in the Hamiltonian, V, contains inter-island couplings. This terms models single-electron tunnelling between the islands, mediated by the Majorana modes. Such a tunnelling process alters the Fermion parity of the island whence the electron departs and that of the island whither it arrives. In other words, the tunnelling link excites the islands which it connects. These tunnelling terms take the form $V_{ij}^{mn} = i\,\gamma_i^m\,\gamma_j^n$. For concreteness, we will from here onwards consider the subsection of the physical system which is framed in figure 3.1 and shown in more detail in figure 3.2.

The set of four Majorana operators on each island can be confined to either the even or odd parity subspace by tuning the gate voltage, V_{gate}. As we saw in section 1.2, this results in each island constituting a two level system, irrespective of whether it is confined to the even or odd parity subspace. For convenience, we will consider the situation where all islands are confined to the even parity subspace. We can map each island to a spin-half system, and talk about the pseudo-spin of the islands. This mapping allows us to map Fermion parity operators, which are products of Majorana operators, into spin operators, which are Pauli operators. This is done by the associations we found in 1.10. We restate the association here, in terms of the new labels u, d, r, l we have assigned to the Majorana operators.

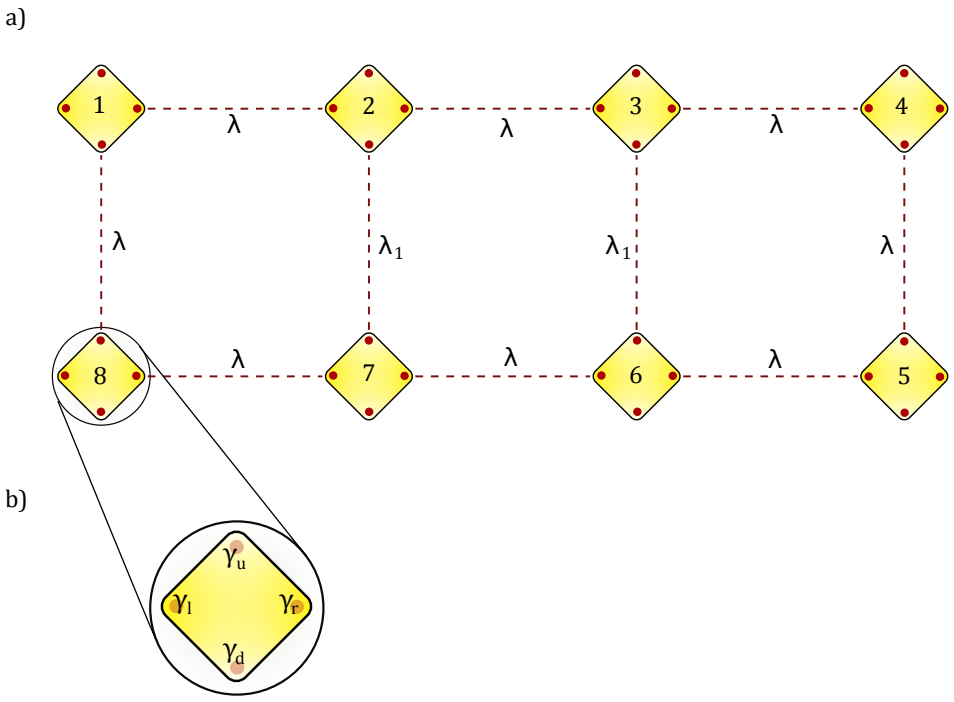

Figure 3.2: a) The section of the system demarcated by the grey rectangle in figure 3.1, with the various coupling strengths labelled. b) An individual island, showing the labelling of the Majorana states. The subscripts indicate the position of the Majorana mode. u indicates up, d down, r right and l left.

$$\boxed{\sigma_z \equiv i\,\gamma_n^r\,\gamma_n^d \equiv i\,\gamma_n^l\,\gamma_n^u, \quad \sigma_x \equiv i\,\gamma_n^l\,\gamma_n^d \equiv i\,\gamma_n^u\,\gamma_n^r, \quad \sigma_y \equiv i\,\gamma_n^l\,\gamma_n^r \equiv i\,\gamma_n^d\,\gamma_n^u} \tag{3.1}$$

As a final introductory note, we add that we in this chapter will work with Pauli operators to a larger extent than we have so far. In order to avoid clutter, we will stop writing them on the form σ_n^a, where n is the island index and a is x, y, z or 0 and instead write A_n, where n remains the island index, and A is either X, Y, Z or I. Thus an operator σ_3^x will in our calculations be written as X_3.

3.2 Perturbation analysis of tunable coupling regime

In this section, we will treat the tunnelling terms as perturbations to the charging Hamiltonian, H_0. This will be done within the framework of Schrieffer-Wolff perturbation theory. We start by outlining this procedure, before we apply it to the system in 3.2. The low-energy sector of this system will reproduce the planar code, without twist defects.

When we introduce a diagonal tunnelling term and repeat the procedure, we will see how the planar code, now with twist defects, emerges.

In the Schrieffer-Wolff framework, pedagogically outlined in [7], we find the effective Hamiltonian as

$$H_{\text{eff}} = E_0 + \Sigma(E_0),$$

where the dependence of the self-energy, Σ, on the energy has been neglected. We define the unperturbed Green's function for excited states only (we require it to vanish when applied to ground states) as

$$G_0'(E) = \left((E - H_0)^{-1}\right)'.$$

The apostrophe indicates that the operator should vanish on ground states. The self energy is calculated as

$$\Sigma(E_0) = \langle GS|(V + VG_0'V + VG_0'VG_0'V + \cdots)|GS\rangle$$

To have non-vanishing terms in this sequence, the perturbations must excite the system, then relax it back into the ground state. In the following, we apply the method, so that the procedure becomes clear.

3.2.1 Planar code in perturbation theory

We will now consider the case where some of the inter-island tunnel couplings in figure 3.2 can be tuned. For ease of reference, we will refer to the term which models the tunnelling between islands i and j as $V_{i,j}$. A perturbation takes the form of a sum of tunnelling terms weighted by the tunnelling amplitude:

$$V = \sum \lambda_{i,j} V_{i,j} \tag{3.2}$$

Where the sum runs over the set of i, j that label the appropriate pairs of Majorana operators on neighbouring islands. When we now treat the system perturbatively, it suffices to consider the four central islands of figure 3.2. The result obtained for this part of the system is easily generalizable to the rest of the system, due to the discrete translational invariance of the array.

When we consider the four central islands, the relevant tunnelling terms are:

$$\begin{aligned} V_{7,2} &= \pm i\gamma_7^u\gamma_2^d, \qquad & V_{2,3} &= \pm i\gamma_2^r\gamma_3^l, \\ V_{3,6} &= \pm i\gamma_3^d\gamma_6^u, \qquad & V_{6,7} &= \pm i\gamma_6^l\gamma_7^r \end{aligned} \tag{3.3}$$

All these operators mutually commute, due to eq. 1.4, as they share no common Majorana operators.

As mentioned, these tunnelling links can be visualized as an excitation of the ground state of the islands it connects, by flipping their respective parities. In the language of

pseudo-spins, this corresponds to flipping the spin of the islands connected by the link. If an electron tunnels away from an island, it must return to the same island for the system to remain in the low-energy regime. This means that we essentially will see two kinds of terms in perturbation theory: The first kind is a sequence of tunnelling terms which transports an electron to an island, before returning it to the original island via the same path. The second kind of term transports an electron to an island, and returns it to the original island via a different path, forming a closed loop. If we make a term of the second kind, and rewrite it in terms of Pauli operators, we can interpret it in terms of the string operators of the toric code model. A closed loop of tunnelling link operators corresponds to a closed loop in the terminology of the toric code. It is a string which nucleates a pair of charges, moves one of them in a loop, and reannihilates the pair. In this way the system is excited, before it relaxes back into the anyonic vaccum state.

Odd orders of perturbation theory will give terms equal to zero, as an odd number of perturbations cannot return the islands to the ground state. Even orders of perturbation can return the islands to the ground state. The second order term of the perturbative expansion, in which one tunnelling link operator is applied twice and moves an electron forth and back along the same path, gives a constant energy shift. This is evident, from the fact that a tunnelling link operator squared gives the identity operator. In the following analysis, constant energy shifts resulting from perturbation terms which belong to the first of the two categories above are neglected.

In fourth order perturbation theory, terms arise where the four-island system is brought back to its ground state with no link operator applied twice. Such terms are qualitatively different from those of second order perturbation theory. The tunnelling link operators do one of three things: A link operator can flip two pseudo-spins, increasing the energy by $4E_C$. It can flip a pair of pseudo-spins where one pseudo-spin is already excited. This amounts to shifting a flipped pseudo-spin, which leaves the energy unchanged. The third possibility is that a link operator flips a pair of pseudo-spins where both spins are already excited. This reduces the energy by $4E_C$. In the terminology of the toric code, these three options correspond to creation of a pair of charges, shifting a charge and annihilation of a pair of charges. We term these two possibilities 'creation', 'shift' and 'annihilation' and see that the order of the link operators fall into two categories, depending on the excitations they create. Creation followed by two shifts and annihilation yields a difference between the energy of the perturbed island system and the ground state of $4E_C$ between perturbations, so that each evaluation of $G_0 = (E_0 - H_0)^{-1}$ gives $(-4E_C)^{-1}$. Two creations followed by two annihilations cause the energy difference to be $4E_C$ after one perturbation, $8E_C$ after two perturbations and $4E_C$ after three perturbations. We employ the notation $4E_C \to 4E_C \to 4E_C$ and $4E_C \to 8E_C \to 4E_C$ for these two energy difference sequences, respectively.

For the central four-island system comprising islands 2, 3, 6 and 7, we find the perturbative expansion to fourth order to be

$$\frac{-5\lambda^2\lambda_1^2}{16E_C^3} Z_2 X_3 Z_6 X_7 \tag{3.4}$$

Where the string of Pauli operators is a string of reordered tunnelling link operators describing possible excitations weighted by their tunelling amplitude. The string of link operators is rewritten according to eq. 3.1:

$$\begin{aligned}\lambda_{7,2}\lambda_{2,3}\lambda_{3,6}\lambda_{6,7}V_{7,2}V_{2,3}V_{3,6}V_{6,7} &= \lambda^2\lambda_1^2(i\gamma_7^u\gamma_2^d)(i\gamma_2^r\gamma_3^l)(i\gamma_3^d\gamma_6^u)(i\gamma_6^l\gamma_7^r)\\ &= \lambda^2\lambda_1^2 i\gamma_7^u Z_2(-X_3)Z_6\gamma_7^r = \lambda^2\lambda_1^2(-1)^2 Z_2X_3Z_6X_7\\ &= \lambda^2\lambda_1^2 Z_2X_3Z_6X_7\end{aligned}$$

The combinatorial factor in front comes from summing the $4! = 24$ terms resulting from the permutations of the order of the four Pauli operators corresponding to flipping four pseudo-spin pairs in a particular order. As the link operators mutually commute, these terms all carry the same sign. Eight of these terms correspond to sequences with intermediate energies $4E_C \to 8E_C \to 4E_C$, while the other 16 correspond to $4E_C \to 4E_C \to 4E_C$ sequences:

$$8\frac{1}{2(-4E_C)^3} + 16\frac{1}{(-4E_C)^3} = \frac{-5}{16E_C^3} \tag{3.5}$$

If we perform a similar analysis for the entire eight-island system, the effective Hamiltonian becomes

$$H_4 = \frac{-5\lambda^3\lambda_1}{16E_C^3}\left(Z_1X_2Z_7X_8 + Z_3X_4Z_5X_6\right) - \frac{-5\lambda^2\lambda_1^2}{16E_C^3} Z_2X_3Z_6X_7 \tag{3.6}$$

It is clear that if we extend this analysis to all the islands in the system, perturbation theory to fourth order yields the planar code Hamiltonian with plaquettes defined as in the Wen model.

The higher order terms in the expansion will also be closed loops made from Pauli operators. It is impossible to get terms where the effective operator is not a product of single Wen plaquettes, however, and as a result all higher order terms commute with the fourth order term. This is because a product of operators commute with any operator which commutes with the factors individually. This means that higher order terms may shift the energies of the eigenstates, but they do not change the eigenstates.

3.2.2 Planar code with twists in perturbation theory

We will now see whether we can introduce dislocations in the lattice by use of additional tunable couplings. We introduce a new, diagonal coupling, $V_{2,6} = i\,\gamma_2^d\,\gamma_6^u$, as shown in 3.2.

We allow for couplings $V_{7,2}$, $V_{3,6}$ and $V_{2,6}$ to be adiabatically turned on and off. Three situations can arise, depending on how the couplings are tuned. Firstly, we have the case where the couplings $V_{7,2}$ and $V_{3,6}$ are on, while the diagonal $V_{2,6}$-coupling is

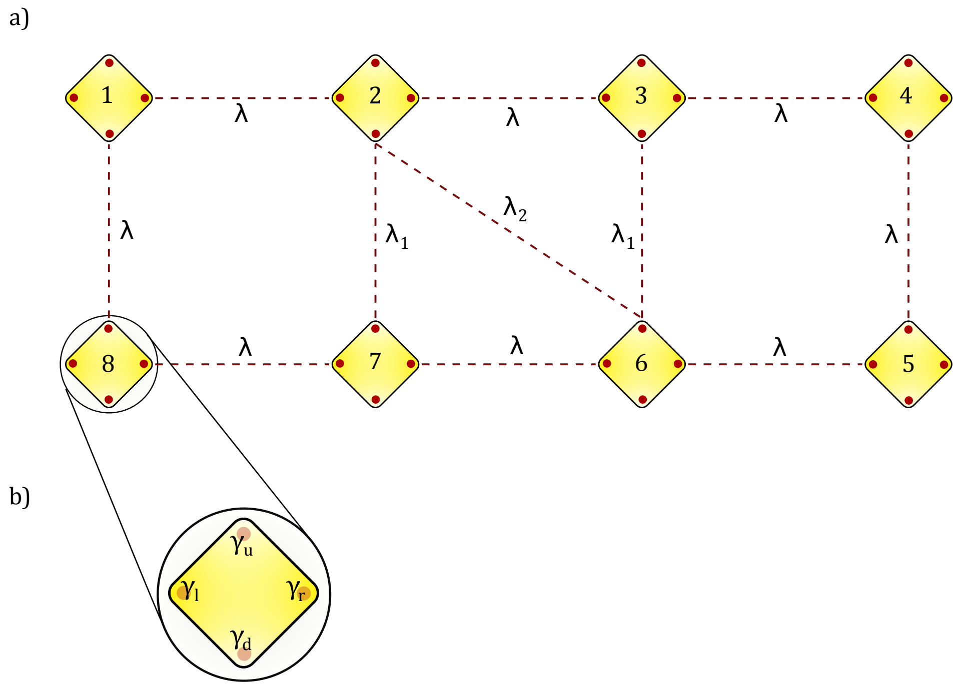

Figure 3.3: a) A diagonal tunnel coupling between islands 2 and 6 is introduced in the system from figure 3.2. All coupling strengths are labelled. b) An individual island, showing the labelling of the Majorana states. The subscripts indicate the position of the Majorana mode. u indicates up, d down, r right and l left.

off. This gives three tetragonal plaquettes framed by islands 1, 2, 7, 8; 2, 3, 6, 7 and 3, 4, 5, 6, respectively. As we have shown, this is equivalent to the planar code without any dislocations. Secondly, there is the case where all three couplings, $V_{7,2}$, $V_{3,6}$ and $V_{2,6}$ are on. This case gives rise to a new kind of plaquette, namely the two triangular plaquettes framed by islands 2, 6, 7 and 2, 3, 6, respectively. Thirdly, there is the case where the $V_{7,2}$- and $V_{3,6}$-couplings are off, while the diagonal $V_{2,6}$-coupling is on. This gives rise to two pentagonal plaquettes framed by islands 1, 2, 6, 7, 8 and 2, 3, 4, 5, 6.

Now we look at the triangular plaquettes. For clarity, we select the leftmost of the two. The relevant link operators for this plaquette are

$$V_{7,2} = i\gamma_7^u\gamma_2^d, \qquad V_{2,6} = i\gamma_2^d\gamma_6^u, \qquad V_{6,7} = i\gamma_6^l\gamma_7^r, \tag{3.7}$$

These link operators do not all mutually commute. We have that $[V_{7,2}, V_{6,7}] = 0$, $[V_{2,6}, V_{6,7}] = 0$ and $\{V_{7,2}, V_{2,6}\} = 0$. The reason why two of the link operators anticommute is that they share a common Majorana operator.

For this plaquette, even orders of perturbation give vanishing terms. The first possible non-zero term is therefore the third order term. The sequence of energy differences in between perturbations is for this plaquette only of one kind: $4E_C \to 4E_C$. There are six different operator strings which excite the three islands from the ground state

before relaxing them after three perturbations. These are:

$$\begin{aligned} &V_{7,2}V_{2,6}V_{6,7}, \quad V_{7,2}V_{6,7}V_{2,6}, \quad V_{6,7}V_{7,2}V_{2,6}, \\ &V_{6,7}V_{2,6}V_{7,2}, \quad V_{2,6}V_{7,2}V_{6,7}, \quad V_{2,6}V_{6,7}V_{7,2}. \end{aligned}$$

From the commutation relations of these link operators we see that three of these orderings have a sign different from that of the other three. As the terms share the same denominator, the perturbations cancel, meaning that the third order term of the perturbation expansion vanishes.

Consider the pentagonal plaquettes. For clarity, we look at the leftmost of the two. The link operators for the plaquette are:

$$\begin{aligned} &V_{8,1} = i\gamma_8^u\gamma_1^d, \qquad V_{1,2} = i\gamma_1^r\gamma_2^l, \qquad V_{2,6} = i\gamma_2^d\gamma_6^u, \\ &V_{6,7} = i\gamma_6^l\gamma_7^r, \qquad V_{7,8} = i\gamma_7^l\gamma_8^r \end{aligned} \tag{3.8}$$

Reordering the operator string describing excitations we get

$$\begin{aligned} \lambda_{8,1}\lambda_{1,2}\lambda_{2,6}\lambda_{6,7}\lambda_{7,8}V_{8,1}V_{1,2}V_{2,6}V_{6,7}V_{7,8} &= \lambda^4\lambda_2(i\gamma_8^u\gamma_1^d)(i\gamma_1^r\gamma_2^l)(i\gamma_2^d\gamma_6^u)(i\gamma_6^l\gamma_7^r)(i\gamma_7^l\gamma_8^r) \\ &= \lambda^4\lambda_2 i\gamma_8^u Z_1(-X_2)Z_6(-Y_7)\gamma_8^r \\ &= -\lambda^4\lambda_2 Z_1X_2Z_6Y_7X_8 \end{aligned}$$

The possible energy difference sequences for the fifth order term in the perturbation expansion are listed below, with the number of different ways Pauli operators can be ordered to achieve the sequence in brackets:

$$\begin{aligned} &4E_C \to 4E_C \to 4E_C \to 4E_C \quad (40) \qquad 4E_C \to 4E_C \to 8E_C \to 4E_C \quad (20) \\ &4E_C \to 8E_C \to 4E_C \to 4E_C \quad (20) \qquad 4E_C \to 8E_C \to 8E_C \to 4E_C \quad (40) \end{aligned}$$

Adding these $5! = 120$ combinatorial pre-factors, with their energy denominators, we have

$$\frac{40}{(-4E_C)^4} + \frac{20}{2(-4E_C)^4} + \frac{20}{2(-4E_C)^4} + \frac{40}{2^2(-4E_C)^4} = \frac{35}{128E_C^4} \tag{3.9}$$

The fifth order terms for both the left and right plaquettes are combined to give

$$H_5 = \frac{-35\lambda^4\lambda_2}{128E_C^4}\left(Z_1X_2Z_6Y_7X_8 + Z_2Y_3X_4Z_5X_6\right). \tag{3.10}$$

We now consider other terms that occur in the perturbation expansion. We can consider the problem pictorially, with a perturbation $V_{2,3}$ represented by a line connecting islands 2 and 3. As previously explained, perturbation sequences that return the system to the ground state must form closed loops. We also note that higher order

perturbation terms, of order n, will be small, compared to the perturbation terms of order 4 and 5, as the terms scale as $\approx \lambda^{n-1}/E_C^{n-2}$.

There are two categories of higher order perturbation terms. If an odd order perturbation term contains one pair of tunnelling link operators that share one common Majorana operator, it vanishes. We saw this in the case of the third order perturbation term, where, due to two link operators anticommuting, the individual terms cancelled each other. For higher orders, this will also happen, with half the terms pertaining to one energy difference sequence cancelling the other half.

The second category is odd order perturbation terms which contain three perturbations $V_{2,7}, V_{2,6}$ and $V_{3,6}$, and do not vanish. $V_{2,6}$ shares one of its Majorana operators with $V_{2,7}$ and the other one with $V_{3,6}$. We have the commutation relations $[V_{2,7}, V_{3,6}] = 0, \quad \{V_{2,7}, V_{2,6}\} = \{V_{2,6}, V_{3,6}\} = 0$, so half the terms pertaining to one energy difference sequence will not cancel the other half in such cases.

An example of a perturbation sequence of the first category is the seventh order term which is pictorially represented in orange in figure 3.4a. An example of the second category is the seventh order term pictorially represented in green in figure 3.4a.

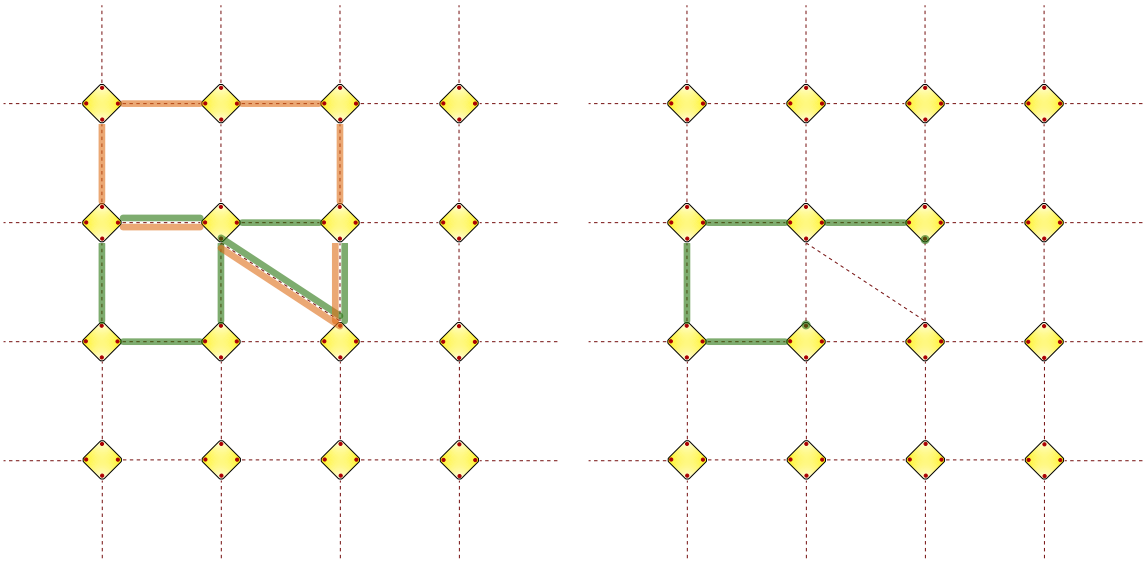

(a) (b)

Figure 3.4: (a) pictorially displays two perturbation terms of seventh order. The orange term vanishes, while the green does not. (b) shows the green term where we remove the Majorana operators which appear twice in the perturbation sequence and square to unity.

We see that the seventh order term reduces to the string operators we found in eq. 2.2, and which we sketched in figure 2.12. The second category of perturbation terms, of which the green seventh order term is an example, generate operators which commute with the Hamiltonian. With another word, they generate symmetries of the system.

3.3 Connecting the physical model and the planar code

We have seen how the introduction of tunable tunnel couplings yields the effective Hamiltonian

$$\begin{aligned} H =& \frac{-5\lambda^3\lambda_1}{16E_C^3}\left(Z_1X_8X_2Z_7 + X_4Z_5Z_3X_6\right) + \frac{-5\lambda^2\lambda_1^2}{16E_C^3}Z_2X_3Z_6X_7 \\ &+ \frac{-35\lambda^4\lambda_2}{128E_C^4}\left(Z_1X_8X_2Z_6Y_7 + X_4Z_5Z_2Y_3X_6\right) \end{aligned} \tag{3.11}$$

when we apply perturbation theory to fifth order. Recall how we in section 2.2 discussed how the transition from the regime with only square plaquettes to one with pentagonal plaquettes allows us to initialize a qubit. The Hamiltonian contains both tetragonal and pentagonal plaquettes. In the limit where $\lambda_2 = 0$, it contains only square plaquettes, and takes the form of the planar code without twists. In the limit where $\lambda_1 = 0$ it contains only the pentagonal plaquettes, and takes the form of the planar code with twists. For this reason, we are interested in tuning the tunnel couplings so that at times $t = 0$ and $t = T$ we have

$$\begin{aligned} \lambda_1(t=0) = \lambda, \quad \lambda_1(t=T) = 0 \\ \lambda_2(t=0) = 0, \quad \lambda_2(t=T) = \lambda \end{aligned} \tag{3.12}$$

The couplings should be tuned adiabatically, to ensure that the system remains in the ground state $|C = +1\rangle$, as discussed, where C is the central plaquette, through which the diagonal coupling runs. The possibility for initialization of the system is our motivation for studying this specific Hamiltonian.

Drawing on the discussion of twist defects, we see that the twist defects of the planar code are actually unpaired Majorana modes in the more physical toy system. In the limit where $\lambda_1 = 0$, when we have pentagonal plaquettes, these Majorana modes do not enter the Hamiltonian. We discussed how strings connecting the twist defects could be used to label the degenerate ground states. These strings took the form

$$\begin{aligned} P_L = CA_{\text{left}} &= -\sigma_z^1\sigma_y^2\sigma_x^3\sigma_z^7\sigma_x^8 \\ P_R = CA_{\text{right}} &= -\sigma_z^3\sigma_x^4\sigma_z^5\sigma_y^6\sigma_x^7 \end{aligned}$$

If we rewrite these two operators in terms of Majorana operators, we see that they constitute strings of Majorana operators which connect the unpaired modes.

3.4 Solving the Hamiltonian

By inspection of the Hamiltonian in 3.11, we see that the four operators Z_1, X_4, Z_5 and X_8 all commute with it, and they furthermore mutually commute. This causes the

Hamiltonian to become block diagonal, with 16 16×16-blocks, if written in the appropriate basis. We arrange the basis so that a basis state is of the form $|z_1x_4z_5x_8\,\sigma_2\,\sigma_7\,\sigma_3\,\sigma_6\rangle$, with the number index referring to the island which hosts the pseudo-spin. The block diagonalization can be seen as fixing the eigenvalues of the operators Z_1, X_4, Z_5 and X_8 as ±1. Thus, the pseudo-spin on island 1 can be seen as a spin fixed as either aligned or anti-aligned with the z-direction. The pseudo-spin on island 2 would then be fixed parallell or anti-parallell to the x-axis. We employ lowercase latin letters to denote the eigenvalues of operators which commute with the Hamiltonian. To get the desired block structure, we note that The Hamiltonian is block diagonal if we rotate the spaces corresponding to islands 1 and 5 so that they are aligned with the x-direction. The spaces corresponding to islands 4 and 8 are diagonal in the z-basis, in which they are already expressed.

The x- and z-bases can be interchanged by a rotation of π about the axis $\mathbf{n}_{xz} = \sqrt{1/2}(1,0,1)$, which is the normalized vector bisecting the angle spanned by the x and z unit vectors in the xz-plane. We have seen this rotation before, in our discussion of basis changes in subsection 1.2.1. Writing this rotation in the Pauli two-component formalism (eq. 1.13) we obtain the well-known Hadamard matrix:

$$\mathbf{R}(\mathbf{n}_{xz},\pi,0) = \sqrt{\frac{1}{2}}\begin{pmatrix}1 & 1\\ 1 & -1\end{pmatrix}. \tag{3.13}$$

We let $\mathbf{R}_n(\mathbf{n}_{xz},\pi,0)$ denote the Hadamard rotation applied to the Hilbert subspace for island number n. By applying the transformation

$$R_4^\dagger(\mathbf{n}_{xz},\pi,0)R_8^\dagger(\mathbf{n}_{xz},\pi,0)H_{256\times256}R_8(\mathbf{n}_{xz},\pi,0)R_4(\mathbf{n}_{xz},\pi,0) = H_{16\times16} \tag{3.14}$$

to the original Hamiltonian we indeed transform it to block diagonal form, with 16 16×16-blocks. By substituting for the operators their two possible eigenvalues, as follows:

$$Z_1 = z_1 = \pm1, \quad X_4 = x_4 = \pm1, \quad Z_5 = z_5 = \pm1, \quad X_8 = x_8 = \pm1. \tag{3.15}$$

we can obtain the form of these 16×16-blocks, which depends on the signs of these eigenvalues:

$$\begin{aligned} H_{16\times16} =& \frac{-5\lambda^3\lambda_1}{16E_C^3}\left(z_1x_8X_2Z_7 + x_4z_5Z_3X_6\right) + \frac{-5\lambda^2\lambda_1^2}{16E_C^3}Z_2X_3Z_6X_7 \\ &+ \frac{-35\lambda^4\lambda_2}{128E_C^4}\left(z_1x_8X_2Z_6Y_7 + x_4z_5Z_2Y_3X_6\right) \end{aligned} \tag{3.16}$$

We will now further block diagonalize these smaller blocks.

Consider the operator $Y_2Y_3Y_6Y_7$. It commutes with the Hamiltonian. We apply a unitary transformation operator $U = (1/2)^{1/2}(Y_2Y_3Y_6Y_7 + X_7)$ and evaluate $U^\dagger H_{16\times16}U$. This transformation yields (see Appendix A for details):

$$\begin{aligned} U^\dagger H_{16\times16} U = H' =& \frac{-5\lambda^3\lambda_1}{16E_C^3}\left(z_1 x_8 Z_2 Y_3 Y_6 + x_4 z_5 Z_3 X_6\right) + \frac{-5\lambda^2\lambda_1^2}{16E_C^3} Z_2 X_3 Z_6 X_7 \\ &+ \frac{-35\lambda^4\lambda_2}{128E_C^4}\left(z_1 x_8 Z_2 Y_3 X_6 X_7 + x_4 z_5 Z_2 Y_3 X_6\right) \end{aligned} \tag{3.17}$$

Where now both Z_2 and X_7 commute with H', meaning that we have effectively reduced the problem to a problem of two pseudo-spins on islands three and six. As was originally done for islands 1, 4, 5 and 8, we fix the eigenvalues of $Z_2 = z_2 = \pm 1$ and $X_7 = x_7 = \pm$. By subjecting X_7 to the Hadamard rotation we reduce the Hamiltonian to block diagonal form, with 64 4×4-blocks, by transforming

$$R_7^\dagger(\mathbf{n}_{xz}, \pi, 0) H' R_7(\mathbf{n}_{xz}, \pi, 0) = H_{4\times4}. \tag{3.18}$$

In terms of the fixed eigenvalues, these blocks take the form:

$$\begin{aligned} H_{4\times4} =& \frac{-5\lambda^3\lambda_1}{16E_C^3}\left(z_1 x_8 z_2 Y_3 Y_6 + x_4 z_5 Z_3 X_6\right) + \frac{-5\lambda^2\lambda_1^2}{16E_C^3} z_2 x_7 X_3 Z_6 \\ &+ \frac{-35\lambda^4\lambda_2}{128E_C^4}\left(z_1 x_8 z_2 x_7 Y_3 X_6 + x_4 z_5 z_2 Y_3 X_6\right) \end{aligned} \tag{3.19}$$

For ease of reading the matrix form of this Hamiltonian, we define

$$x_8 z_1 z_2 \equiv \alpha, \quad x_7 z_2 \equiv \beta, \quad x_4 z_5 \equiv \gamma \quad x_7 x_8 z_1 z_2 \equiv \delta \quad x_4 z_2 z_5 \equiv \varepsilon \tag{3.20}$$

and label

$$\frac{-5\lambda^3\lambda_1}{16E_C^3} \equiv A_1, \quad \frac{-5\lambda^2\lambda_1^2}{16E_C^3} \equiv A_2, \quad \frac{-35\lambda^4\lambda_2}{128E_C^4} \equiv B. \tag{3.21}$$

The Hamiltonian matrix then takes the form

$$H = \begin{pmatrix} 0 & \gamma A_1 & \beta A_2 & -\alpha A_1 - iB(\delta+\varepsilon) \\ \gamma A_1 & 0 & \alpha A_1 - iB(\delta+\varepsilon) & -\beta A_2 \\ \beta A_2 & \alpha A_1 + iB(\delta+\varepsilon) & 0 & -\gamma A_1 \\ -\alpha A_1 + iB(\delta+\varepsilon) & -\beta A_2 & -\gamma A_1 & 0 \end{pmatrix} \tag{3.22}$$

With the eigenvalues

$$\begin{aligned} E_{s_1' s_2'} =& s_1' \frac{-5\lambda^2\lambda_1^2}{16E_C^3} x_7 z_2 \\ &+ s_2' \sqrt{2\left[\left(\frac{35\lambda^4\lambda_2}{128E_C^4}\right)^2 (1 + x_4 x_7 x_8 z_1 z_5) + \left(\frac{5\lambda^3\lambda_1}{16E_C^3}\right)^2 (1 + s_1' x_4 x_8 z_1 z_2 z_5)\right]} \end{aligned} \tag{3.23}$$

where $s_1' = \pm 1$ and $s_2' = \pm 1$.

Consider the four quantities in the expression for the energy that can take the value ± 1. They are $s_2', s_1' x_7 z_2, x_4 x_7 x_8 z_1 z_5$ and $s_1' x_4 x_8 z_1 z_2 z_5$. The three latter ones are not independent; fixing two of them determines the third, resulting in the system having eight distinct energy levels. By using variables s_i that take values ± 1 we can write the energies as

$$E_{s_1 s_2 s_3} = s_1 \frac{-5\lambda^2 \lambda_1^2}{16 E_C^3} + s_2 \sqrt{2\left[\left(\frac{35\lambda^4 \lambda_2}{128 E_C^4}\right)^2 (1+s_3) + \left(\frac{5\lambda^3 \lambda_1}{16 E_C^3}\right)^2 (1+s_1 s_3)\right]} \tag{3.24}$$

where now $s_1 = s_1' x_7 z_2$, $s_2 = s_2'$, $s_3 = x_4 x_7 x_8 z_1 z_5$, $s_1 s_3 = s_1' x_7 z_2 x_4 x_7 x_8 z_1 z_5 = s_1' x_4 x_8 z_1 z_2 z_5$.

There are seven different energies, as $E_{++-} = E_{+--}$. We wish to model the scenario with time dependent couplings, in accordance with 3.12. We choose units so that $\lambda = 1$, and let λ_1 and λ_2 depend on time: $\lambda_1 = \cos(\omega t)$, $\lambda_2 = \sin(\omega t)$. If we demand that the process has ended when a time T has passed, so that at $t = T$, $\cos(\omega t) = 0, \sin(\omega t) = 1$, we have $\omega = \pi/(2T)$.

Plotting the different energies, for $t \in [0, T]$, we can see how the two ground state energies become degenerate in the limit where $\lambda_1 = 0, \lambda_2 = 1$.

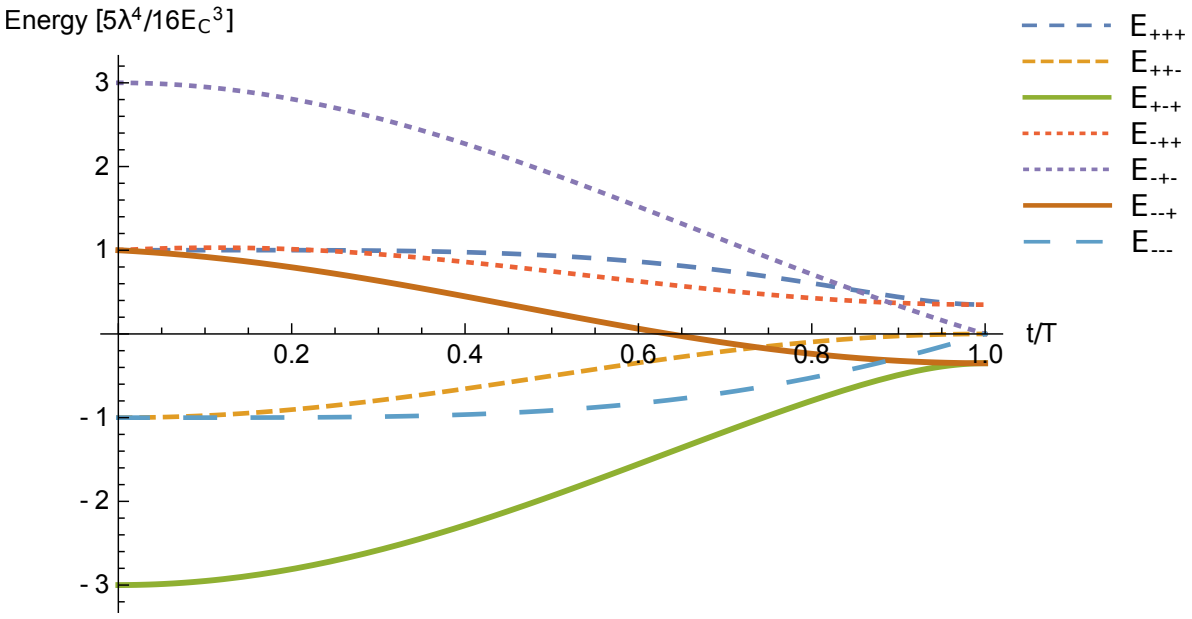

Figure 3.5: The energy levels of the system are plotted as a function of t/T. Units are chosen so that $\lambda = 1$. The ratio λ/E_C is $1/5$. The pair of full lines are the energy levels that are degenerate ground state energies in the limit $\lambda_1 = 0, \lambda_2 = 1$.

In this limit, the possible energies reduce to

$$E_{s_2 s_3} = s_2 \frac{35\lambda^4 \lambda_2}{128 E_C^4} \sqrt{2(1+s_3)} \tag{3.25}$$

It is clear that the two energies E_{+-+} and E_{--+} take the value $-2(35\lambda^4\lambda_2)/(128E_C^4)$, are degenerate in this limit, and belong to the ground states. The ground states therefore have $s_3 = 1$ and $s_2 = -1$. It can be difficult to see the details of the plot in figure 3.5, so we plot the same energies for the range $t/T \in [0.75, 1]$ in figure 3.6

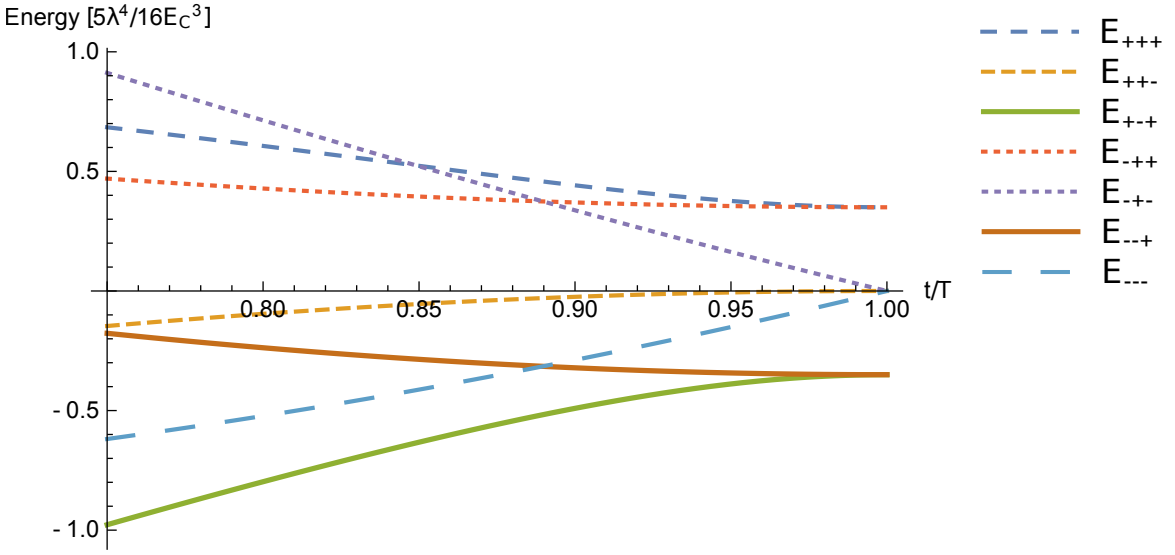

Figure 3.6: An enlarged part of the spectrum shown in figure 3.5, for $t/T \in [0.75, 1]$. The ratio λ/E_C is 1/5. As before, the fully drawn lines are the pair of energies that become degenerate ground state energies for $\lambda_1 = 0, \lambda_2 = 1$.

Diagonalizing the Hamiltonian in eq. 3.22, and imposing that $\lambda_1 \to 0$ and thus $A_1 \to 0$, $A_2 \to 0$, we find the vector representation of the two ground states with energies in terms of the fixed eigenvalues:

$$\begin{pmatrix} i(s_4+s_5)\sqrt{2+2s_4s_5} \\ 1 \\ -i(s_4+s_5)\sqrt{2+2s_4s_5} \\ 1 \end{pmatrix}, \qquad \begin{pmatrix} i(s_4+s_5)\sqrt{2+2s_4s_5} \\ -1 \\ i(s_4+s_5)\sqrt{2+2s_4s_5} \\ 1 \end{pmatrix} \tag{3.26}$$

where $s_4 = x_4 z_2 z_5$, $s_5 = x_7 x_8 z_1 z_2$ and $s_4 s_5 = s_3 = z_1 x_4 z_5 x_7 x_8$. For the ground states, $s_4 s_5 = 1$, and so the possibilities are reduced to

$$|\psi_a'\rangle = \begin{pmatrix} is_6 \\ 1 \\ -is_6 \\ 1 \end{pmatrix}, \qquad |\psi_b'\rangle = \begin{pmatrix} is_6 \\ -1 \\ is_6 \\ 1 \end{pmatrix} \tag{3.27}$$

where $s_6 = 1$ if $s_4 = s_5 = 1$ and $s_6 = -1$ if $s_4 = s_5 = -1$.

Recalling the transformation in eq. 3.18, we know that eigenstates of the 4×4-blocks are expressed in the basis defined by $R_7^\dagger(\mathbf{n}_{xz}, \pi, 0)U^\dagger|v_i\rangle$, where the $|v_i\rangle$s are the basis states of the 16×16 Hamiltonian. We re-express the eigenstates in the original basis by subjecting them to the transformation $UR_7(\mathbf{n}_{xz}, \pi, 0)R_7^\dagger(\mathbf{n}_{xz}, \pi, 0)U^\dagger|v_i\rangle = |v_i\rangle$. These states will be vectors of a 16-dimensional subspace of the Hilbert space, multiplied by some simple product state of pseudo-spins in the x- or z-direction, for islands 1, 4, 5 and 8. We label $|\psi_a'\rangle$ expressed in the non-rotated basis $|\psi_a\rangle$ and likewise for $|\psi_b'\rangle$. By explicitly computing the matrix form of the central plaquette operator, and applying it to the states $|\psi_a\rangle$ and $|\psi_b\rangle$, one finds that they both are eigenstates of the central plaquette operator, $C = Z_2X_3Z_6X_7$:

$$C|\psi_a\rangle = -|\psi_a\rangle, \quad C|\psi_b\rangle = |\psi_b\rangle, \tag{3.28}$$

and have opposite eigenvalues under this operation.

We have shown how, by adiabatically tuning inter-island couplings in the system, so that at $t = 0$, $\lambda_1 = \lambda$ and $\lambda_2 = 0$ and at some later time T, $\lambda_1 = 0$ and $\lambda_2 = \lambda$, we can double the number of ground states. At$t = 0$ the system will be in the state $|C = +1\rangle$. At $t = T$, the system has two degenerate ground states, namely $|C = +1\rangle$ and $|C = -1\rangle$. As long as the evolution from the planar code with only square plaquettes to the one with twist defects is adiabatic, the system will remain in the ground state, and thus be initialized in the state $|C = +1\rangle$. The ratio of coupling strengths to charging energy should be small, to keep the perturbation theory valid, but still large enough to allow for adiabatic evolution. This becomes hard if the gap between the ground state prior to the introduction of twist defects and the excited states becomes very small. This way of introducing twist defects in the system corresponds to the creation of an initialized logical qubit, as previously discussed.

Chapter 4

Adiabatic manipulation of Majorana modes

4.1 Motion of dislocations

In this section, we will see how dislocations can be adiabatically shifted across the lattice. We will see how information about the state of the system is transferred between Majorana modes.

4.1.1 Horizontal motion

We will now explore how dislocations can be adiabatically shifted across the lattice.

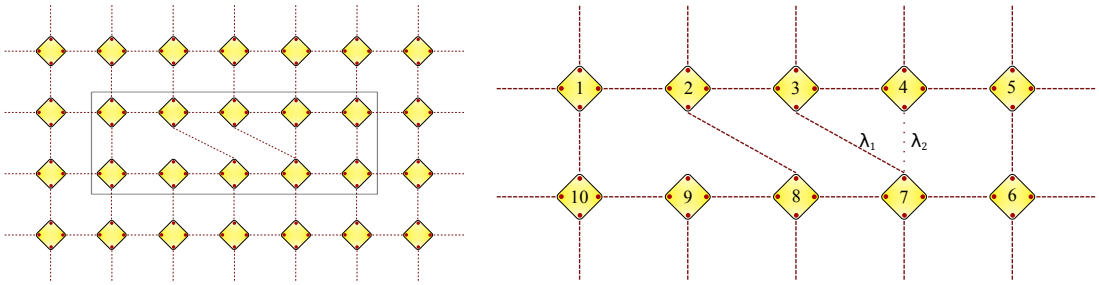

(a) (b)

Figure 4.1: (a) Pictorial representation of the physical setup, with the section of interest demarcated by a grey line. (b) Sketch labelling the coupling strengths relevant for the horizontal motion of an unpaired Majorana mode.

Consider figure 4.7. At time $t = 0$, the coupling λ_2 is on, while the coupling λ_1 is off. Dislocations can be moved by adiabatically switching on λ_1, before adiabatically switching off λ_2. In terms of Majorana modes, the process is as follows:

Initially, the unpaired Majorana modes are γ_9^u and γ_3^d, respectively. By switching on the coupling $i\,\gamma_3^d\,\gamma_7^u$ and switching off the coupling $i\,\gamma_4^d\,\gamma_7^u$, the unpaired modes become γ_9^u and γ_4^d.

If the change is adiabatic, the system will remain in the ground state. At time $t = T$, λ_1 is on, while λ_2 is off. The process gives a new Hamiltonian, where the pentagonal plaquette operator is shifted to a new position, and where we introduce a parallelogram plaquette. This scenario was discussed in section 2.2. Using the numbering in figure 4.1b, the parallelogram plaquette, in terms of Pauli operators, takes the form

$$A_{\text{para}} = \sigma_2^z\,\sigma_3^x\,\sigma_7^z\,\sigma_8^x\,.$$

In the ground state, these parallelogram stabilizers take the value 1.

Information transfer

We have seen how a pair of dislocations introduce a qubit. We have seen how information about the state of this qubit is encoded by the eigenvalue of a string connecting the unpaired Majorana modes. We will now look briefly at how this information can be transferred by tuning the couplings between Majorana modes in the system. This has previously been considered by Sau, Tewari and Clarke [49]. Here we summarize their argument

Only two couplings are tuned in the transfer process, and so only three Majorana operators are contained in the tunnelling Hamiltonian of the system. For ease of notation, we relabel the three Majorana operators involved in the process as $\gamma_1 \equiv \gamma_3^d, \gamma_7^u \equiv \gamma_2, \gamma_4^d \equiv \gamma_3$. The Hamiltonian is

$$H(t) = \alpha(t)\lambda_1 i\,\gamma_1\,\gamma_2 + (1-\alpha(t))\lambda_2 i\,\gamma_2\,\gamma_3$$

where $\alpha(t)$ is an adiabatically varying parameter, which satisfies $\alpha(0) = 0$, $\alpha(T) = 1$. If we formulate an effective magnetic field $\mathbf{B}(t) = (\alpha(t)i\lambda_1, 0, [1-\alpha(t)]i\lambda_2)$, this Hamiltonian can be restated as

$$H(t) = \sum_{a,b,c=1,2,3} \varepsilon_{abc} B_a(t)\,\gamma_b(t)\,\gamma_c(t)$$

where we now treat the Majorana operators in the Heisenberg picture. By application of the Heisenberg equation of motion (in units where $\hbar$ is 1), the time dependence of γ_a is found as

$$\dot{\gamma}_a = 2\varepsilon_{abc} B_b(t)\,\gamma_c(t)$$

where repeated indices are implicitly summed over. We recognize this as having the same form as the equation of motion for a spin-1/2 in a magnetic field which depends on time. If we think of the system in this way, we know that at $t = 0$, $\gamma(0) = \gamma_1$, which would correspond to a spin operator $\sigma(0) = \sigma_1$ for a spin in the field $\mathbf{B}(0) = (i\lambda_1, 0, 0)$. If the magnetic field changes adiabatically, the spin magnetic moment stays aligned with the field, so that at $t = T$, $\sigma(T) = \sigma_3$. By analogy, the Majorana operator will also align with the effective field. The 'direction' of the mode depends on the sign of the field, and we have at $t = T$ that

$$\gamma_3(T) = \mathrm{sgn}(\lambda_1\lambda_2)\,\gamma_1(0)$$

Having established this result, we are ready to consider the remainder of the system. The string connecting the unpaired Majorana modes distinguishes the degenerate pair of ground states.

- At $t = 0$, with $\lambda_2 = \lambda, \lambda_1 = 0$, the left string, which we call P_L, takes the form $(i\,\gamma_9^u\,\gamma_9^l)(i\,\gamma_{10}^r\,\gamma_{10}^u)(i\,\gamma_1^d\,\gamma_1^r)(i\,\gamma_2^l\,\gamma_2^r)(i\,\gamma_3^l\,\gamma_3^d)$.
- At $t = T$, with $\lambda_2 = 0, \lambda_1 = \lambda$, the left string, which we call P_L, takes the form $(i\,\gamma_9^u\,\gamma_9^l)(i\,\gamma_{10}^r\,\gamma_{10}^u)(i\,\gamma_1^d\,\gamma_1^r)(i\,\gamma_2^l\,\gamma_2^r)(i\,\gamma_3^l\,\gamma_3^r)(i\,\gamma_4^l\,\gamma_4^d)$.

Consider the collection of Majorana modes consisting of all Majorana operators contained in the two different string operators. Only three of them enter them Hamiltonian. The time evolution of the ones that do not enter the Hamiltonian is trivial.

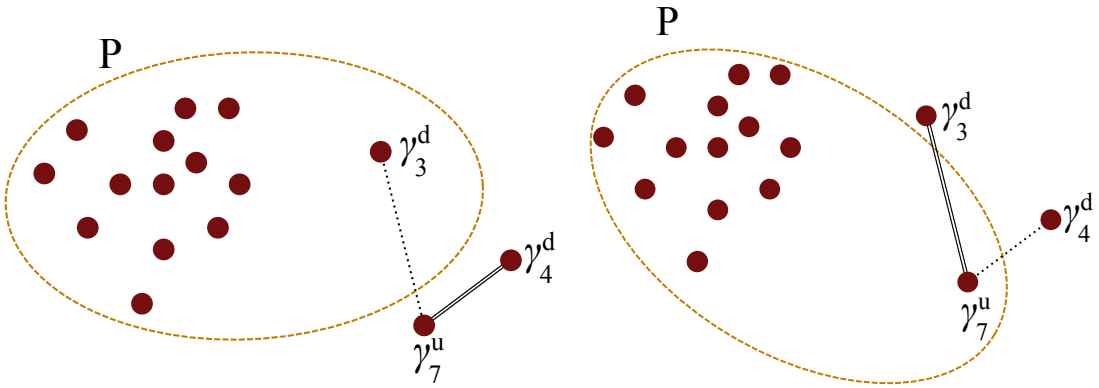

Figure 4.2: Sketch showing how information about the Fermion parity P can be transferred between γ_3^d and γ_4^d by adiabatically turning couplings on and off. The sketch in (a) represents the system at $t = 0$, and the one in (b) at $t = T$.

Figure 4.2 shows the Majorana modes that do not enter the Hamiltonian collected to the left, while the three Majorana operators in the Hamiltonian are to the right. In figure

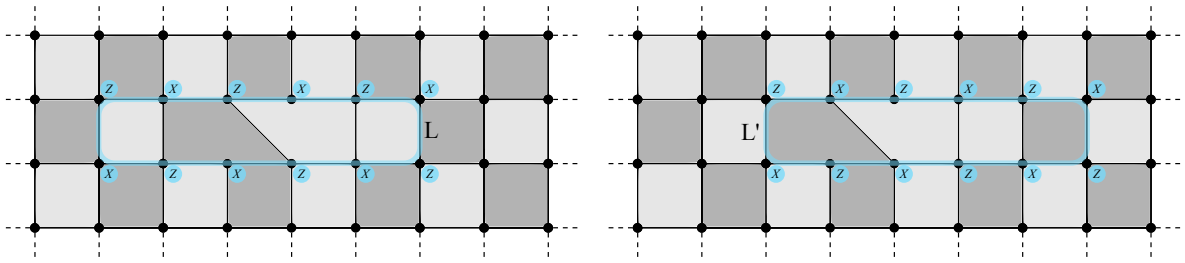

(a) (b)

Figure 4.3: (a) A loop L which is a symmetry of the system. (b) A loop L' which is a symmetry of the system.

4.2a, the dashed line encircles a set of Majorana modes which have a parity $P = \pm 1$. As we tune the tunnel couplings as discussed, we have seen how $\gamma_3(T) = \mathrm{sgn}(\lambda_1\lambda_2)\,\gamma_1(0)$, or in the original notation $\gamma_4^d(T) = \mathrm{sgn}(\lambda_1\lambda_2)\,\gamma_3^d(0)$. Figure 4.2b shows the situation at $t = T$, and because the total parity is conserved, the parity P is now the parity of the same set of Majoranas as before, but with γ_3^d replaced by γ_4^d. In this sense, information about the parity P has been transferred from γ_3^d to γ_4^d.

Protection of the ground states

Previously, a string symmetry connecting the twist defects of the toric code was used to characterize the ground states. We have seen how this amounts to a string connecting the unpaired Majoranas in the physical system. This string plays the role of the parity operator for the pair of unpaired Majoranas.

If we recall the discussion about the transfer of parity information above, we see that the tuning of the couplings λ_1 and λ_2 is the transfer of parity information from the initially unpaired Majorana mode to the finally unpaired one. This means that we can employ a string operator connecting the two unpaired Majorana modes to distinguish between the two ground states, both before and after the adiabatic horizontal shift of the defect. By employing several shifts, the uncoupled Majorana mode can be translated through the system.

We wish to show that the horizontal translation of the Majorana mode in this way does not mix the ground states, or destroy the degeneracy between them. We start by considering the system at $t = 0$. We can construct loop operators, denoted L and L', as shown in 4.3a and 4.3b, respectively.

L and L' both commute with the Hamiltonian, for both $t = 0$ and $t = T$, as well as during the adiabatic process. Both loops could in principle be extended, as long as the alternating order of operators is kept. In the case of many successive translations of the unpaired Majorana mode, this would be necessary for the loops to commute with the Hamiltonian. The loops L and L' are not independent. If we construct the product of the two pentagonal plaquettes and all parallelogram plaquettes separating them at the end of the adiabatic process, we have an operator which, when applied to L (L')

transforms it into L' (L). The transformation of L into L' in this fashion is shown in 4.4. In conclusion, we have that L, at $t = 0$ is equivalent to L' at $t = T$.

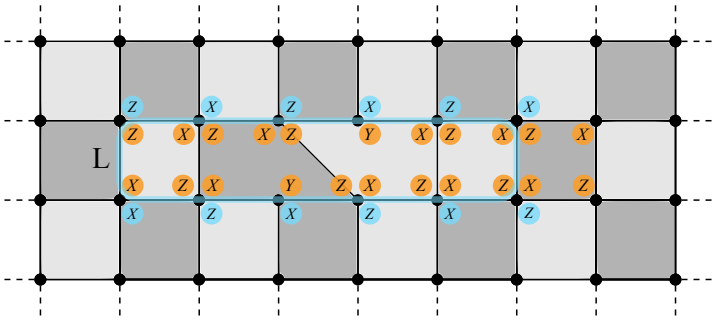

Figure 4.4: By multiplication with all the plaquettes contained within the area demarcated by both L and L', L can be transformed into L', and *vice versa*.

Next, we note that L and L' can be transformed into the parity strings that can be used to differentiate the degenerate ground states. We recall these strings from the discussion in section 2.2 and in particular from eq. 2.2. This is done by multiplying the loops by stabilizers that take the value 1 in the ground states. Figure 4.5a shows how L by multiplication with the appropriate stabilizers is reduced to the parity string connecting the unpaired Majorana modes (figure 4.5c), at $t = 0$. As we have done previously, we label this string P_R. Similarly, figure 4.5b shows how L by multiplication with the appropriate stabilizers is reduced to the symmetry string connecting the unpaired Majorana modes (figure 4.5d), at $t = T$. We label this string P'_R.

To make the argument, we summarize: At $t = 0$, $P_R = L$. At $t = T$, $P'_R = L'$. Furthermore, $L = L'$, and as it commutes with the Hamiltonian at all times, it does not change its eigenvalue during the process. This leads to the conclusion that $P_R = P'_R$. The parity string connecting the unpaired Majorana modes at $t = 0$ and $t = T$, respectively, does not change its value during the process, and thus there are no transitions among the different ground states during the motion of the mode.

This argument extends to further motion. For the process taking the system from the case where there is one parallelogram plaquette, at $t = T$, to the case where there are two, at $t = 2T$, we can apply the same logic. Consider, as above, how L' is equivalent to P'_R. At $t = 2T$, we take a loop L'' which is similar in structure to L, but extended two tetragonal plaquettes further right. This operator i shown in figure 4.6.

At $t = 2T$, there will be two parallelogram plaquettes between the pentagons. Keeping this in mind, we see that by multiplication with the right pentagonal plaquette, the leftmost parallelogram plaquette and the two tetragonal plaquettes adjacent to the pentagons, L'' reduces to a symmetry string, P''_R connecting the unpaired Majorana modes. At $t = 2T$,L'' is equivalent to L' at $t = T$. This can be seen by multiplying L'' by all the plaquettes it encircles. Both loops commute with the Hamiltonian at all times and we can again conclude that P'_R at $t = T$ is equivalent to P''_R at $t = 2T$, and that there are not transitions among different ground states during the process.

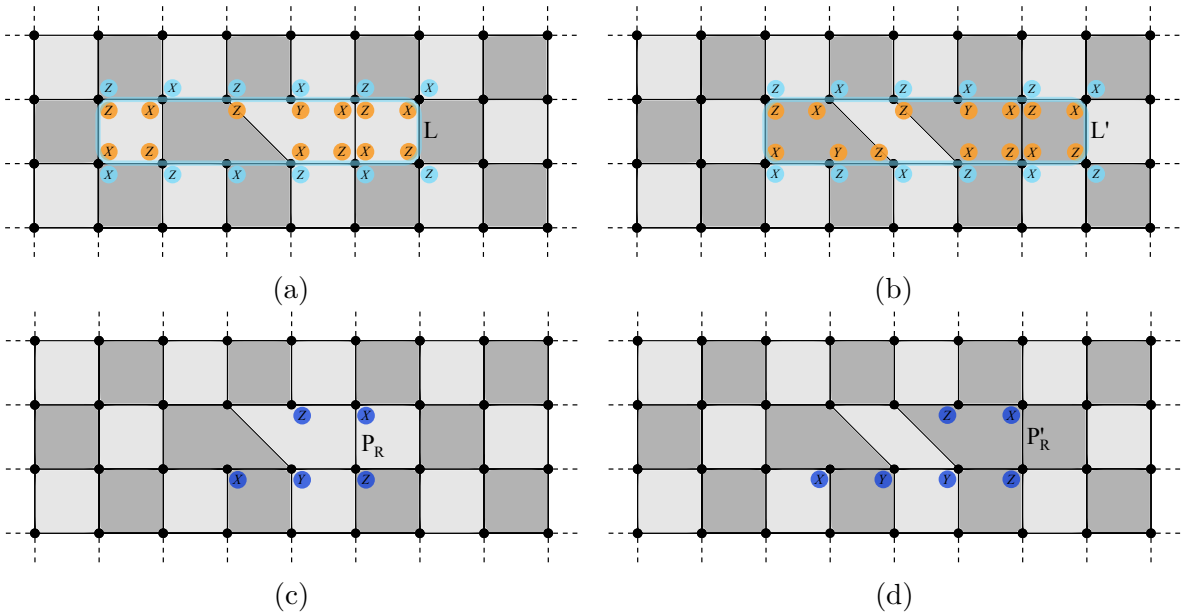

Figure 4.5: (a) The multiplication of L with the plaquettes denoted with orange operators transforms it into the operator P_R as shown in (c). (b) The multiplication of L' with the plaquettes denoted with orange operators transforms it into the operator P'_R as shown in (d).

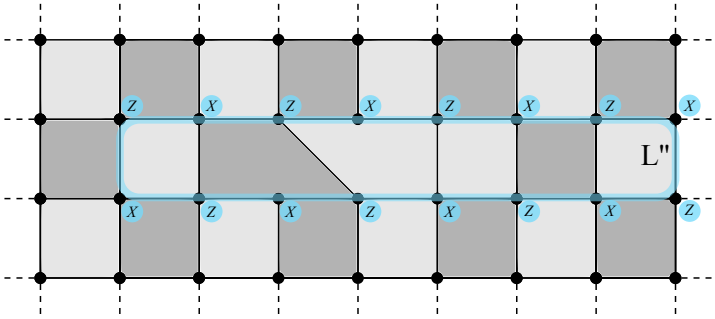

Figure 4.6: A loop L which is a symmetry of the system.

4.1.2 Motion around corners

The Majorana modes can also be moved around corners. Consider the architecture in figure 4.7a. Initially, all couplings except λ_1 and λ_3 (dotted) are on, and the unpaired Majorana mode is γ_1^d. By adiabatically turning λ_1 on, and λ_2 off, we shift the free Majorana mode to γ_6^r. By then adiabatically turning λ_3 on, and λ_4 off, we shift the free Majorana mode to γ_5^r. If we consider the process as consisting of three distinct stages, at times $t = 0, t = T_1$ and $t = T_2$, we can summarize the order in which the couplings are tuned on and off as follows:

1. At $t = 0$, we have $\lambda_1 = 0$, $\lambda_2 = \lambda$, $\lambda_3 = 0$, $\lambda_4 = \lambda$.

2. At $t = T_1$, we have $\lambda_1 = \lambda$, $\lambda_2 = 0$, $\lambda_3 = 0$, $\lambda_4 = \lambda$.

3. At $t = T_2$, we have $\lambda_1 = \lambda$, $\lambda_2 = 0$, $\lambda_3 = \lambda$, $\lambda_4 = 0$.

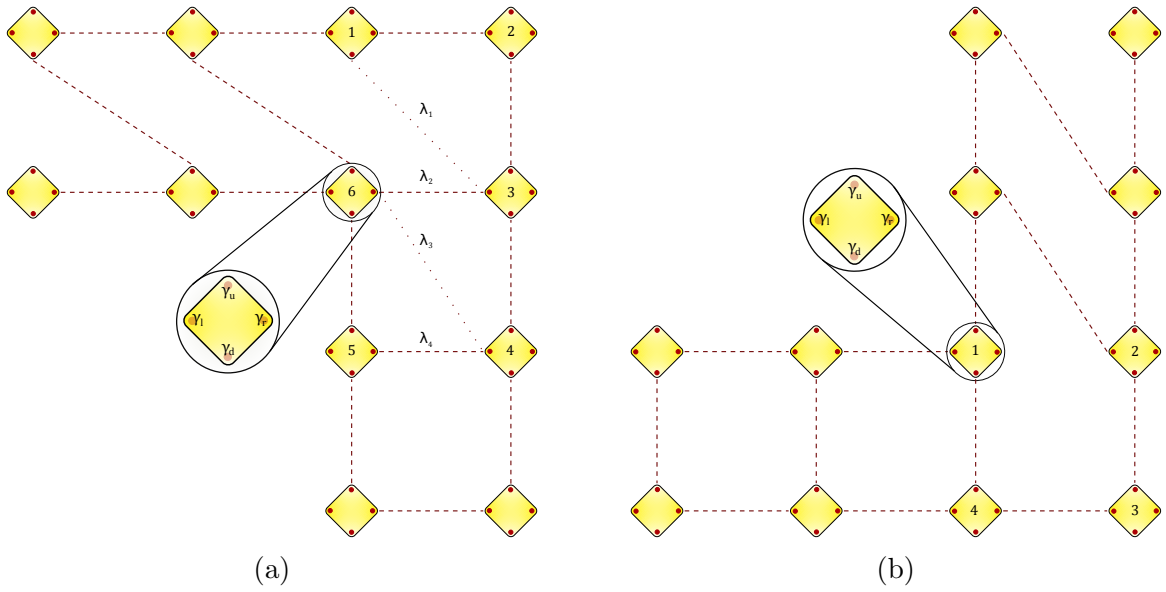

Figure 4.7: (a) A bend structure, where the couplings involved in the adiabatic shift of a Majorana mode around a corner are indicated. (b) The problem with traversing the other kind of corner is illustrated. The unpaired mode γ_1^r cannot be moved around the corner.

The previous argument, using loop operators, extends easily to the scenario where we shift an unpaired mode around a corner. One should define two loops, L and L', related by the operator consisting of all plaquettes between the pair of pentagonal plaquettes. This would be the set of plaquette operators encircled by the product LL'. By multiplication with appropriate stabilizers, L and L' reduce to parity strings. The argument we employed for horizontal motion can then be repeated to show that motion around the corner does not allow transitions between the ground states.

After moving the uncoupled Majorana mode around the corner, it can be shifted vertically by a similar approach as the one used for horizontal shifts. All discussion of loop and string operators is seen to be essentially the same.

Unpaired modes can by this approach be shifted horizontally, vertically, and around the kind of corner shown above. There is also a second kind of corner, shown in figure 4.7b. The difference between the two corners is the following: When moving a mode around the corner in figure 4.7a, we have no diagonal tunnel couplings connected to island 2. When we have the configuration shown in figure 4.7b and want to move the Majorana mode around the bend, we might try to introduce a tunnel coupling $i\,\gamma_1^r\,\gamma_3^u$.

This does not work. We cannot introduce diagonal tunnel couplings to island 3, and so we need a different solution to traverse this kind of corner.

A way around this is to introduce a new kind of superconducting island, which allows for additional intra-island couplings. In the following, we assume that such an island can be made, and show how this solves the problem. We postpone the detailed treatment of this island structure to section 4.9.

Under the assumption that we can make an island allowing for intra-island couplings, we construct a protocol for shifting dislocations around the second kind of corner. With the aid of figure 4.8 we describe this protocol:

1. Initially, couplings λ_1 and λ_3 (dotted in figure 4.8) are off, and the uncoupled Majorana mode is γ_1^r.
2. Switching λ_1 on and λ_2 off, the uncoupled mode becomes γ_4^u.
3. Switching λ_3 on and λ_4 off, the uncoupled mode becomes γ_5^u, and the corner has been traversed.

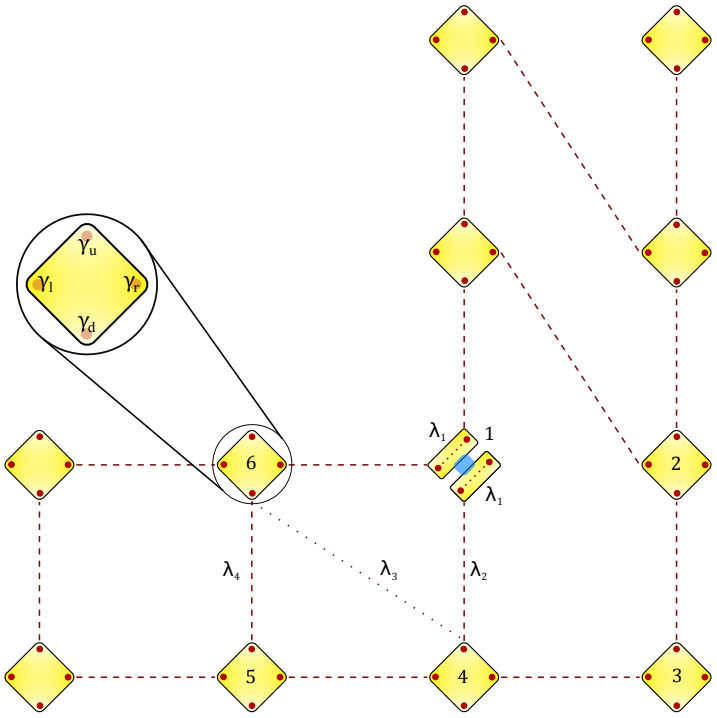

Figure 4.8: Introducing a split island structure (island 1) we are able to shift a Majorana mode around the kind of corner shown in figure 4.7b.

With such a split island structure, we can move Majorana modes both horizontally and vertically. The next section looks at the split island in greater detail, to show that it has the desired properties.

4.2 A split island

To circumvent the problem of traversing the second kind of corner, we look at a modified version of the superconducting islands previously considered. Figure 4.9 shows such an island, which consists of two sub-islands. The two sub-islands are capacitively coupled, and coupled through a Josephson junction, as indicated. Our physical intuition of such a system suggests that in the limit of very strong Josphson coupling, the system of two sub-islands behaves essentially as one island. Conversely, in the limit of very weak Josephson coupling, the islands behave as separate islands. Experimental setups allow for the tuning of the Josephson couplings, so an architecture where that is done is physically realizable [50].

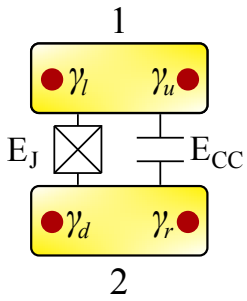

Figure 4.9: The structure of a split island, with capactive and Josephson couplings labelled E_{CC} and E_J, respectively.

The goal of this section is to find out how the two limits of large or small Josephson coupling result in different effective Hamiltonians. The Hamiltonian for this two-island system takes the form

$$\begin{aligned} H =& E_{C_1}\left(Q_1 + q_{\text{ind},1} + P_1\right)^2 + E_{C_2}\left(Q_2 + q_{\text{ind},2} + P_2\right)^2 \\ &+ E_{CC}\left(Q_1 + q_{\text{ind},1} + P_1\right)\left(Q_2 + q_{\text{ind},2} + P_2\right) \\ &- E_J \cos(\phi_1 - \phi_2) - \frac{\Delta}{2}\left((-1)^{Q_1} + (-1)^{Q_2}\right) \end{aligned}$$

The first and second terms are charging terms for the two islands. These take the normal form, with a charging energy coefficient multiplied by the square of the number of charges on the island. The charge on an island is given by the sum of the charge operator, Q_i, the induced charge, $q_{\text{ind},i}$, due to a backgate voltage and the Fermion number operator for the Majorana modes, P_i. The Fermion number operator P_i takes the value 0 (1) if the Majorana modes on island i host 0 (1) fermion.

$$P_1 = \frac{1 + i\,\gamma^l\,\gamma^u}{2}, \quad P_2 = \frac{1 + i\,\gamma^d\,\gamma^r}{2}$$

The third term is the cross capacitance. This is the term describing the capacitive coupling between the two islands. The fourth term is the usual Josephson coupling term, which depends on the relative superconducting phase between the two islands. The last term is a term describing the superconducting pairing in the two separate islands. This effect has been mentioned previously, and it is the energetic penalization of odd electron number in a superconductor.

We relabel

$$Q_i + q_{\text{ind},i} \equiv Q_i'. \tag{4.1}$$

and can rewrite the Hamiltonian as

$$\begin{aligned} H =& E_{C_1}(Q_1' + P_1)^2 + E_{C_2}(Q_2' + P_2)^2 + E_{CC}(Q_1' + P_1)(Q_2' + P_2) \\ & - E_J \cos(\phi_1 - \phi_2) - \frac{\Delta}{2}\left((-1)^{Q_1} + (-1)^{Q_2}\right). \end{aligned} \tag{4.2}$$

There is an amount of charge on each of the two islands. The Josephson term allows for Cooper pair tunnelling between them, and accordingly, there is a commutation relation between the charge operator and the phase operator associated with the tunnelling. For each of the two islands, we have

$$[Q_i', \phi_i] = -2ei \tag{4.3}$$

Where the charge is the charge of all Cooper pair. The charge of a cooper pair is twice that of an electron, which here is accounted for by the factor 2.

We wish to decouple the Hamiltonian into two parts, one related to the total charge of the two islands, and one related to the charge difference. To this end, we define the sum and difference of the charges on the individual islands. For convenience, we also define a label for the total charge of each island:

$$Q_i^t = Q_i + q_{\text{ind},i} + P_i \tag{4.4}$$

$$\begin{pmatrix} Q \\ Q_r \end{pmatrix} = \begin{pmatrix} 1 & 1 \\ 1 & -1 \end{pmatrix} \begin{pmatrix} Q_1' + P_1 \\ Q_2' + P_2 \end{pmatrix} = \begin{pmatrix} 1 & 1 \\ 1 & -1 \end{pmatrix} \begin{pmatrix} Q_1^t \\ Q_2^t \end{pmatrix} \tag{4.5}$$

Finally, we also introduce the relative phase, given by $\phi_r = \phi_1 - \phi_2$.

With the above definitions, and by imposing that $E_{C_1} = E_{C_2} = E_C$ we get

$$H = \left(\frac{E_C}{2} + E_{CC}\right) Q^2 + \left(\frac{E_C}{2} - E_{CC}\right) Q_r^2 - E_J \cos(\phi_1 - \phi_2) - \frac{\Delta}{2}\left((-1)^{Q_1} + (-1)^{Q_2}\right) \tag{4.6}$$

Having rewritten the Hamiltonian in this form, we observe that we have split it in two commuting parts, where one is related to the relative charge and phase, and the

other with the total charge. Symbolically we have $[Q, \cos(\phi_r)] = 0$ and $[Q, Q_r] = 0$ while $[Q_r, \cos(\phi_r)] \neq 0$ and $[Q_r, \phi_r] = -4ei$. Based on the last commutator, we know that ϕ_r and Q_r are conjugate quantities. We have that $Q_r = Q_1' - Q_2'$, and by letting this operator work on the function $g(\phi_r(\phi_1, \phi_2)$ we find its explicit form:

$$\begin{aligned} Q_r g\left(\phi_r(\phi_1, \phi_2)\right) &= (Q_1' - Q_2')g\left(\phi_r(\phi_1, \phi_2)\right) \\ &= -2ei(\partial_{\phi_1} - \partial_{\phi_2})g\left(\phi_r(\phi_1, \phi_2)\right) \\ &= -2ei\left(\frac{\partial g}{\partial \phi_r}\frac{\partial \phi_r}{\partial \phi_1} - \frac{\partial g}{\partial \phi_r}\frac{\partial \phi_r}{\partial \phi_2}\right) \\ &= -2ei\left(2\frac{\partial g}{\partial \phi_r}\right) \end{aligned} \tag{4.7}$$

By removing the test function we obtain

$$Q_r = -4ei\frac{\partial}{\partial \phi_r}, \quad \text{and we define} \quad n_r \equiv \frac{Q_r}{4e} = -2i\frac{\partial}{\partial \phi_r} \tag{4.8}$$

Where the operator n_r now counts the difference in the number of Cooper pairs on each island, when it is divided by two. Thus, if the relative number of Cooper pairs between the islands were four, the operator n_r would return the value two.

The Hamiltonian has effectively been split into two commuting parts, which can be solved separately. The part related to the total charge is not affected by the introduction of E_J, and therefore we focus on the part in Q_r, which reads

$$\begin{aligned} H_r &= \left(\frac{E_C}{2} - E_{CC}\right)Q_r^2 + E_J\cos(\phi_r) \\ &= E_r Q_r^2 + E_J\cos(\phi_r) \end{aligned}$$

We can take the total charge, Q, to be zero, at the cost of a constant energy shift. We can thus consider only one sector of the Hamiltonian, labelled by the value of Q. The different sectors are equivalent, up to an energy shift. Within one such sector, the total charge of both islands does not change.

We can express the Hamiltonian in the number basis of n_r to clarify the effect of the Josephson term. We rewrite the Josephson term as $E_J\cos(\phi_r) = E_J/2(e^{i\phi_r} + e^{-i\phi_r})$. The matrix elements of these operators are

$$\langle n|e^{\pm i\phi_r}|m\rangle = \frac{1}{\sqrt{2\pi}}\int e^{-in\phi_r}e^{\pm i\phi_r}e^{im\phi_r}d\phi_r = \frac{1}{\sqrt{2\pi}}\int e^{i(m\pm 1-n)\phi_r}d\phi_r = \delta_{m\pm 1,n}$$

The Hamiltonian takes the form

$$H = \sum_n 16E_r\left(n_r + p_1 - p_2\right)^2|n\rangle\langle n| + \frac{E_J}{2}\left(|n+1\rangle\langle n| + |n\rangle\langle n+1|\right)$$

where the labels n, m denote half the number of difference of the number of Cooper pairs, and not single Cooper pairs nor single charges.

We consider the sector for which $Q = 0$. We will label states of the system by the charges and parities (the even- or oddness of the Fermion occupation number) of the the two islands. We write these states as $|Q_1, Q_2, P_1, P_2\rangle$. These states can be grouped into two categories: Those with $P_1 = P_2 = 0$ and $P_1 = P_2 = 1$, respectively. States belonging to these two parity sectors were degenerate on the four-Majorana islands we have been considering up until now. In the limit of small Josephson coupling, where we effectively have two separated islands, they are not degenerate, due to the superconducting pairing effect. This is accounted for by the term $\Delta/2((-1)^{Q_1} + (-1)^{Q_2})$ in the Hamiltonian.

We proceed now to analyze two different regimes: that where the relative charge term dominates, and that where the Josephson tunnelling term dominates. First, we neglect the Josephson term, and consider states where the number of charges on individual islands is well-defined.

The ground state is the state $|0, 0, 0, 0\rangle$, as it minimizes the terms of the Hamiltonian in eq. 4.2. If the parity effect is neglected, we see that the state $|-1, -1, 1, 1\rangle$ would also be a ground state.

If the Josephson tunnelling term becomes large, due to the ratio E_C/E_J being small, quantum fluctuations are dominant. In this regime, the Josephson term is the important one and we can neglect the charging terms.

With this term as the dominant one, we have two different kind of eigenstates. One kind is of the form $|\pm 2n, \mp 2n, 0, 0\rangle$, of which $|0, 0, 0, 0\rangle$ is an example, while the other is of the form $|-(2n+2), 2n, 1, 1\rangle$ of which $|-2, 0, 1, 1\rangle$ is an example. The second kind of state differs from the first by belonging to the parity sector where $P_1 = P_2 = 1$. If the ratio E_C/E_J is large, these two states are not degenerate.

In order to see how the energy levels of the system change with changing E_J/E_r-ratio, we truncate the Hamiltonian and calculate the eigenvalues numerically as functions of E_J, with E_r set to one.

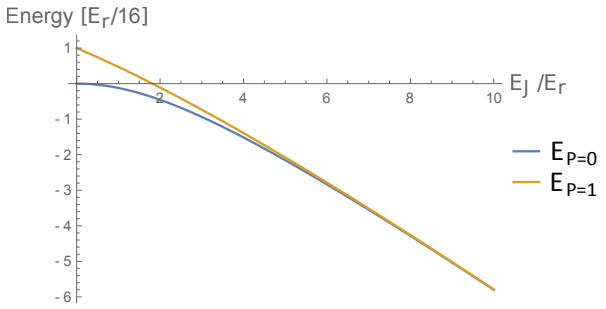

Figure 4.10: Plot of the two lowest energy levels of the system. In the limit of small E_J/E_r-ratio, states of parity sectors $P = 0$ and $P = 1$ are not degenerate. In the limit of large E_J/E_r-ratio, they become degenerate.

Figure 4.10 shows that in the limit of strong E_J, the two separate islands behave as

one, and that the two parity states become degenerate. In the following, we will find an analytical mapping to the transmon model, which will allow us to establish the result beyond numerics.

Equivalence with the transmon model

Following van Heck *et al* [51], we impose the restriction on the wavefunction that

$$\Psi(\phi_1 + 2\pi, \phi_2) = e^{iP_1\pi}\Psi(\phi_1, \phi_2)$$
$$\Psi(\phi_1, \phi_2 + 2\pi) = e^{iP_2\pi}\Psi(\phi_1, \phi_2)$$

In terms of the relative phase $\phi_r = \phi_1 - \phi_2$ we have

$$\phi_1 \to \phi_1 + 2\pi \Rightarrow \phi_r \to \phi_r + 2\pi$$
$$\phi_2 \to \phi_2 - 2\pi \Rightarrow \phi_r \to \phi_r + 2\pi$$

Thus we can write the boundary conditions for $\Psi(\phi_r)$ by attaching a global phase $U = e^{-iP\phi_r/2}$ to the wavefunction. The number P is 1 for the parity sector where $P_1 = P_2 = 1$, and 0 for the parity sector where $P_1 = P_2 = 0$. The number P can be expressed as $P = Q_r/2 \mod 2$.

$$\Psi(\phi_r + 2\pi) = e^{iP\pi}\Psi(\phi_r)$$

This new boundary condition ensures that the charge operator returns the correct number of charges when applied to the wave function.

There are two cases:

- If $P = 0$, $\Psi(\phi_r + 2\pi) = \Psi(\phi_r)$. Writing this in the plane wave basis, we have $\exp(iq_r(\phi_r + 2\pi)) = \exp(iq_r\phi_r)$. It is clear that q_r must take an integer value to satisfy this. As $Q_r = -4ei\partial_{\phi_r}$, applying it to the wave function returns an even number of charges of the form $4en$, with n an integer. We have already seen how this is the relative charge between the islands in the $P = 0$-sector.
- If $P = 1$, $\Psi(\phi_r + 2\pi) = -\Psi(\phi_r)$. Now, $\exp(iq_r(\phi_r + 2\pi)) = -\exp(iq_r\phi_r)$ is satisfied for q_r being a half-integer, and so, applying Q_r to the wave function yields a relative charge of the form $4en + 2e$, which is the form the relative charge must take for the $P = 1$-sector.

Having seen that these twisted boundary conditions are a necessary requirement, we consider how this gauge transformation changes the operator Q_r^2.

$$\hat{Q}_r'^2\Psi' = (U\hat{Q}_rU^\dagger)^2U\Psi = U\hat{Q}_r{}^2U^\dagger U\Psi = U\hat{Q}_r{}^2U^\dagger\Psi'$$

$$
\begin{aligned}
e^{-iP\phi_r/2}\hat{Q}_r^2 e^{iP\phi_r/2} e^{-iP\phi_r/2}\Psi(\phi_r) &= (-4ei\partial_{\phi_r})^2 e^{iP\phi_r/2}\Psi'(\phi_r) \\
&= (-4ei)^2\left(\left(\frac{iP}{2}\right)^2 + iP\partial_{\phi_r} + \partial_{\phi_r}^2\right)\Psi'(\phi_r) \\
&= (4e)^2\left(\left(\frac{P}{2}\right)^2 - iP\partial_{\phi_r} - \partial_{\phi_r}^2\right)\Psi'(\phi_r) \\
&= (4e)^2\left(-i\partial_{\phi_r} + \frac{P}{2}\right)^2\Psi'(\phi_r) \\
&= (-4ei\partial_{\phi_r} + 2eP)^2\,\Psi'(\phi_r) \\
&= \left(\hat{Q}_r + 2eP\right)^2\Psi'(\phi_r)
\end{aligned}
$$

The gauge transformation sends $\hat{Q}_r^2 \to (\hat{Q}_r + 2eP)^2$, and the Hamiltonian is brought to the form

$$H_{\text{tr}} = 16e^2E_r(-i\partial_{\phi_r} + \alpha P)^2 - E_J\cos(\phi_r)$$

,

where $\alpha = 1/2$.

This is the same model as that of a Cooper-pair box system [52], and that of the transmon system explored by Koch *et al* [53]. The charging energy in that model corresponds to $4E_re^2$ in our model. We absorb the square of the electron charge in our energy by letting $e^2E_r = E_r'$.

In the transmon model, the difference in energy of the mth eigenstate of the Hamiltonian when the gate charge is respectively $1/2$ and 0, is given by

$$\epsilon_m' = E_m(n_g = 1/2) - E_m(n_g = 0)$$

In our model, this corresponds to the energy difference

$$\epsilon_m = E_m(P = 1) - E_m(P = 0)$$

For the transmon model, this energy difference has been shown to decay exponentially with increasing E_J/E_r-ratio. The difference in terms of the original transmon parameters is

$$\epsilon_m \simeq (-1)^m E_C\frac{2^{4m+5}}{m!}\sqrt{\frac{2}{\pi}}\left(\frac{E_J}{2E_C}\right)^{\frac{m}{2}+\frac{3}{4}}\exp\left(-\sqrt{\frac{8E_J}{E_C}}\right)$$

We are only interested in the ground state. Setting $m = 0$ and rewriting the difference in terms of the parameters of the split island system, we have

$$\begin{aligned}\epsilon_0 &\simeq 4E_r' 2^5 \sqrt{\frac{2}{\pi}} \left(\frac{E_J}{8E_r'}\right)^{\frac{3}{4}} \exp\left(-\sqrt{\frac{2E_J}{E_r'}}\right) \\ &\simeq E_r' 2^7 \sqrt{\frac{2}{\pi}} \left(\frac{E_J}{8E_r'}\right)^{\frac{3}{4}} \exp\left(-\sqrt{\frac{2E_J}{E_r'}}\right)\end{aligned}$$

By adjusting the ratio E_J/E_C, one can go from a situation in which the splitting is vanishingly small, and states belonging to separate parity sectors are degenerate, to a situation in which the splitting is large, and they are not degenerate. The question is essentially when the two separate superconducting islands are so strongly coupled that they reduce to one superconducting island, which corresponds to the four-Majorana islands that we have discussed previously.

In the limit of large E_J/E_C, Koch *et al* show how the Hamiltonian takes the form

$$\begin{aligned}H_{\text{eff}}(P) &= H_{\text{tr}}(\alpha P = 1/4) - \frac{\epsilon_0}{2}\cos(2\pi\alpha P) \\ &= H_{\text{tr}}(\alpha P = 1/4) - \frac{\epsilon_0}{2}\cos(\pi P)\end{aligned}$$

The cosine function takes the value 1 (-1) for P = 0 (P=1). Recalling that the parities for the individual islands takes the form $P_1 = i\,\gamma_1\,\gamma_2$, $P_2 = i\,\gamma_3\,\gamma_4$, we can write the effective Hamiltonian as

$$\begin{aligned}H_{\text{eff}}(P) &= H(\alpha P = 1/4) - \frac{\epsilon_0}{2} i\,\gamma_1\,\gamma_2 \\ &= H(\alpha P = 1/4) - \frac{\epsilon_0}{2} i\,\gamma_3\,\gamma_4\,.\end{aligned}$$

Thus effective intra-island couplings are introduced in the Hamiltonian. This concludes our discussion of this system, where we have seen that we can get the kind of coupling required to traverse the second kind of corner by tuning the Josephson coupling strength, E_J.

4.3 Braiding

With the split island structure, it also becomes possible to perform braiding operations. We will look at the small section of the planar code marked in figure 4.11. We show how two Majorana modes can be braided in four steps. We employ figure 4.12 as a visual aid. The two Majorana modes that are braided are referred to as γ_2 and γ_3. To avoid clutter in figure 4.12, we only label the islands in the top-left panel. This labelling should be understood as valid for all panels in 4.12.

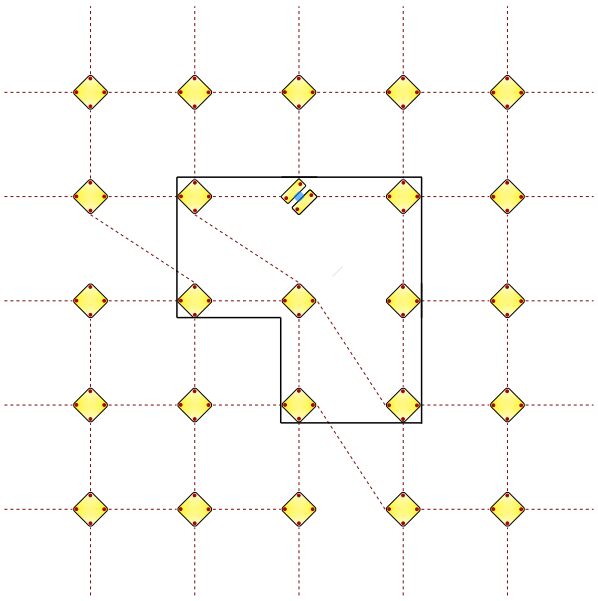

Figure 4.11: A sketch of the system, with the black line demarcating the subsection of the system relevant to the braiding procedure.

1. For this step, we use figure 4.12a and 4.12b as a visual aid. Initially, the unpaired Majorana modes γ_2 and γ_3 are γ_1^d and γ_3^l, respectively. By switching on the coupling $i\,\gamma_1^d\,\gamma_1^r$ of the split island and switching off the coupling $i\,\gamma_1^r\,\gamma_2^l$, γ_2 is moved to γ_2^l.

2. For this step, we use figure 4.12b and 4.12c as a visual aid. Initially, the unpaired Majorana modes γ_2 and γ_3 are γ_2^l and γ_3^l, respectively. By switching on the coupling $i\,\gamma_1^r\,\gamma_3^l$ and switching off the coupling $i\,\gamma_1^d\,\gamma_1^r$, γ_3 is moved to γ_1^d.

3. For this step, we use figure 4.12c and 4.12d as a visual aid. Initially, the unpaired Majorana modes γ_2 and γ_3 are γ_2^l and γ_1^d, respectively. By switching on the coupling $i\,\gamma_1^r\,\gamma_2^l$ and switching off the coupling $i\,\gamma_1^r\,\gamma_3^l$, γ_2 is moved to γ_3^l. This successfully exchanges γ_2 and γ_3.

4.3.1 Calculation of the Berry phase of the braiding

We wish to calculate how the wave function changes under the braiding operation which was described in detail above. At the beginning and end of the process, the Hamiltonian is the same. The process is therefore a closed loop in the parameter space of the Hamiltonian. We can compute the Berry phase associated with this evolution. We start by noticing that the braiding essentially concerns four Majorana modes. The mode circled in green in figure 4.12 is the central mode, and throughout the process, it is always strongly coupled to one of three other modes. This central mode is γ_1^r. In

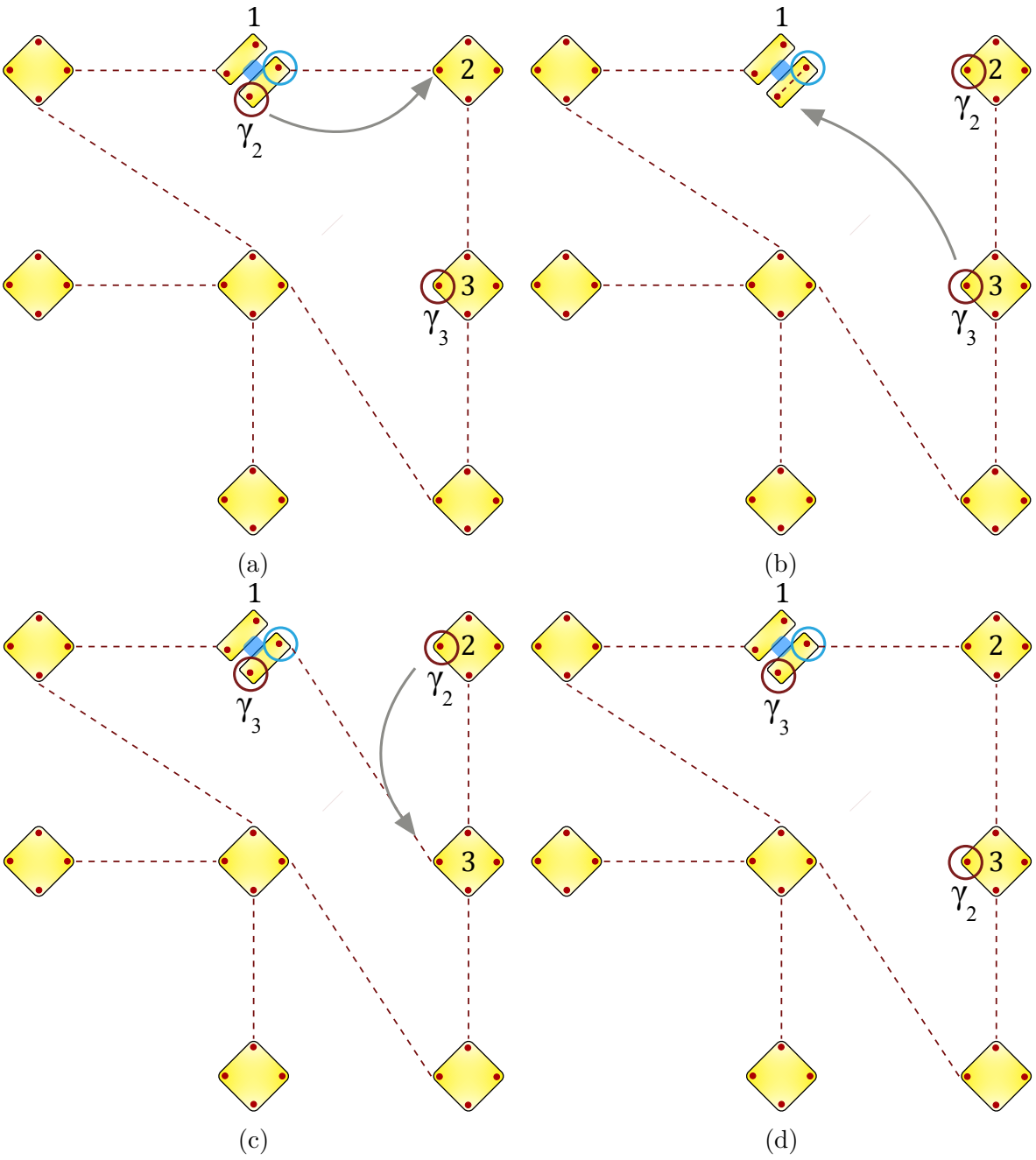

Figure 4.12: The various steps in the braiding process are illustrated. (a) is at $t = 0$ and (d) at $t = T$.

figure 4.12a, γ_1^r is coupled to the mode γ_2^l, in figure 4.12b to the mode γ_1^d and in figure 4.12c to the mode γ_3^l. We label this central mode γ_a. Furthermore, we label γ_2^l, γ_1^d and γ_3^l by γ_b, γ_2 and γ_3, respectively.

Two of these modes, namely γ_2 and γ_3, belong to the set of four unpaired Majorana modes we have been considering so far. The two other ones, γ_a and γ_b, are auxiliary

modes, and constitute a Fermion mode which we label c_{aux}. This system has been considered in the literature, and in the following, our approach mimics that presented in [54]. Recall the definitions of the Majorana modes in eq. 1.9. We then have two Fermion modes given by

$$c_{23} = \frac{\gamma_2 + i\,\gamma_3}{2}, \quad c_{\text{aux}} = \frac{\gamma_a + i\,\gamma_b}{2}$$

We formulate a Hamiltonian containing the relevant couplings and Majorana modes:

$$H = \sum_n \lambda_n i\,\gamma_a\,\gamma_n$$

Here, λ_n denotes the coupling strength between the central Majorana mode, γ_a, and the mode γ_n, where n is either $b, 2$ or 3. If we consider each panel of figure 4.12 as a step in the adiabatic process, labelling the steps by the subfigure indices a), b) and so on, we can construct a table:

Table 4.1: Table showing the various coupling strengths at the different stages of the braiding process.

	λ_b	λ_2	λ_3
a)	M	0	0
	M	M	0
b)	0	M	0
	0	M	M
c)	0	0	M
	M	0	M
d)	M	0	0

We see that the Hamiltonian goes through a closed loop in parameter space, so that it at points a) and d) is the same. By finding the ground states of the Hamiltonian, we may calculate the Berry connections and thereby the Berry phase.

Recall the definitions of the Majorana modes in eq. 1.9. If we express the Majorana modes of the Hamiltonian in terms of Fermion modes, we can find the Hamiltonian matrix elements. In the basis spanned by the states

$$c_{23} = \frac{\gamma_2 + i\,\gamma_3}{2}, \quad c_{\text{aux}} = \frac{\gamma_a + i\,\gamma_b}{2}$$

$$\gamma_a = c^\dagger_{\text{aux}} + c_{\text{aux}}, \quad \gamma_b = i(c^\dagger_{\text{aux}} - c_{\text{aux}}), \quad \gamma_2 = c^\dagger_{23} + c_{23}, \quad \gamma_3 = i(c^\dagger_{23} - c_{23})$$

In terms of the Fermion operators, the Hamiltonian takes the form

$$\begin{aligned} H_{int} = H_1 + H_2 + H_3 &= \sum_{k=1}^{3} \lambda_k i\gamma_0\gamma_k \\ &= -\lambda_b(c^\dagger_{\text{aux}} + c_{\text{aux}})(c^\dagger_{\text{aux}} - c_{\text{aux}}) \\ &\quad + i\lambda_2(c^\dagger_{\text{aux}} + c_{\text{aux}})(c^\dagger_{23} + c_{23}) \\ &\quad - \lambda_3(c^\dagger_{\text{aux}} + c_{\text{aux}})(c^\dagger_{23} - c_{23}) \end{aligned}$$

In the Fock basis $\{|0_{23}0_{\text{aux}}\rangle, |0_{23}1_{\text{aux}}\rangle, |1_{23}0_{\text{aux}}\rangle, |1_{23}1_{\text{aux}}\rangle\}$ we can find the matrix elements of the Hamiltonian. We use that

$$|0_{23}1_{\text{aux}}\rangle = c^\dagger_{\text{aux}}|0_{23}0_{\text{aux}}\rangle, \quad |1_{23}0_{\text{aux}}\rangle = c^\dagger_{23}|0_{23}0_{\text{aux}}\rangle, \quad |1_{23}1_{\text{aux}}\rangle = c^\dagger_{23}c^\dagger_{\text{aux}}|0_{23}0_{\text{aux}}\rangle,$$

As before, the total Fermion parity of the system is conserved, and the Hamiltonian therefore splits into two blocks; one for the even and one for the odd parity subsector.

We find the matrix element $\langle n_{23}n_{\text{aux}}|H_b|n'_{23}n'_{\text{aux}}\rangle$, where we allow for the two occupation number states to be different, indicated by the prime, as follows:

$$\begin{aligned} \langle n_{23}n_{\text{aux}}|H_b|n'_{23}n'_{\text{aux}}\rangle &= -\lambda_b\langle n_{23}n_{\text{aux}}|(c_{\text{aux}}c^\dagger_{\text{aux}} - c^\dagger_{\text{aux}}c_{\text{aux}}|n'_{23}n'_{\text{aux}}\rangle \\ &= -2\lambda_b\langle n_{23}n_{\text{aux}}|\hat{n}_{\text{aux}}|n'_{23}n'_{\text{aux}}\rangle + \lambda_1\langle n_{23}n_{\text{aux}}|n'_{23}n'_{\text{aux}}\rangle \end{aligned}$$

This means that for different occupation number states, the element $\langle n_{23}n_{\text{aux}}|H_b|n'_{23}n'_{\text{aux}}\rangle$ is zero, while the elements $\langle 0_{23}0_{\text{aux}}|H_b|0_{23}0_{\text{aux}}\rangle = \langle 1_{23}0_{\text{aux}}|H_b|1_{23}0_{\text{aux}}\rangle = \lambda_b$ and $\langle 0_{23}1_{\text{aux}}|H_b|0_{23}1_{\text{aux}}\rangle = \langle 1_{23}1_{\text{aux}}|H_b|1_{23}1_{\text{aux}}\rangle = -\lambda_b$.

For the anti-diagonal elements, the matrix elements containing H_b are zero, while the other two terms do not vanish. For ease of reading, we suppress the subscripts on the occupation numbers below, and show how to calculate one of these elements:

$$\begin{aligned} \langle 00|H|11\rangle &= \langle 00|H_2|11\rangle + \langle 00|H_3|11\rangle = i\lambda_2\langle 00|c_{\text{aux}}c_{23}|11\rangle - \lambda_3\langle 00| - c_{\text{aux}}c_{23}|11\rangle \\ &= i\lambda_2 + \lambda_3 \end{aligned}$$

The remaining elements are calculated similarly, and the Hamiltonian matrix takes the form

$$H = \begin{pmatrix} \lambda_b & 0 & 0 & i\lambda_2 + \lambda_3 \\ 0 & -\lambda_b & i\lambda_2 + \lambda_3 & 0 \\ 0 & -i\lambda_2 + \lambda_3 & \lambda_b & 0 \\ -i\lambda_2 + \lambda_3 & 0 & 0 & -\lambda_b \end{pmatrix}$$

The Hamiltonian found in the paper by Van Heck *et al* [54] becomes the Hamiltonian above under a simple relabelling of the coupling strengths. The two degenerate ground states of the Hamiltonian are

$$|e\rangle = \sqrt{\frac{\varepsilon+\lambda_b}{2\varepsilon}}\begin{pmatrix} i\frac{\lambda_b-\varepsilon}{\lambda_2+i\lambda_3} \\ 0 \\ 0 \\ 1 \end{pmatrix}, \qquad |o\rangle = \sqrt{\frac{\varepsilon-\lambda_b}{2\varepsilon}}\begin{pmatrix} 0 \\ i\frac{\lambda_b+\varepsilon}{\lambda_2+i\lambda_3} \\ 1 \\ 0 \end{pmatrix}$$

The ground state vectors are labelled by e and o, indicating even or odd quasiparticle number. We can compute the Berry connection matrices from these vectors as

$$\mathcal{A}_k = \begin{pmatrix} \langle e|\frac{d}{d\lambda_k}|e\rangle & 0 \\ 0 & \langle o|\frac{d}{d\lambda_k}|o\rangle \end{pmatrix}$$

Explicitly calculating the connection matrices yields

$$\mathcal{A}_b = \begin{pmatrix} 0 & 0 \\ 0 & 0 \end{pmatrix}, \quad \mathcal{A}_2 = \frac{\lambda_3}{\lambda_2^2+\lambda_3^2}\begin{pmatrix} i\frac{\varepsilon-\lambda_b}{2\varepsilon} & 0 \\ 0 & i\frac{\varepsilon+\lambda_b}{2\varepsilon} \end{pmatrix}, \quad \mathcal{A}_3 = \frac{-\lambda_2}{\lambda_2^2+\lambda_3^2}\begin{pmatrix} i\frac{\varepsilon-\lambda_b}{2\varepsilon} & 0 \\ 0 & i\frac{\varepsilon+\lambda_b}{2\varepsilon} \end{pmatrix}$$

The closed path in parameter space followed by the Hamiltonian gives the Berry phase, contained in the adiabatic time evolution operator:

$$U = \exp\left(-\oint_{\mathcal{C}} \sum_k A_k d\lambda_k\right) \tag{4.9}$$

The details of the calculation of this operator are deferred to the appendices. The result of the computation is that

$$U = \exp\left(-i\frac{\pi}{4}\sigma_z\right) \tag{4.10}$$

This is in the basis spanned by $\{|e\rangle, |o\rangle\}$, with the even and odd subspace being those of the number states for the Fermion modes (c_{23}, c_{aux}). We may write this as

$$U = e^{-i\pi/4}|e\rangle\langle e| + e^{i\pi/4}|o\rangle\langle o|$$

Thus, if we at time $t = 0$ have the state $|e\rangle$, we at time $t = T$ have $U|e\rangle = e^{-i\pi/4}$.

We assume that the occupation of the number state for c_{aux} at $t = 0$ and $t = T$ is 1, as the tunnel coupling $i\lambda_b\gamma_a\gamma_b$ at these times is on, making the occupation number 1 more stable than 0. We select the matrix elements

$$\langle 0_{23}1_{\text{aux}}|U|0_{23}1_{\text{aux}}\rangle = e^{i\pi/4}, \quad \langle 1_{23}1_{\text{aux}}|U|1_{23}1_{\text{aux}}\rangle = e^{-i\pi/4},$$
$$\langle 0_{23}1_{\text{aux}}|U|1_{23}1_{\text{aux}}\rangle = \langle 1_{23}1_{\text{aux}}|U|0_{23}1_{\text{aux}}\rangle^* = 0$$

If we now remove the auxiliary Fermion, we get the even and odd subspace blocks of the braiding operator in the basis of number states for the Fermion modes (c_{23}, c_{14}). Ordering the basis as $(|00\rangle, |11\rangle, |01\rangle, |10\rangle)$, we have

$$U = \begin{pmatrix} e^{i\pi/4} & 0 & 0 & 0 \\ 0 & e^{-i\pi/4} & 0 & 0 \\ 0 & 0 & e^{i\pi/4} & 0 \\ 0 & 0 & 0 & e^{-i\pi/4} \end{pmatrix}.$$

We can now rotate the even and odd subspace blocks into the representation spanned by number states of (c_{12}, c_{34}), by recalling the discussion in section 1.2.1; in particular eq. 1.12. If we select the even subspace block, we see that it can be written as $e^{i\pi\,\sigma_z/4}$. The matrix connecting the bases (c_{23}, c_{14}) and (c_{12}, c_{34}) is

$$\mathbf{U}_{12\to 14} = \sqrt{\frac{1}{2}} \begin{pmatrix} 1 & 1 \\ 1 & -1 \end{pmatrix}.$$

We find the time evolution operator in the basis (c_{12}, c_{34}) as

$$\boxed{U(T) = \mathbf{U}_{12\to 14} e^{i\pi\,\sigma_z/4} \mathbf{U}^{\dagger}_{12\to 14} = e^{i\,\sigma_x\,\pi/4}} \tag{4.11}$$

These results are consistent with the expected outcome of a braiding of the Majorana modes, as discussed in chapter 1.

Had we instead assumed that the occupation number state for the auxiliary Majorana Fermion was 0 we would have found

$$\langle 0_{23}0_{\text{aux}}|U|0_{23}0_{\text{aux}}\rangle = e^{-i\pi/4}, \quad \langle 1_{23}0_{\text{aux}}|U|1_{23}0_{\text{aux}}\rangle = e^{i\pi/4},$$
$$\langle 1_{23}0_{\text{aux}}|U|0_{23}0_{\text{aux}}\rangle = \langle 0_{23}0_{\text{aux}}|U|1_{23}0_{\text{aux}}\rangle^* = 0$$

And we get the opposite result. This is related to the 'chirality' of the junction. The word chirality is used here to illustrate that depending on the negative or positive value of the quantity $\text{sgn}(\lambda_b\lambda_2\lambda_3)$, we find the braiding operator $e^{-i\,\sigma_x\,\pi/4}$ or $e^{i\,\sigma_x\,\pi/4}$. We saw this effect at the start of chapter 4, where the calculation due to Sau, Tewari and Clarke provided a similar result. One could imagine that in a real system, the sign of the coupling constants might not be known, and one would perform measurements to determine the chiralities of the junctions. This information could then be used to realize whether one should perform a given adiabatic process or its inverse to obtain the desired quantum gate.

4.3.2 Calculation of braiding outcome using string operators

We can also obtain this braiding result from a simpler calculation, using string symmetries.

Consider the three operators shown in 4.13. At the start of the process ($t = 0$), the stings labelled P_L and A commute with the Hamiltonian, and are therefore symmetries. At the end of the process ($t = T$), P'_L commutes with the Hamiltonian and is a symmetry of the system.

These operators are string operators connecting unpaired Majoranas. We used such string symmetries extensively in chapters 2 and 3. Recall for example the discussion relating to the horizontal motion of a Majorana mode. Such string symmetries square to unity. Consider the split island in the figure. We will number this split island as island N. The product of P_L and A will trivially give the factors of P'_L on all islands but this one. For this specific island, we have the product $(i\,\gamma_N^l\,\gamma_N^d)(i\,\gamma_N^d\,\gamma_N^r) = i(i\,\gamma_N^c\,\gamma_N^a)$. We therefore have that

$$P_L A = iP'_L.$$

In addition, because the pair of operators P_L and A share a single Majorana mode, we have

$$\{P_L, A\} = 0 \quad \Rightarrow \quad \{P'_L, A\} = 0$$

and as a consequence

$$P_L P'_L = P_L P_L A = -P_L A P_L = -P'_L P_L \quad \Rightarrow \quad \{P_L, P'_L\}$$

We recall from 1.10 that the parity of the left dislocation pair is encoded by the operator $i\,\gamma_2\,\gamma_1$, corresponding to σ_z. The parity operator $i\,\gamma_1\,\gamma_3$ corresponds to σ_y, and $i\,\gamma_3\,\gamma_2$ to σ_x. Based on this we make the association

$$\boxed{P_L \equiv -\sigma_z, \quad A \equiv -\sigma_x, \quad P'_L \equiv \sigma_y} \tag{4.12}$$

the operators fulfil the appropriate commutation and product relations. Prior to the braiding operation, the Fermion parity operator of the left Majorana pair will be the string operator B_1. The braiding process exchanges Majoranas, so that the Fermion parity operator for the left pair becomes B'_1. In the Heisenberg picture, this transformation can be written as

$$U(T) P_L U^\dagger(T) = P'_L$$

which in terms of Pauli operators reads

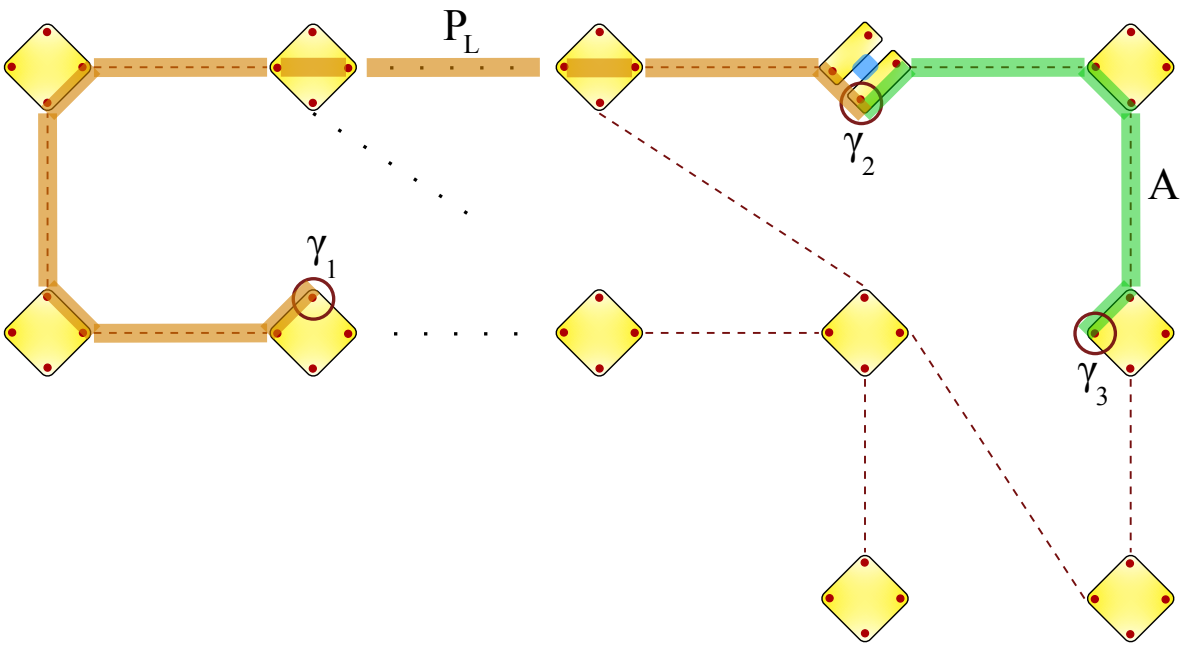

(a)

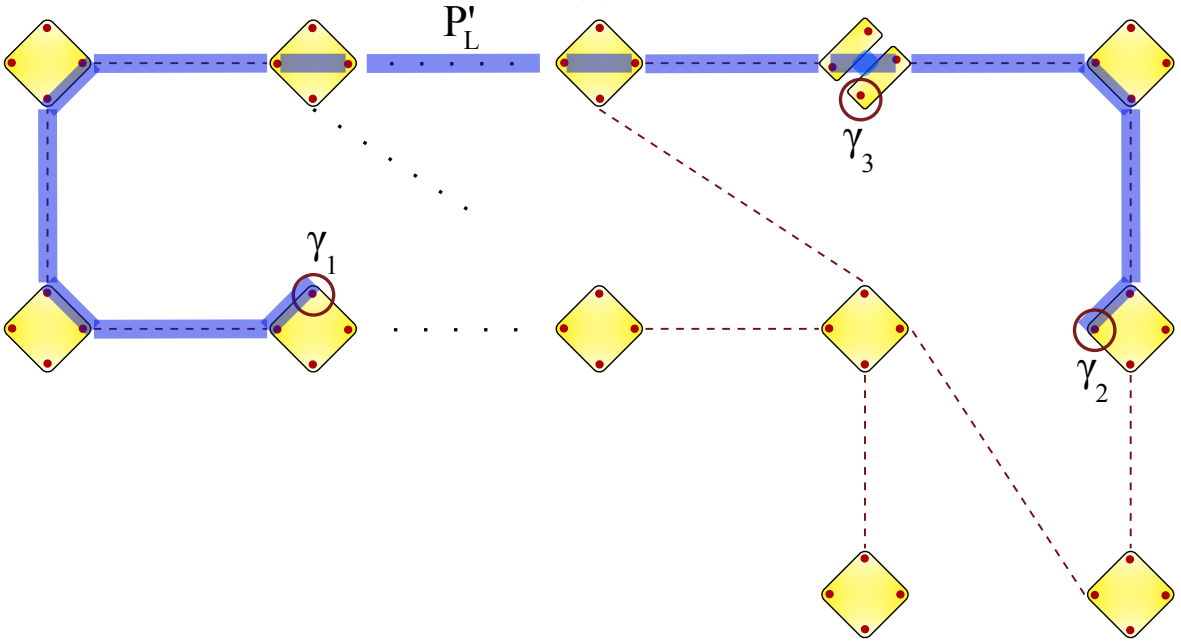

(b)

Figure 4.13: (a) The system at the start (t=0) of the adiabatic brading process. The operators P_L and A are both symmtries of the system. (b) The system at the end ($t = T$) of the process. Note that the dotted lines are not couplings that are turned off, but indicate the continuation of the system for an undetermined length.

$$U(T)\,\sigma_z\,U^\dagger(T) = -\,\sigma_y\,.$$

This transformation is (up to a phase) a rotation of $\pi/2$ radians about the x-axis. Such rotations were discussed previously, and we have that

$$\mathbf{R}(\mathbf{n}_x, \pi/2) = e^{-i\,\sigma_x\,\pi/4} = \sqrt{\frac{1}{2}}\begin{pmatrix} 1 & i \\ i & 1 \end{pmatrix}.$$

So we find the form of the braiding operator as

$$\boxed{U(T) = e^{-i\,\sigma_x\,\pi/4}}. \tag{4.13}$$

4.4 Readout strategy

The final part of this chapter will discuss a strategy for the readout of the qubits of the system. A strategy using quantum interferometry is presented in [35], building on [55, 56]. In the following, we explain how this approach can be applied to the qubits we consider in this thesis.

Consider figure 3.3. If we take the diagonal coupling λ_2 to be on, and the vertical couplings labelled λ_1 to be off, we have a system with two unpaired Majorana modes. We couple each unpaired mode to a lead, and also connect the two leads by a wire which we will model by a single tunnelling amplitude. If a small bias voltage is applied between the two leads, a current will flow. By measuring the conductance, we can gain information about the state of the qubit. This scenario is effectively the same as the one in [35].

The Schrieffer-Wolff perturbation theory outlined in chapter 3 can be used to find an effective, low-energy Hamiltonian describing the transfer process. In addition to the tunnel couplings introduced in chapter 3, we will now also have the direct link between the two leads, labelled by Ψ_1 and Ψ_2, as well as tunnel couplings between the unpaired Majorana modes (labelled by γ_1 and γ_2) and the leads. The Hamiltonian would then take the form

$$H = H_{\textit{surface code}} + it_1(\Psi_1 + \Psi_1^\dagger)\,\gamma_1 + it_2(\Psi_2 + \Psi_2^\dagger)\,\gamma_2 + t_{\textit{wire}}(\Psi_2^\dagger\Psi_1 + \text{H. c.})$$

Where $t_{\textit{wire}}$ is the tunnel coupling between the two leads, and t_i is the tunnel coupling between γ_i and Ψ_i, with i taking one of the two values 1, 2.

We assume that the tunnel couplings are small compared to the charging energies. Our effective Hamiltonian will contain three tunnelling terms: two for paths through the unpaired Majoranas and through either the left (P_L) or right (P_R) string connecting

them, and one through the wire connecting Ψ_1 and Ψ_2. Referring to [35] we have that the low-energy Hamiltonian becomes

$$H_{12} = \alpha(\xi + c_L P_L + c_R P_R)\Psi_1^\dagger \Psi_2 + \text{ H. c.}$$

and with our labelling of the coupling strengths, $\alpha = -32t_1 t_2/(t^*_{wire} E_C)$ while $\xi = 5|t_{wire}|^2/(16E_C)$. The coefficients of the Majorana strings P_L and P_R depend on the length of these strings, which is determined by how far the Majorana modes are located from each other. The resulting conductance coincides with eq. of [35]:

$$\frac{G_{12}}{e^2/h} = 4\pi^2 \nu_1 \nu_2 (g + g_L P_L + g_R P_R + g_{LR} P_L P_R) \tag{4.14}$$

Thus, we should be able to measure the values of the strings P_L and P_R. The product $P_L P_R$ is also a symmetry of the system. A measurement of P_L and P_R is a measurement of the logical value of the qubit defined by the dislocation.

Conclusion

We have reviewed the basic aspects of Majorana modes and the toric and planar code models. We have shown how the planar code emerges in fourth order perturbation theory in a Majorana bound state (MBS) network. We introduced dislocations into this network by means of tunable tunnel couplings, and saw how, in fifth order perturbation theory, the planar code with twist defects emerged.

By going from the system without twist defects, and only tetragonal plaquettes to one with a pair of pentagonal plaquettes we were able to initialize the system in a specific state. The introduction of tunable couplings enabled us to move unpaired Majorana modes through the MBS network in the horizontal and vertical directions, as well as around one kind of corner. To enable motion around an oppositely oriented corner, and to thereby be able to perform braiding operations, we introduced a split island structure, and saw how it allowed us to shift between regimes of inter-and intra-island couplings.

We defined a protocol for braiding Majorana modes in the MBS network with twist defects, and calculated the associated Berry phase in two different ways. The obtained result agreed with expectations. Finally, we proposed a strategy for measuring the state of logical qubits in the system.

Bibliography

[1] H Bombin. Topological order with a twist: Ising anyons from an Abelian model. *Physical Review Letters*, 105(3), 2010.

[2] Huaixiu Zheng, Arpit Dua, and Liang Jiang. Demonstrating non-Abelian statistics of Majorana fermions using twist defects. *Physical Review B*, 92(October):1–10, 2015.

[3] Sergey Bravyi and Alexei Kitaev. Universal quantum computation with ideal Clifford gates and noisy ancillas. *Physical Review A - Atomic, Molecular, and Optical Physics*, 71(2):022316, feb 2005.

[4] Barbara M. Terhal. Quantum error correction for quantum memories, apr 2015.

[5] Martin Leijnse and Karsten Flensberg. Introduction to topological superconductivity and Majorana fermions. *Semiconductor Science and Technology*, 1:1–21, 2012.

[6] Frank Wilczek. Magnetic flux, angular momentum, and statistics. *Physical Review Letters*, 48(17):1144–1146, apr 1982.

[7] Alexei Kitaev. Anyons in an exactly solved model and beyond, 2006.

[8] Sankar Das Sarma, Michael Freedman, and Chetan Nayak. Topologically protected qubits from a possible non-abelian fractional quantum hall state. *Physical Review Letters*, 94(16):166802, apr 2005.

[9] Parsa Bonderson, Alexei Kitaev, and Kirill Shtengel. Detecting non-abelian statistics in the î=5/2 fractional quantum hall state. *Physical Review Letters*, 96(1):016803, jan 2006.

[10] Chetan Nayak, Steven H. Simon, Ady Stern, Michael Freedman, and Sankar Das Sarma. Non-Abelian anyons and topological quantum computation. *Reviews of Modern Physics*, 80(3):1083–1159, sep 2008.

[11] Alexei Kitaev. Unpaired Majorana fermions in quantum wires. *Physics-Uspekhi*, 44(10S):131–136, oct 2000.

[12] Liang Fu and C. L. Kane. Superconducting proximity effect and majorana fermions at the surface of a topological insulator. *Physical Review Letters*, 100(9):1–4, 2008.

[13] V. Gurarie, L. Radzihovsky, and A. V. Andreev. Quantum phase transitions across a p-wave feshbach resonance. *Physical Review Letters*, 94(23):230403, jun 2005.

[14] Johan Nilsson, A. R. Akhmerov, and C. W.J. Beenakker. Splitting of a cooper pair by a pair of majorana bound states. *Physical Review Letters*, 101(12):120403, sep 2008.

[15] Pavan Hosur, Pouyan Ghaemi, Roger S. K. Mong, and Ashvin Vishwanath. Majorana modes at the ends of superconductor vortices in doped topological insulators. *Physical Review Letters*, 107(9):097001, aug 2011.

[16] Jay D. Sau and S. Das Sarma. Realizing a robust practical Majorana chain in a quantum-dot-superconductor linear array. *Nature Communications*, 3(1):964, jan 2012.

[17] Yuval Oreg, Gil Refael, and Felix Von Oppen. Helical liquids and Majorana bound states in quantum wires. *Physical Review Letters*, 105(17):1–4, 2010.

[18] Roman M. Lutchyn, Jay D. Sau, and S. Das Sarma. Majorana fermions and a topological phase transition in semiconductor-superconductor heterostructures. *Physical Review Letters*, 105(7), 2010.

[19] K. T. Law, Patrick A. Lee, and T. K. Ng. Majorana Fermion Induced Resonant Andreev Reflection. *Physical Review Letters*, 103(23):237001, dec 2009.

[20] Karsten Flensberg. Tunneling characteristics of a chain of Majorana bound states. *Physical Review B - Condensed Matter and Materials Physics*, 82(18):180516, nov 2010.

[21] Jay D Sau, Sumanta Tewari, Roman M Lutchyn, Tudor D Stanescu, and S Das Sarma. Non-Abelian quantum order in spin-orbit-coupled semiconductors: Search for topological Majorana particles in solid-state systems. *Physical Review B - Condensed Matter and Materials Physics*, 82(21), 2010.

[22] V. Mourik, K. Zuo, S. M. Frolov, S. R. Plissard, E. P. A. M. Bakkers, and L. P. Kouwenhoven. Signatures of Majorana Fermions in Hybrid Superconductor-Semiconductor Nanowire Devices. *Science*, 336(6084):1003–1007, 2012.

[23] M. T. Deng, C. L. Yu, G. Y. Huang, M. Larsson, P. Caroff, and H. Q. Xu. Anomalous zero-bias conductance peak in a Nb-InSb nanowire-Nb hybrid device. *Nano Letters*, 12(12):6414–6419, dec 2012.

[24] Anindya Das, Yuval Ronen, Yonatan Most, Yuval Oreg, Moty Heiblum, and Hadas Shtrikman. Zero-bias peaks and splitting in an Al–InAs nanowire topological superconductor as a signature of Majorana fermions. *Nature Physics*, 8(12):887–895, nov 2012.

[25] H. O.H. Churchill, V. Fatemi, K. Grove-Rasmussen, M. T. Deng, P. Caroff, H. Q. Xu, and C. M. Marcus. Superconductor-nanowire devices from tunneling to the multichannel regime: Zero-bias oscillations and magnetoconductance crossover. *Physical Review B - Condensed Matter and Materials Physics*, 87(24):241401, jun 2013.

[26] A. D. K. Finck, D. J. Van Harlingen, P. K. Mohseni, K. Jung, and X. Li. Anomalous modulation of a zero-bias peak in a hybrid nanowire- superconductor device. *Physical Review Letters*, 110(12):126406, mar 2013.

[27] Fabrizio Nichele, Asbjørn C.C. Drachmann, Alexander M. Whiticar, Eoin C.T. O'Farrell, Henri J. Suominen, Antonio Fornieri, Tian Wang, Geoffrey C. Gardner, Candice Thomas, Anthony T. Hatke, Peter Krogstrup, Michael J. Manfra, Karsten Flensberg, and Charles M. Marcus. Scaling of Majorana Zero-Bias Conductance Peaks. *Physical Review Letters*, 119(13):136803, sep 2017.

[28] T D Stanescu and S Tewari. Majorana fermions in semiconductor nanowires: Fundamentals, modeling, and experiment, jun 2013.

[29] R. M. Lutchyn, E. P.A.M. Bakkers, L. P. Kouwenhoven, P. Krogstrup, C. M. Marcus, and Y. Oreg. Majorana zero modes in superconductor-semiconductor heterostructures, may 2018.

[30] Hao Zhang, Chun Xiao Liu, Sasa Gazibegovic, Di Xu, John A. Logan, Guanzhong Wang, Nick Van Loo, Jouri D.S. Bommer, Michiel W.A. De Moor, Diana Car, Roy L.M. Op Het Veld, Petrus J. Van Veldhoven, Sebastian Koelling, Marcel A. Verheijen, Mihir Pendharkar, Daniel J. Pennachio, Borzoyeh Shojaei, Joon Sue Lee, Chris J. Palmstrøm, Erik P.A.M. Bakkers, S. Das Sarma, and Leo P. Kouwenhoven. Quantized Majorana conductance. *Nature*, 556(7699):74–79, mar 2018.

[31] Jiannis Pachos. *Introduction to topological quantum computation*. Cambridge University Press, 1st edition, 2012.

[32] A.Yu. Kitaev. Fault-tolerant quantum computation by anyons. *Annals of Physics*, 303(1):2–30, 2003.

[33] Barbara M Terhal, Fabian Hassler, and David P Divincenzo. From Majorana Fermions to Topological Order. *Physical Review Letters*, 108:1–8, 2012.

[34] L A Landau, S Plugge, E Sela, A Altland, S M Albrecht, and R Egger. Towards Realistic Implementations of a Majorana Surface Code. *Physical Review Letters*, 116(5), 2016.

[35] S. Plugge, L. A. Landau, E. Sela, A. Altland, K. Flensberg, and R. Egger. Roadmap to Majorana surface codes. *Physical Review B*, 94(17):1–21, 2016.

[36] Liang Fu. Electron teleportation via Majorana bound states in a mesoscopic superconductor. *Physical Review Letters*, 104(5):1–4, 2010.

[37] Alexander Altland and Reinhold Egger. Multiterminal coulomb-majorana junction. *Physical Review Letters*, 110(19):196401, may 2013.

[38] Stephan Plugge, Alex Zazunov, Pasquale Sodano, and Reinhold Egger. Majorana entanglement bridge. *Physical Review B - Condensed Matter and Materials Physics*, 91(21):214507, jun 2015.

[39] A. R. Akhmerov, Jay D. Sau, B. Van Heck, S. Rubbert, and R. Skolasinski. Topology in Condensed Matter.

[40] Alexei Kitaev and Chris Laumann. Topological phases and quantum computation. *Spectrum*, cond-mat.m(January):31, 2009.

[41] D A Ivanov. Non-Abelian statistics of half-quantum vortices in p-wave superconductors. *Physical Review Letters*, 86(2):268–271, 2001.

[42] Xiao-Gang Wen. Quantum Orders in an Exact Soluble Model. *Physical Review Letters*, 90(1):016803, 2003.

[43] Frank Wilczek. Remarks on dyons. *Physical Review Letters*, 48(17):1146–1149, apr 1982.

[44] Frank Wilczek. Magnetic Flux, Angular Momentum, and Statistics. *Physical Review Letters*, 48(17):1144–1146, apr 1982.

[45] Benjamin J. Brown, Katharina Laubscher, Markus S. Kesselring, and James R. Wootton. Poking holes and cutting corners to achieve clifford gates with the surface code. *Physical Review X*, 7(2):021029, may 2017.

[46] David P. DiVincenzo. The physical implementation of quantum computation. *Fortschritte der Physik*, 48(9-11):771–783, sep 2000.

[47] M. T. Deng, C. L. Yu, G. Y. Huang, M. Larsson, P. Caroff, and H. Q. Xu. Anomalous Zero-Bias Conductance Peak in a Nb–InSb Nanowire–Nb Hybrid Device. *Nano Letters*, 12(12):6414–6419, dec 2012.

[48] T. W. Larsen, K. D. Petersson, F. Kuemmeth, T. S. Jespersen, P. Krogstrup, J. Nygård, and C. M. Marcus. Semiconductor-Nanowire-Based Superconducting Qubit. *Physical Review Letters*, 115(12):127001, sep 2015.

[49] Jay D. Sau, David J. Clarke, and Sumanta Tewari. Controlling non-Abelian statistics of Majorana fermions in semiconductor nanowires. *Physical Review B - Condensed Matter and Materials Physics*, 84(9):094505, sep 2011.

[50] J. A. Schreier, A. A. Houck, Jens Koch, D. I. Schuster, B. R. Johnson, J. M. Chow, J. M. Gambetta, J. Majer, L. Frunzio, M. H. Devoret, S. M. Girvin, and R. J. Schoelkopf. Suppressing charge noise decoherence in superconducting charge qubits. *Physical Review B - Condensed Matter and Materials Physics*, 77(18):180502, may 2008.

[51] B. Van Heck, F. Hassler, A. R. Akhmerov, and C. W.J. Beenakker. Coulomb stability of the 4π-periodic Josephson effect of Majorana fermions. *Physical Review B - Condensed Matter and Materials Physics*, 84(18):2–5, 2011.

[52] V. Bouchiat, D. Vion, P. Joyez, D. Esteve, and M. H. Devoret. Quantum Coherence with a Single Cooper Pair. *Physica Scripta*, T76(1):165, 1998.

[53] Jens Koch, Terri M Yu, Jay Gambetta, A A Houck, D I Schuster, J Majer, Alexandre Blais, M H Devoret, S M Girvin, and R J Schoelkopf. Charge-insensitive qubit design derived from the Cooper pair box. *Physical Review A - Atomic, Molecular, and Optical Physics*, 76(4), 2007.

[54] B. Van Heck, A. R. Akhmerov, F. Hassler, M. Burrello, and C. W J Beenakker. Coulomb-assisted braiding of Majorana fermions in a Josephson junction array. *New Journal of Physics*, 14, 2012.

[55] Parsa Bonderson, Kirill Shtengel, and J. K. Slingerland. Decoherence of anyonic charge in interferometry measurements. *Physical Review Letters*, 98(7):070401, feb 2007.

[56] Parsa Bonderson, Michael Freedman, and Chetan Nayak. Measurement-only topological quantum computation. *Physical Review Letters*, 101(1):010501, jun 2008.

Appendices

Appendix A

Unitary transformation of the Hamiltonian

We subject the Hamiltonian of eq. 3.16 to the transformation $U^\dagger H_{16\times16}U$, where $U = (1/2)^{1/2}(Y_2Y_3Y_6Y_7 + X_7)$.

Under this unitary transformation, terms with the identity operator on the seventh island remain unchanged. The same is true for the term with an X-operator on island seven. We label the operators part of this term h_x:

$$h_x = Z_2X_3Z_6X_7$$

and see that cross terms from $U^\dagger h_x U$ vanish, as:

$$Y_2Y_3Y_6Y_7h_xX_7+X_7h_xY_2Y_3Y_6Y_7 = h_xY_2Y_3Y_6Y_7X_7+X_7Y_2Y_3Y_6Y_7h_x = [h_x, Y_2Y_3Y_6Y_7X_7] = 0 \tag{A.1}$$

Where we have used $Y_2Y_3Y_6Y_7X_7 = -X_7Y_2Y_3Y_6Y_7$.

We label terms with either the Z- or Y-operator on the seventh island by h_{yz}:

$$h_{yz} = z_1x_8X_2Z_7, \quad \text{or} \quad h_{yz} = z_1x_8X_2Z_6Y_7.$$

For these terms we have that

$$Y_2Y_3Y_6Y_7h_{yz}Y_2Y_3Y_6Y_7 = h_{yz}, \quad X_7h_{yz}X_7 = -h_{yz}. \tag{A.2}$$

So only cross-terms do possibly not cancel out in these two cases. We find

$$\frac{1}{2}(Y_2Y_3Y_6Y_7(z_1x_8X_2Z_7)X_7 + X_7(z_1x_8X_2Z_7)Y_2Y_3Y_6Y_7) = z_1x_8Z_2Y_3Y_6 \tag{A.3}$$

and

$$\frac{1}{2}(Y_2Y_3Y_6Y_7(z_1x_8X_2Z_6Y_7)X_7 + X_7(z_1x_8X_2Z_6Y_7)Y_2Y_3Y_6Y_7) = z_1x_8Z_2Y_3X_6X_7 \quad \text{(A.4)}$$

So the unitary transformation yields the Hamiltonian of eq. 3.17.

Appendix B

Calculational details of the Berry phase of the braiding process

In the following, we treat the situation where the coupling strengths cannot necessarily be tuned to zero. We label the maximum value of the couplings by M, and the minimum value by m. We split the integral over a closed path up into integrals over the segments of the path defined by the six steps shown in table 1 of the article.

$$\oint_{\mathcal{C}} \sum_k \mathcal{A}_k d\lambda_k = \int_{\text{step 1}} \sum_k \mathcal{A}_k d\lambda_k + \int_{\text{step 2}} \sum_k \mathcal{A}_k d\lambda_k + \cdots + \int_{\text{step 6}} \sum_k \mathcal{A}_k d\lambda_k$$

The connection matrices mutually commute, so that we for two connection matrices have $[\mathcal{A}_k, \mathcal{A}_{k'}] = 0$.

In the first step, only λ_2 changes. For this reason, the integrals over λ_b and λ_3 in step 1 vanish. This reduces the expression to

$$\oint_{\mathcal{C}} \sum_k \mathcal{A}_k d\lambda_k = \int_{\lambda_2,\text{min}}^{\lambda_2,\text{max}} \mathcal{A}_2 d\lambda_2 + \int_{\lambda_b,\text{max}}^{\lambda_b,\text{min}} \mathcal{A}_b d\lambda_b + \cdots + \int_{\lambda_3,\text{max}}^{\lambda_3,\text{min}} \mathcal{A}_3 d\lambda_3 \tag{B.1}$$

$\mathcal{A}_b$ is a zero matrix. For this reason, the second and fifth terms vanish. In the first step, λ_3 takes its minimal value, while λ_b takes its maximal value. We label the minimal and maximal values of λ_k by m_k and M_k, respectively.

The matrix we need to integrate in the first step could then be written as $\mathcal{A}_2(M_1, \lambda_2, m_3)$. The integral over the closed path can be written

$$\begin{aligned}\oint_{\mathcal{C}} \sum_k \mathcal{A}_k d\Delta_k = &\int_{m_2}^{M_2} \mathcal{A}_2(M_b, \lambda_2, m_3) d\lambda_2 + \int_{m_3}^{M_3} \mathcal{A}_3(m_b, M_2, \lambda_3) d\lambda_3 \\ &- \int_{m_2}^{M_2} \mathcal{A}_2(m_b, \lambda_2, M_3) d\lambda_2 - \int_{m_3}^{M_3} \mathcal{A}_3(M_b, m_2, \lambda_3) d\lambda_3\end{aligned}$$

Where the negative signs come from swapping the integration limits. Inserting the explicit form of the connections and integrating yields a long expression, with the diagonal matrix elements consisting of sixteen terms. If we introduce two restraints $m_b = m_2 = m_3 = m$ and $M_b = M_2 = M_3 = M$, this reduces greatly, as we shall see. With these restraints we consider the explicit form of the connections. We see that integrating the connection $\mathcal{A}_2(M, \lambda_2, m)$ with respect to λ_2 is equivalent to integrating the connection $-\mathcal{A}_3(M, m, \lambda_3)$ with respect to λ_3. The same is true for the pair of connections $\mathcal{A}_2(m, \lambda_2, M)$ and $-\mathcal{A}_3(m, M, \lambda_3)$. We can handle the expression in terms of only $\mathcal{A}_2$:

$$\oint_{\mathcal{C}} \sum_k \mathcal{A}_k d\Delta_k = 2\int_m^M \mathcal{A}_2(M, \lambda_2, m) d\lambda_2 - 2\int_m^M \mathcal{A}_2(m, \lambda_2, M) d\lambda_2$$

By inserting the explicit forms of $\mathcal{A}_2(M, \lambda_2, m)$ and $\mathcal{A}_2(m, \lambda_2, M)$ and integrating, we obtain

$$-\oint_{\mathcal{C}} \sum_k \mathcal{A}_k d\Delta_k = -i\alpha\, \sigma_z + i\beta\, \sigma_0$$

where

$$\begin{aligned}
\alpha = &- \arctan\left(\frac{M}{\sqrt{2m^2 + M^2}}\right) - \arctan\left(\frac{m}{\sqrt{m^2 + 2M^2}}\right) \\
&+ \operatorname{arcCot}\left(\frac{M\sqrt{2m^2 + M^2}}{m^2}\right) + \operatorname{arcCot}\left(\frac{m\sqrt{m^2 + 2M^2}}{M^2}\right) \\
\beta = &\frac{\pi}{2} - \arctan\left(\frac{M}{m}\right) - \arctan\left(\frac{m}{M}\right)
\end{aligned}$$

We label the quantity m/M by ε and consider the case $\varepsilon \ll 1$. By rewriting the expressions for α and β we can perform a Maclaurin expansion in ε. We use that $\arctan(A/B) = \operatorname{arcCot}(B/A)$ and that $\operatorname{arcCot}(A) = \pi/2 - \arctan(A)$.

$$
\begin{aligned}
\alpha &= \Bigg[- \arctan\left(\frac{1}{\sqrt{2\varepsilon^2+1}}\right) - \arctan\left(\frac{\varepsilon}{\sqrt{\varepsilon^2+2}}\right) \\
&\quad + \operatorname{arcCot}\left(\frac{\sqrt{2\varepsilon^2+1}}{\varepsilon^2}\right) + \operatorname{arcCot}\left(\varepsilon\sqrt{\varepsilon^2+2}\right) \Bigg] \\
&= \Bigg[- \arctan\left(\frac{1}{\sqrt{2\varepsilon^2+1}}\right) - \arctan\left(\frac{\varepsilon}{\sqrt{\varepsilon^2+2}}\right) \\
&\quad + \arctan\left(\frac{\varepsilon^2}{\sqrt{2\varepsilon^2+1}}\right) + \frac{\pi}{2} + \arctan\left(\varepsilon\sqrt{\varepsilon^2+2}\right) \Bigg] \\
&\approx -\frac{\pi}{4} - \mathcal{O}(\varepsilon^2) - \frac{\varepsilon}{\sqrt{2}} + \mathcal{O}(\varepsilon^3) + \mathcal{O}(\varepsilon^2) + \frac{\pi}{2} - \frac{2\varepsilon}{\sqrt{2}} + \mathcal{O}(\varepsilon^3) \\
&\approx \frac{\pi}{4} - \frac{3\varepsilon}{\sqrt{2}} + \mathcal{O}(\varepsilon^2) \\
\beta &= \left[\frac{\pi}{2} - \arctan\left(\frac{1}{\varepsilon}\right) - \arctan\left(\varepsilon\right)\right] \\
&= \frac{\pi}{2} - \Big(\frac{\pi}{2} - \arctan(\varepsilon)\Big) - \arctan(\varepsilon) = 0
\end{aligned}
$$

Consider the limit $\varepsilon \to 0^+$, where $\varepsilon = m/M$. We rewrite the expression for α in terms of ε. It reduces to

$$
\begin{aligned}
\alpha &\approx \lim_{\varepsilon\to 0} \Bigg[- \arctan\left(\frac{1}{\sqrt{2\varepsilon^2+1}}\right) - \arctan\left(\frac{\varepsilon}{\sqrt{\varepsilon^2+2}}\right) \\
&\quad + \operatorname{arcCot}\left(\frac{\sqrt{2\varepsilon^2+1}}{\varepsilon^2}\right) + \operatorname{arcCot}\left(\varepsilon\sqrt{\varepsilon^2+2}\right) \Bigg] \\
&\approx -\arctan\left(1\right) - \arctan\left(0\right) + \operatorname{arcCot}\left(\infty\right) + \operatorname{arcCot}\left(0\right) \\
&\approx -\frac{\pi}{4} - 0 + 0 + \frac{\pi}{2} = \frac{\pi}{4}
\end{aligned}
$$

In this limit, in the adiabatic approximation, the time evolution operator reduces to

$$\mathcal{U} = \exp\left(-i\frac{\pi}{4}\sigma_z\right)$$